NSR-2-2

C00-2263-2

MASTER

ADVANCED THERMIONIC ENERGY CONVERSION

Progress Report by:

E. J. Britt
G. O. Fitzpatrick
L. K. Hansen
N. S. Rasor

Rasor Associates, Inc.
420 Persian Drive
Sunnyvale, California 94086

September 1, 1973 – August 31, 1974

PREPARED FOR THE U.S. ATOMIC ENERGY COMMISSION
UNDER CONTRACT NO. AT-(11-1)-2263

DISCLAIMER

NSR-2-2

C00-2263-2

ADVANCED THERMIONIC ENERGY CONVERSION

Progress Report by:

E. J. Britt
G. O. Fitzpatrick
L. K. Hansen
N. S. Rasor

Rasor Associates, Inc.
420 Persian Drive
Sunnyvale, California 94086

September 1, 1973 – August 31, 1974

PREPARED FOR THE U.S. ATOMIC ENERGY COMMISSION
UNDER CONTRACT NO. AT-(11-1)-2263

ACKNOWLEDGMENT

This work was performed for the USAEC Space Nuclear Systems Division. The encouragement and imaginative guidance of the project by Glen A. Newby, Associate Director, is gratefully acknowledged.

Additional assistance through supplemental funding by the NASA Office of Aeronautics and Space Technology, and the active interest of F. Carl Schwenk, Director, Research Division OAST and Dr. Joseph G. Lundholm, Program Manager, Research Division OAST, are also acknowledged gratefully.

ABSTRACT

During this reporting period basic analytical and experimental exploration was conducted on several types of advanced thermionic energy converters, and preliminary analysis was performed on systems utilizing advanced converter performance. The Pt-Nb cylindrical diode which exhibited a suppressed arc drop, as described in the preceeding annual report, was reassembled and the existence of the postulated hybrid mode of operation was tentatively confirmed. Initial data obtained on ignited and unignited triode operation in the demountable cesium vapor system essentially confimed the design principles developed in earlier work, with a few exceptions. Three specific advanced converter concepts have been selected as candidates for concentrated basic study and for practical evaluation in fixed-configuration converters. Test vehicles and test stands for these converters and a unique controlled-atmosphere station for converter assembly and processing were designed, and procurement has been initiated. System analysis has shown that the thermionic heat exchanger concept for topping of electric power plants is economically and technically attractive if 2nd generation converter performance is achieved, and if identified structural, heat transfer and output coupling innovations are reduced to engineering practice.

TABLE OF CONTENTS

INTRODUCTION

The primary objective of the project is to achieve advanced thermionic converter performance which will make thermionic energy conversion practical for applications having high priority in the national energy program. The overall project strategy for the development of advanced methods of thermionic energy conversion and their applications is illustrated in Figure 1. Figure 2 shows the detail of this strategy as applied to the THX applications. An outline of the objectives of the various work areas in the project follows:

Preliminary System Analysis

Emphasis is on applications where fuel conservation and costs are dominant. Primary attention is being given to terrestrial applications of the thermionic heat exchanger (THX) concept, although increasing attention will be given to space-nuclear applications as the advanced thermionic technology matures. System design activity has emphasized performance estimates. Further parametric analysis and a specific preliminary design of a reference THX are objectives for next year (FY 1975).

Basic Converter Characterization

A phenomenological description of elementary diode and advanced converter operation is maintained, consistent with current experimental data, in an analytical form which is useful for converter innovation and diagnosis, and for system design analysis.

Advanced Converter Research

Advanced converter configurations and modes of operation are conceived, analyzed, and explored experimentally in demountable cesium vapor systems which permit convenient and relatively rapid iteration as the exploratory cycle. The primary objective is to provide input data for converter characterization and development. Phenomenological descriptions of electrode surface characteristics are developed and maintained. The results of work in the New Concept Analysis, Surface Physics, and Demountable Converter Tasks are included in this section.

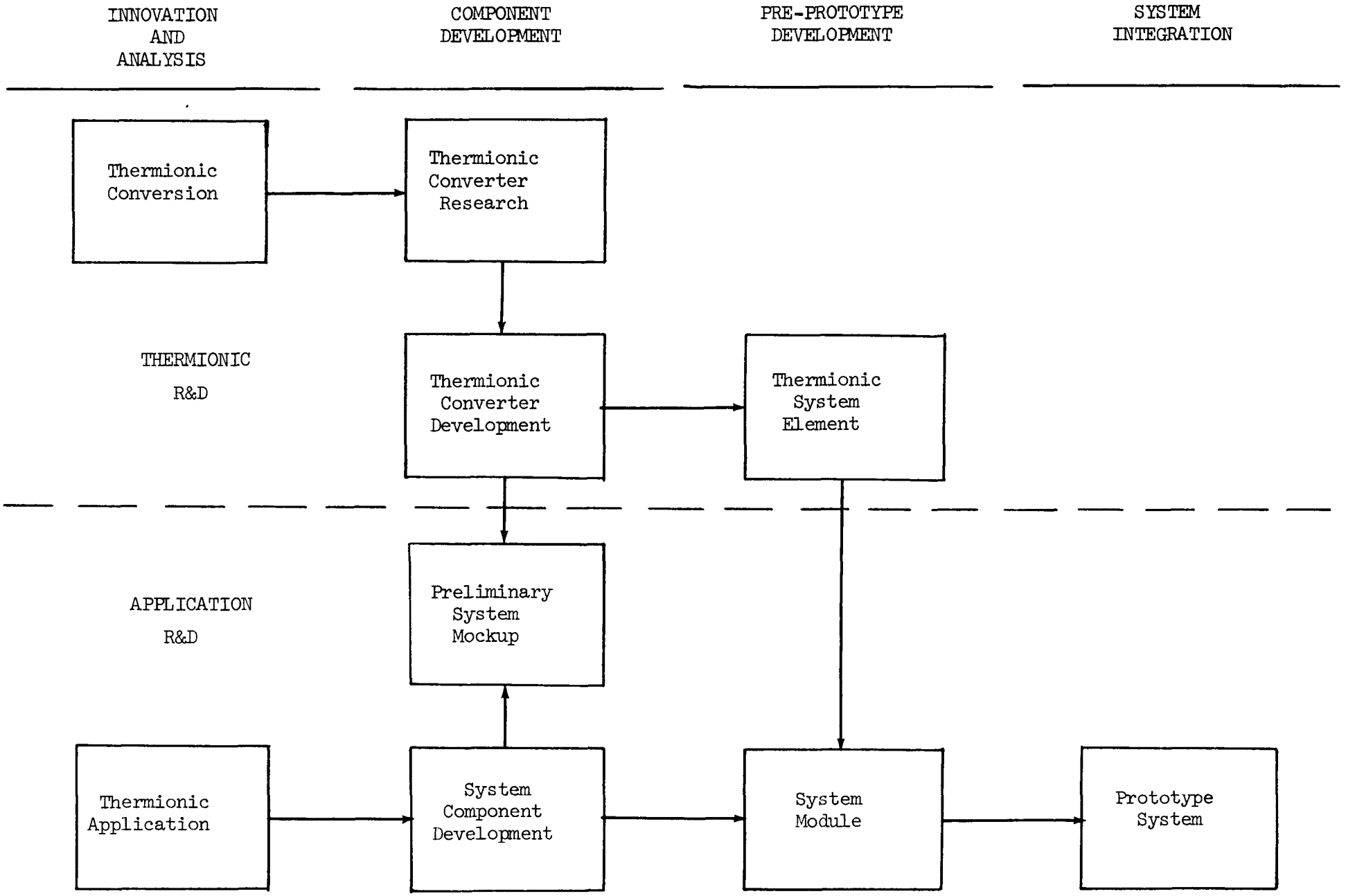

Figure 1 Advanced Thermionic Energy Conversion Program

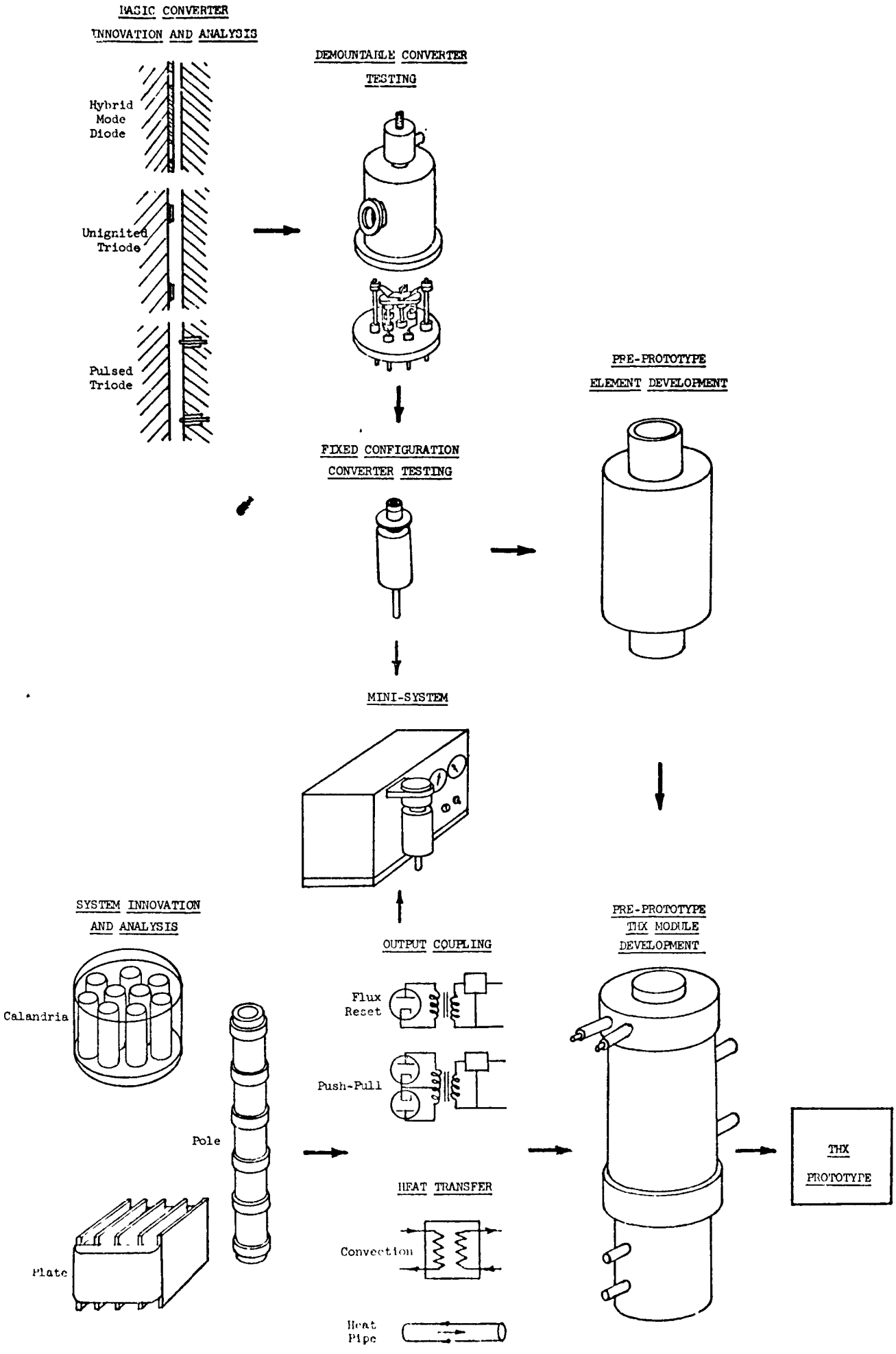

Figure 2 Advanced Thermionic Energy Conversion Program with THX Applications

Advanced Converter Development

Based on data obtained through converter research, and on the practical region of converter operation defined by the System Analysis Task, fixed-configuration converters are constructed and tested to parametrically map and credibly demonstrate the performance available for engineering analysis and design. Facilities for construction and processing of all converters are provided. The Fixed Configuration and Processing Station Tasks are included in this work area.

System Development

Converters and ancillary components are constructed and operated as a system to evaluate problems of physical scale, heat transfer, and output coupling, and to credibly demonstrate specific applications of current technology. During this year work in this area has concentrated on the development of the mini-system.

Program Review

The work during this reporting period proceeded in two phases. During the first half-year, Drs. Rasor and Britt initiated operation of the demountable cesium vapor system, conducted experiments on the Pt-Nb cylindrical diode converter, and performed basic converter analysis and preliminary system analysis under sponsorship by the AEC Space Nuclear Systems Division.

During the second half-year, this activity was supplemented by additional funding from the Research Division of NASA Office of Aeronautics and Space Technology. This additional funding permitted the initiation of parallel evaluation of advanced converter concepts instead of the sequential evaluation procedure used previously. This primarily involved the design and construction of additional test stations and a new processing station for more rapid iterations of test vehicles. A small-scale experimental system itegration activity ("mini-system") was initiated to obtain early practical experience with advanced output coupling techniques and advanced modes of operation as they are developed in the more basic experimental program.

Based on the results obtained during this period, three specific advanced converter concepts have been tentatively selected as candidates for concentrated basic study in the Converter Research Task and for practical evaluation in the Converter Development Task. As shown schematically in Figure 2, they are:

1. Hybrid Mode Diode Converter
2. Unignited Triode Converter
3. Pulsed Triode Converter

Also shown schematically in Figure 2 are the three candidate THX configurations defined during this period, which will be analyzed in more detail under the System Analysis Tasks:

1. Calandria (parallel-tube) THX
2. Coaxial (series-tube) THX
3. Parallel Plate THX

A major objective for FY1975 is to obtain enough experimental and analytical data to permit unambiguous selection of the best converter concept and the best THX configuration for further detailed study in a reference THX design. It should be recognized, however, that the candidate converter and THX selections listed are tentative. Further work may define additional concepts which also must be considered. However, it is hoped that the field can be narrowed at an early stage to permit concentration of available resources on reducing the most promising concept to engineering practice.

In March, 1974, Lorin Hansen and Gary Fitzpatrick joined this project. Dr. Hansen was project manager in the former thermionic conversion program at Atomic International, and is responsible for the advanced converter research activities in this project. Mr. Fitzpatrick was formerly in charge of in-pile thermionic converter testing at Gulf General Atomic and is responsible for advanced converter development activities here. He also is serving as overall project manager of this project.

PROGRAM HIGHLIGHTS SUMMARY

Progress in each of the project tasks during the year is summarized below.

Preliminary System Analysis

System studies in this period concentrated on the application of THX modules as topping units for a central station power plant. Several qualitatively attractive THX designs incorporating the potential performance capabilities of advanced thermionic converters were studied, and an early "calandria" version was analyzed as a topping cycle for the Bull Run steam power plant. The results indicate an attractive cost-effective system could probably be provided with second generation thermionic performance, and that third generation performance would almost certainly provide a cost-effective system. Thus, the addition of a topping cycle to a steam power plant may not only provide an increase in plant efficiency (saving of fuel resources), but may also significantly reduce electric power production costs.

Further analysis will be performed with other THX designs, and more complete system studies will be conducted to better accertain the potential performance of a THX in this application.

Basic Converter Characterization

During this year the phenomenological description of the elementary ignited cesium diode operation derived in NSR-1-1 was incorporated into a program for use with the Hewlett-Packard 9820A desk top programmable calculator. A preliminary comparison of calculated and experimental IV curves has provided new insight into the physical processes which dominate the diodes performance. For example, it was found that a virtual collector probably existed for most of the data used in the past to compute arc drops. The effective ionization potential, and the ion conservation and electrode scattering factors found to characterize the data are consistent with estimates computed from the fundamental atomic properties of cesium. The present formulation becomes inaccurate for current densities greater than 10 amp/cm^2 and pressure-spacing products greater then 60 torr-mil. Work is continuing to extend the accurate region.

Advanced Converter Research

The limitations and possibilities of thermionic energy conversion are discussed based on general statements such as energy balance, particle flux boundary conditions, and existence conditions for virtual electrodes. In this way the limitations of present converters are better defined, the way is pointed for possible enhancement of the elementary diode, and promising indications are given for advanced mode energy conversion.

Three demountable converters were fabricated in this contract period and experimental tests were conducted with two of them. Operation in three advanced modes were demonstrated: the unignited triode, the pulsed triode, and the ignited triode. The unignited triode behaved as expected, except that pulsing to remove a Hernqvist "z-state" was not required. This work produced the important practical result that the converter optimized with the third electrode bias at plasma floating potential. The pulse triode results were encouraging, showing that this method could be used effectively for arc drop suppression. The pulse triode has many advantages over the pulse diode. The ignited triode showed the ability to completely suppress the arc drop. Too great an interaction between the auxiliary discharge and the main discharge, however, presented this arc drop suppression technique from being an efficient process in the test vehicle used.

Advanced Converter Development

The cylindrical converter with which the hybrid mode of operation was discovered was reassembled and retested. Enhanced performance was again achieved, confirming the previous observations. The degree of enhancement was found to be a sensitive function of the position of the platinum emitter sleeve. The dominant process thus is a function of converter interelectrode geometry, and appears to be due to a multi-region discharge.

The design of a cylindrical fixed configuration converter was completed and acquisition of materials for fabrication was initiated.

The design of a processing station was completed. It will enable a converter to be fabricated, instrumented, tested, and disassembled without exposure to air. The acquisition of equipment for the station was initiated.

System Development

A "mini-system" was developed which incorporates a converter and its output coupling circuitry in a compact, self-contained unit. The converter is designed to run in air. Initial operation will be with flux-reset inductive output coupling. The converters have been fabricated and are awaiting cesiation. The flux reset circuit has been built and sucessfully tested with a simulated converter.

I SYSTEM ANALYSIS

Introduction

The purpose of the work conducted under this Task was to survey potential thermionic system applications and to define the performance and cost characteristics of the most promising. A brief initial review of the requirements for a variety of applications was made, including solar energy conversion, transportation power sources, underwater power sources, aluminum refinement, hydrogen production from water, and central station electric production. Thermionic topping of central station electric power plants, using the thermionic heat exchanger (THX) concept, was selected as the most appropriate application for initial detailed study.

There are two aspects to this specific initial choice. First, although cost requirements probably make this the most demanding application technically, it has the greatest and clearest potential yield: i.e., a significant reduction in fuel requirements and cost of producing the nation's primary electric power. This is a real, enduring, and amply-recognized requirement, and thermionics is well suited to fulfill it by virtue of the inherent match between thermionic heat rejection and steam plant heat input conditions. Therefore, if thermionic conversion technology can advance as rapidly toward this new objective as it did in the difficult reactor- space-power application, the thermionic topping application should provide the stability and continuity which is essential for coherent development of the field.

The second aspect is the decision to emphasize the THX approach initially. It is felt that at least one approach in the national thermionic program should be dominated by the ultimate development of thermionic technology, rather than by the constraints and problems of a specific heat source. The THX can, in principle, accept heat from any source, e.g., combustion, nuclear, solar, etc. It is expected that demonstrated THX performance, as a function of its heat input and output conditions, will stimulate heat source development in response to the associated economic incentives. It is the purpose of this Task to define such performance and to anticipate such incentives through system analysis, rather than to become directly involved in the design and development of the heat source.

As the new thermionic technology matures, however, other areas of application probably will appear which are less demanding in cost and scale than power plant topping, and which therefore can take advantage of this technology at an earlier date. The early anticipation and definition of such applications is a corollary purpose of this Task.

Several qualitatively attractive thermionic heat exchanger (THX) designs incorporating the potential performance capabilities of advanced thermionic converters have been studied. The resulting THX module designs are intermediate in size and are distinct from the heat source. The modular design provides maximum flexibility in application, permits high system reliabilities due to component redundancy, and results in relatively size-independent system costs and performance.

An early "calandria" version of the THX was analyzed as a topping cycle for the Bull Run steam power plant. The results indicate that second generation thermionic performance may provide an attractive cost-effective system, and that third generation performance almost certainly would. The THX design configurations developed and the results of this study are discussed in detail below.

THX Design Studies

A ground rule established early in the work was to design a thermionic heat exchanger (THX) which is modular, and distinct from the heat source. The latter requirement enables us to investigate the properties required of the thermionic conversion unit with a minimum of information about the source. Consequently, the designs which result are generally applicable to any heat source, be it a coal-fired furnace, nuclear reactor, or solar power. It is desirable for the thermionic generating unit to be an intermediate-sized module, i.e., one which can be installed in the economically optimum number of units, but which is small enough not to impose insurmountable initial development problems and large enough to gain experience in high power regions of operation. The efficiency and performance data obtained with a single module are then representative of the entire system. Thus, system data can be obtained with a small capital investment, in contrast to an MHD system, where cost and performance are strongly size dependent.[1] The overall plant reliability is also high with a modular design since loss of a single THX module does not result in plant

shutdown. Thus, the modular thermionic system has distinct advantages in development time and cost, and in operational flexibility and maintainability.

In the presently-favored designs, all converter current is collected in parallel, and the power is taken out with inductive coupling[10] to the load. This type of design could feature all-metal construction, without moving parts or ceramic seals, and thus should have reduced complexity and cost and higher reliability.

THX Configuration

A configuration of THX with inductive coupling is shown in Figure I-1 to illustrate the basic concept. The device is a hollow metal tank filled with liquid sodium. It incorporates two adjacent planar electrodes connected at their edges to a single-turn-primary transformer. The path of current flow in the primary circuit is shown by the dashed arrows. High voltage electric output is removed from a multi-turn secondary winding.

Heat input may be accomplished on the emitter side by sodium convection from a heat source. Heat is removed by electromagnetic convection of the sodium on the collector side through the coils of a steam generator. Sodium is attractive as a heat transfer fluid in this application because of its exceptionally low cost and high electrical conductivity. A disadvantage of sodium is that its relatively high vapor pressure (approximately 100 psia @ 2100^{o}F) adds to structural problems at the higher emitter temperatures. The materials of construction can be ferrous super-alloys on the collector side; however, refractory metals probably are required for creep limitation on the emitter side except at the lowest emitter temperatures. Oxidation-resistant superalloys are available, which can withstand 2300^{o} - 2400^{o}F continuous exposure to air, and these might be used to clad refractory metal tubes in a furnace heat source. Appendix I-2 describes these considerations in more detail, including the sodium flow requirements and the effect of operating temperature on costs. Heat pipes also may be used for heat input, and in some designs their special heat transfer capabilities are a distinct advantage. A third alternative is a system in which combustion gas from a furnace or a high temperature gas cooled reactor flows directly through the THX. Its disadvantages are the associated large temperature drops and heat transfer areas required for gaseous heat transfer.

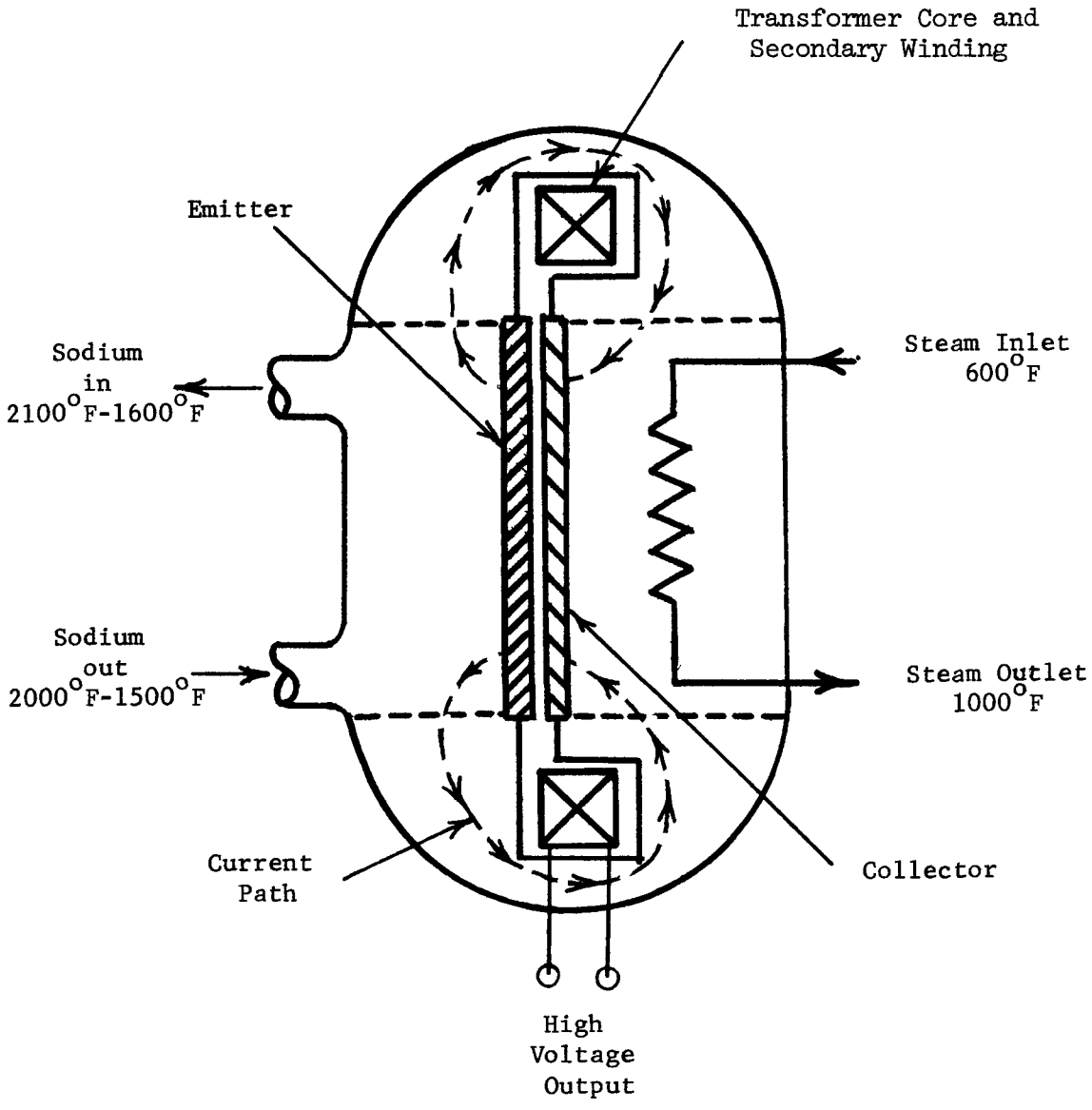

Figure I-1 Schematic Section of A Planer THX with Sodium Coolant

In these designs the primary converter currents are very large (much greater than 10^4 amperes typically), driven by less than a volt. Resistive losses must be minimized, therefore, and this makes inductive output coupling very attractive. No insulators are needed since negligable current is lost by completing the converter envelope with a thin section of a high resistance metal such as stainless steel. The transformer core and secondary winding must be thermally insulated from the hot surroundings, and cooled. Large magnetic fields exist, and effects of flux leakage and eddy currents must be carefully considered. Appendix I-3 describes the initial calculations of such losses.

Several practical THX configurations are under study. Examples are shown in Figures I-2, 3, and 4. The calandria design with a single transformer core at each end (Figure I-2) received early attention, but it was found to have intolerably large eddy current and resistive power losses. These losses can be suppressed by placing a transformer core around each tube, but this results in higher complexity. The plate design appears to have several advantages with regard to power density, costs, and end losses, but it is more complex to fabricate. The pole concept has many attractive features, particularly with respect to end effects, eddy current and resistive losses, and fabrication, but heat transfer may be more difficult.

Thermionic Performance

In order to be able to economically generate large amounts (megawatts) of electric power with thermionic conversion, innovations are necessary to overcome the problems of small size, high cost, close electrode spacings and high temperature requirements (2300 ^{o}F) associated with the familiar elementary cesium diode converter. Fortunately, there are a number of advanced converter concepts which can be applied to meet these new requirements. Some are discussed elsewhere in this report. Many of these advanced devices were demonstrated many years ago,[2-8] but they were not developed because they could not immediately compete with the elementary diode in the high temperature regimes. Improved performance in these advanced converters is achieved by reducing the electronic energy losses in the interelectrode plasma and/or at the collector surface. These new generation converters are capable of efficient operation at substantially lower emitter temperatures (1400^{o} - 2000^{o} F) and larger spacings.

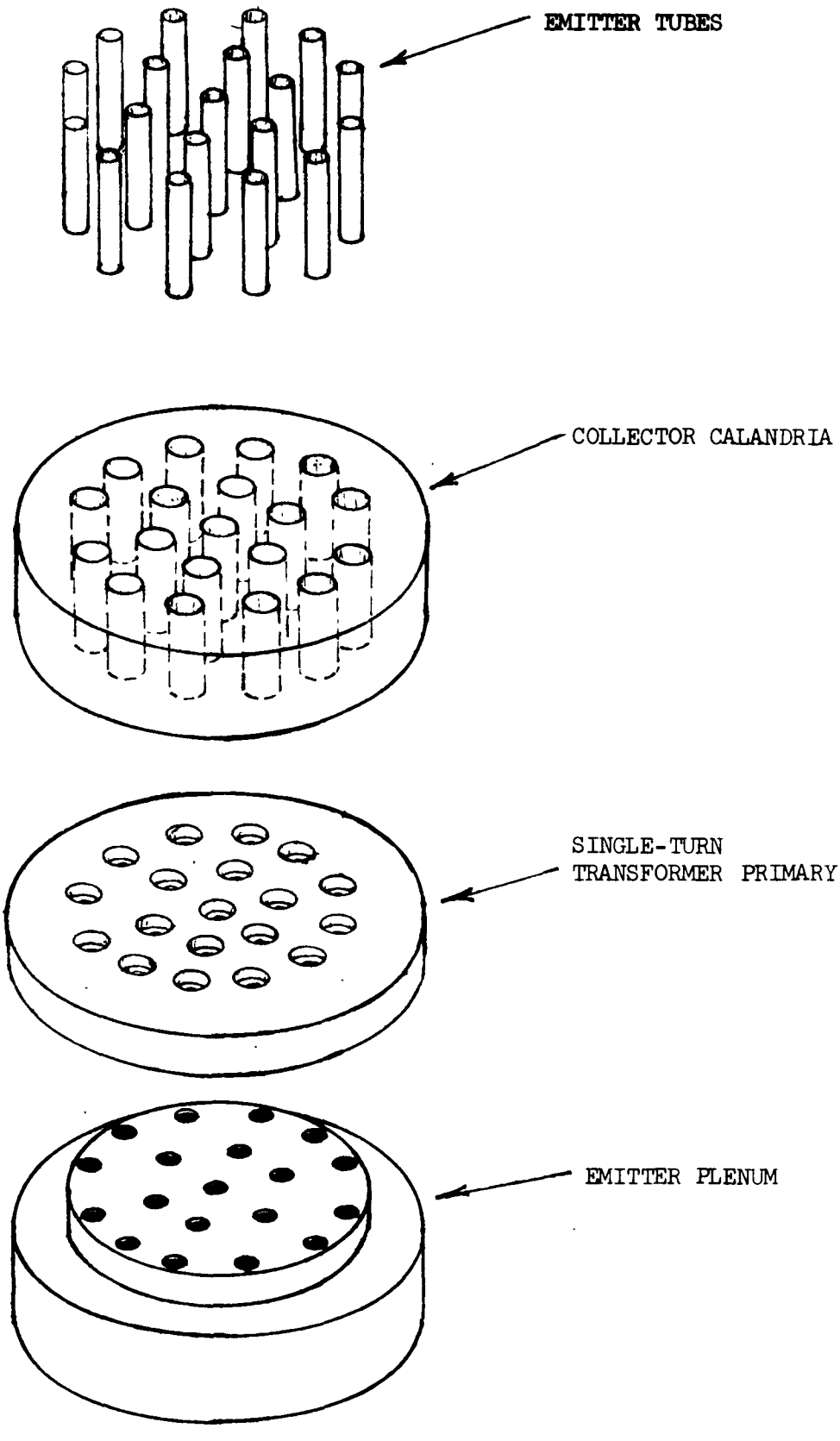

Figure I-2 Schematic of a Calandria THX Configuration

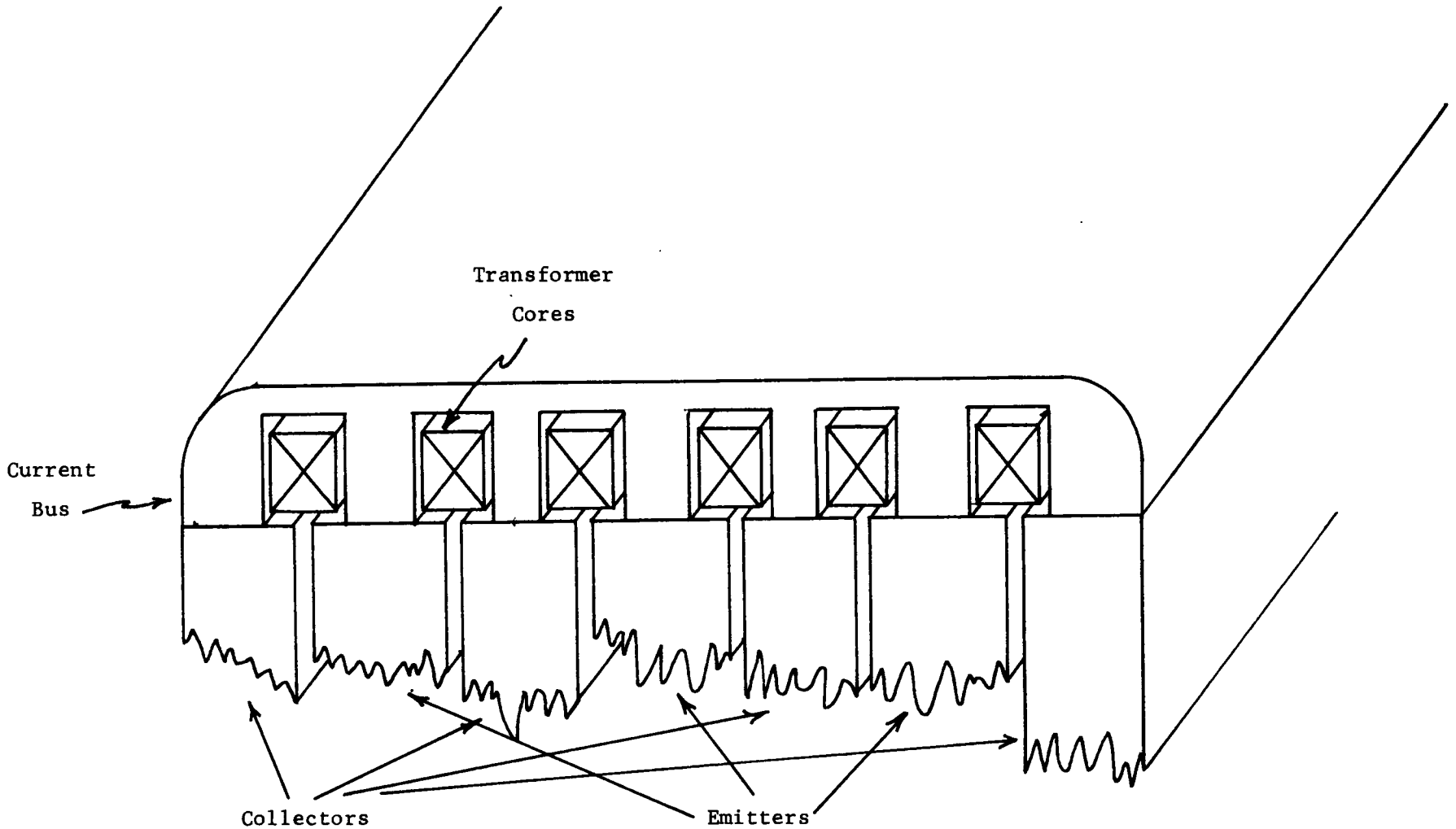

Figure I-3 Schematic Section of a Plate Configuration THX

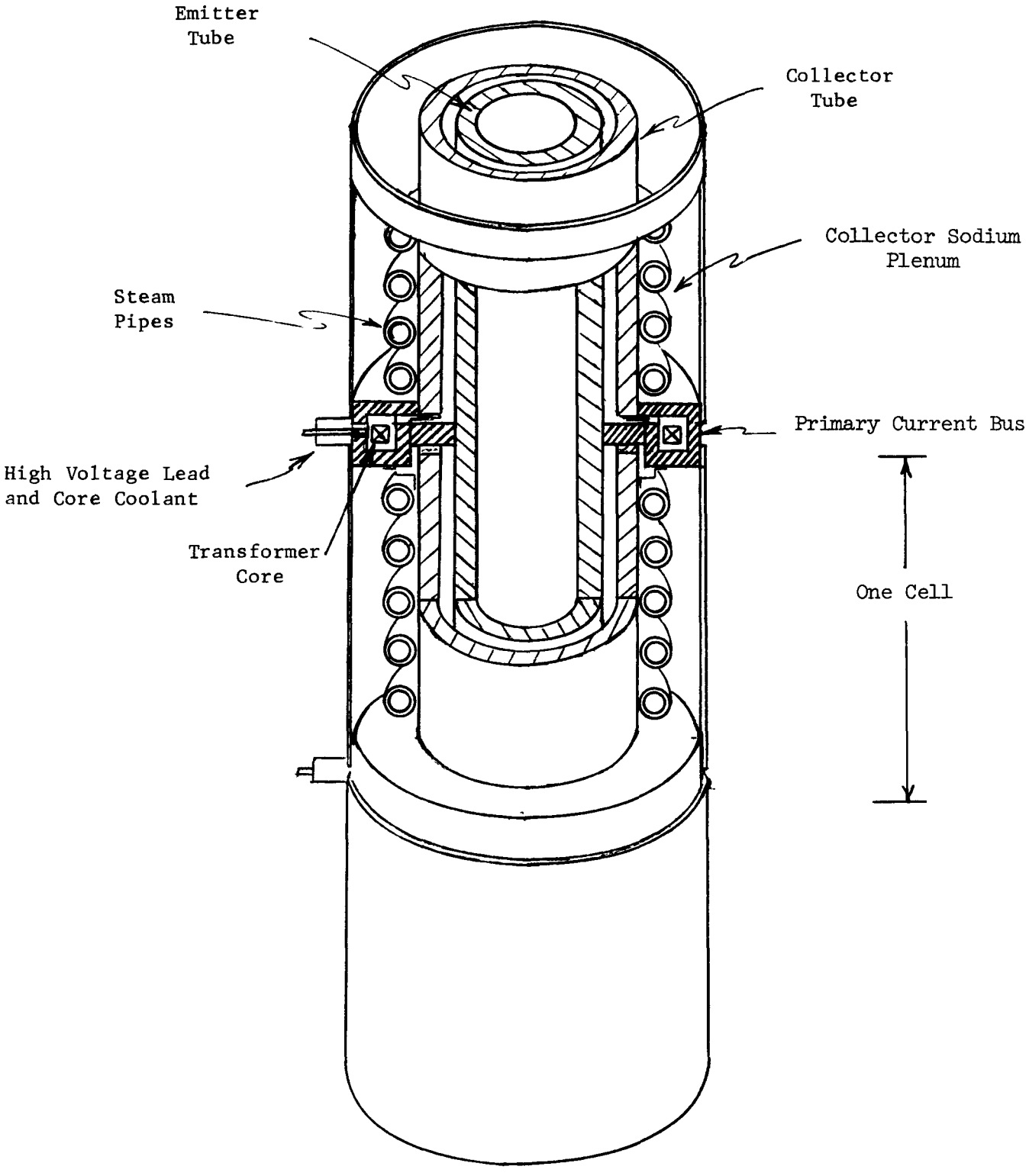

Figure I-4 Schematic Section of a Pole Configuration THX

In order to parametrically survey the performance of systems incorporating a variety of converter types a calculational model is employed which permits each type of converter to be characterized by an "effective" collector work function and an "equivalent" arc drop.[9] Some other non-idealities affecting converter performance, such as electron-neutral scattering, collector back emission, resistive losses in the electrodes and auxiliary power inputs are included in the equations used:[15]

$$P = 0.86\, J(V' - V_d^*)$$

$$V' = \psi - \phi_C' - \Delta V$$

$$\psi = kT_E \ln(AT_E^2/J_S)$$

$$J_s = J\,\frac{1 + 3/4(d/\lambda)}{1 + 1/3(d/\lambda)} + J_C$$

$$J_C = AT_C^2 \exp(-\phi_C/kT_C)$$

$$\Delta V = (\pi H/2)(\rho_E/A_E + \rho_C/A_C)$$

where P = output power per unit area of emitter (watts/cm^2)

J = current density (amps/cm^2)

V' = output voltage (volts)

T_E, T_C = emitter and collector temperatures ($^\circ$K)

A = Richardson constant (120 amp/cm^2 - $^\circ$K^2)

$\phi_C' = \phi_C + V_d'$ = effective collector work function[9] (ev)

ϕ_C = actual collector work function (ev)

V_d' = arc voltage drop (volts)

ΔV = resistive voltage drop in the electrodes (volts)

d/λ = ratio of interelectrode spacing to electron mean free path

V_d^* = "equivalent" arc drop due to auxiliary power inputs[9] (volts)

I = total output current from a converter element (amps)

H = length of electrode (cm)

A_E = cross sectional area of emitter (cm^2)

A_C = cross sectional area of collector (cm^2)

ρ_E = electrical resistivity of the emitter (ohm-cm)

ρ_C = electrical resistivity of collector (ohm-cm)

The thermal input power per unit area has been approximated by[16]

$$P_{in} = 1.14\ J(\bar{\psi} + 2k\bar{T}_E - 0.25) + 1.5\ (\bar{T}_E/1000)^4 - (\bar{T}_C/1000)^4 + 1.5\ \left(\frac{watt}{cm^2}\right)$$

where $\bar{\psi}$, $\bar{T}_E$, and $\bar{T}_C$ are the average values for temperature drops T_E and T_C along the emitter and collector. The factors of .86 and 1.14 appearing in the equations for the electric power output and thermal input are a result of assumming an optimized emitter lead.[14]

Inductive Output Coupling

Inductively coupling to the output of a thermionic converter has several advantages. Among these are the ability to increase the normally low output voltage of a device to more useful levels, to greatly reduce the distance high currents must travel and the associated resistive power losses, and the possbility of eliminating ceramic insulating seals. All-metal construction sould significantly reduce system costs and increase both life and reliability for many applications.

Two methods of inductively coupling to the output of thermionic converters have been demonstrated. In "push-pull" operation one converter delivers power while another one is switched off or deignited for half of the cycle. During the next half-cycle, the roles of the converters are interchanged.[13] In the "flux reset" method of inductive coupling a converter is alternately turned on and off.[10] While the converter is off, the transformer flux is reset. In both methods, the various phase of the cycle are initiated by programmed pulses from a self-powered pulse generator. The output of a flux reset device is high-duty-cycle chopped DC at a higher voltage. The push-pull type of output produces square-wave AC power. Further power conditioning thus may be necessary for some applications.

Thermionic Topped Bull Run Plant

In order to develop a comparison of performance and also a model for cost estimates, a thermionic topping cycle for a plant with the same steam characteristics as the Bull Run station was studied. The calandria THX module shown in Figure I-2 was chosen as a reference case. Figure I-5 shows a simplified

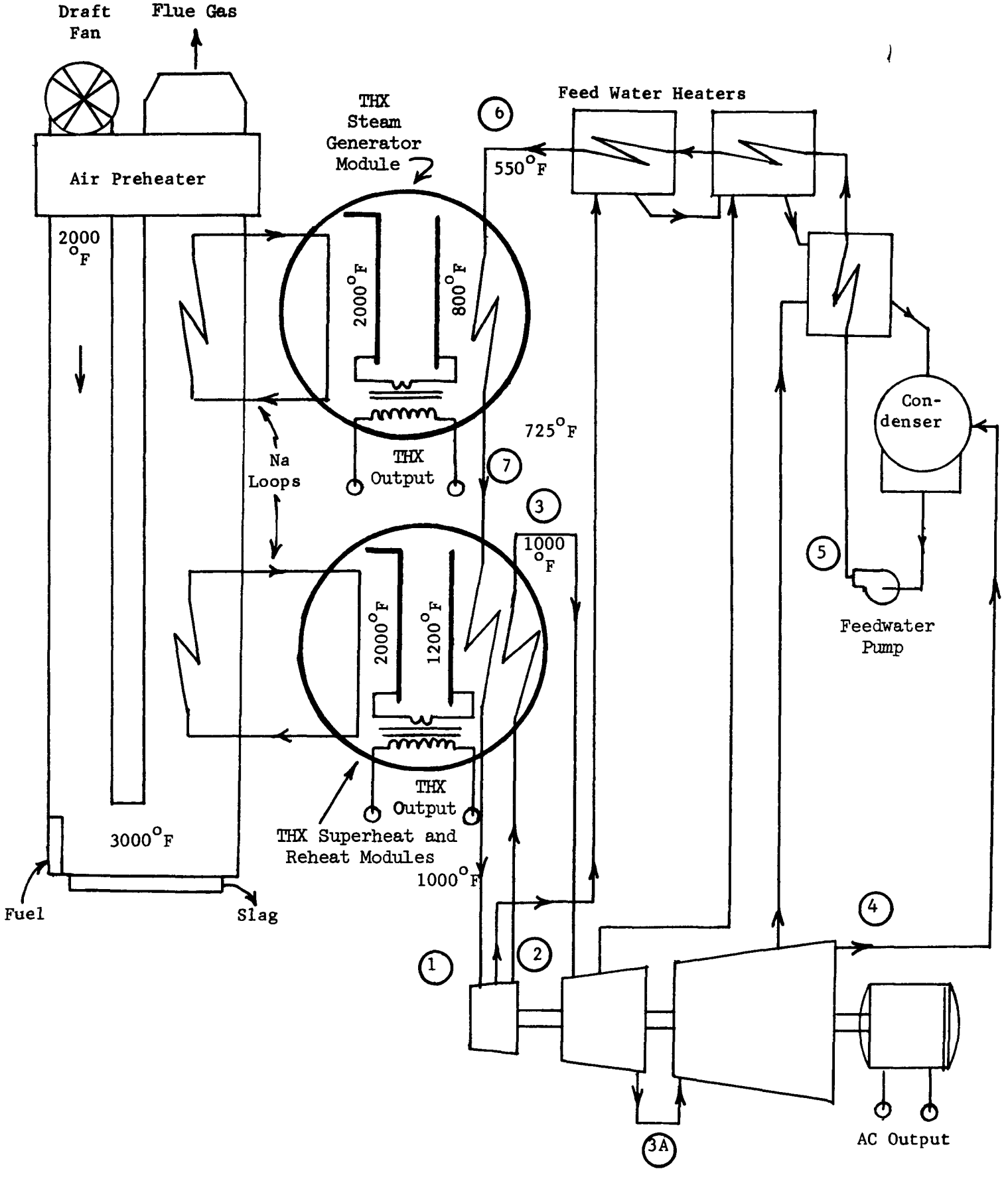

Figure I-5 Thermionic Topped Bull Run Station

schematic of the total system configuration assumed for this study. Examples of the calculated performance characteristics of the standard and thermionic topped systems are summarized below.

Performance Summary

- o Bull Run Station (no topping)
  Generating capacity 914 MWe
  Thermal efficiency 41.3%
- o Bull Run Station (2000°F thermionic topping, 2nd generation)
  Power from steam cycle 914 MWe
  Power from thermionic 215 MWe
  Generating capacity 1166 MWe
  Combined thermal efficiency 47%
- o Bull Run station (2000°F thermionic topping 3rd generation)
  Power from steam cycle 914 MWe
  Power from thermionics 528 MWe
  Generating capacity 1442 MWe
  Combined thermal efficiency 58%

THX Design

The design model studied for the reference case was a calandria THX (Figure I-2). Sodium is pumped through the emitter tubes between large phenums at each end. Calculated values of the required pumping power are less than 1% for 100°F temperature drop along the emitters. Heat transfer from the collector side occurs by electromagnetic convection of the sodium around steam tubes imbedded in the calandria annulus. The emitter material is assumed to be TZM molybdenum alloy, and the calandria is assumed to be constructed of Inconel 601. The static stresses are the vapor pressure of the sodium and the weight of the structure. A dynamic stress is produced by the alternating magnetic field.

THX Performance

The most sensitive variable affecting system performance is the emitter temperature. The dimensions of the THX calandria must be optimized for each

emitter temperature. A calculational algorithm was devised which allows the THX output power and efficiency to be computed and iteratively optimized with an HP-9820A programable calculator.

The outer diameter D of the THX module was arbitrarily fixed at two meters for all of the designs studies (see Figure I-6 below).

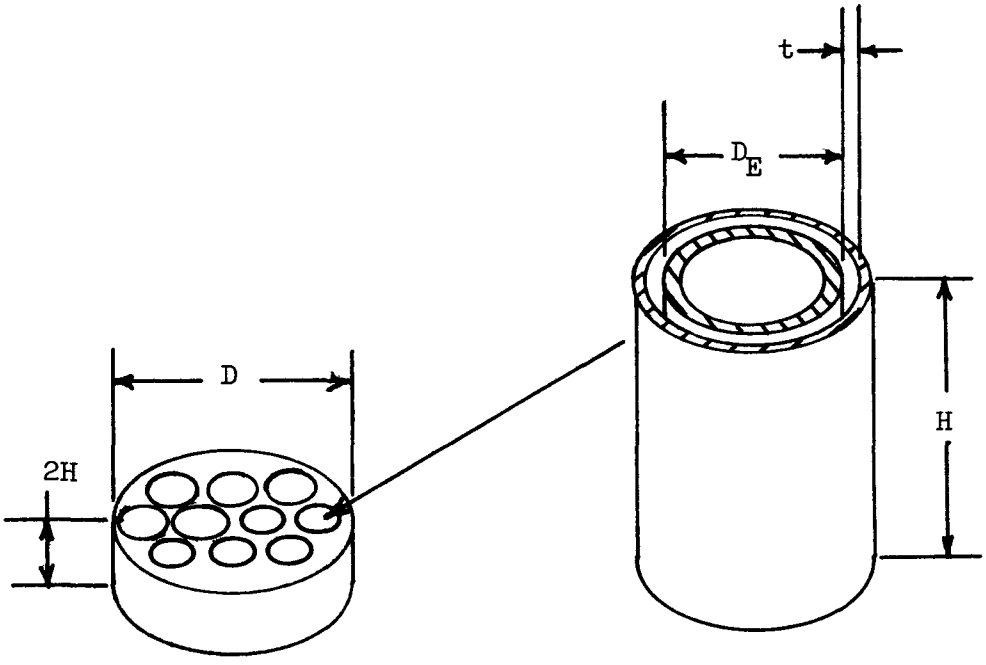

Figure I-6

The diagram also shows an enlarged view of a unit cell of the calandria with emitter diameter D_E, inter-electrode gap t, and half-height of calandria H.

The cross-sectional area A_E of the emitter and its perimeter S_E are respectively $A_E = \pi D_E^2/4$ and $S_E = \pi D_E$, and the emitting area is $S_E H$. Similarly, the effective flow cross sectional area of the unit cell collector is

$$A_C = \pi\left[D^2/N - (D_E + t)^2\right]/4$$

where N is the number of emitter tubes. Since current flows toward both ends the voltage drop ΔV from the center to one end of the electrodes is given by

$$\Delta V = \tfrac{1}{2} S_E H^2 J \left[\rho_E/A_E + \rho_C/A_C\right]$$

The total electric output of the THX is then given by

$$P_{total} = .86\ NJ\ S_E H\ (V' - V_d^*)$$

The total thermal input power for a module is given by

$$Q_{in} = NS_E H\ \ (P_{in} - \tfrac{1}{2}J\Delta V)$$

The module efficiency is then

$$\eta = P_{total}/Q_{in}$$

Optimization

A particular case for a given emitter temperature is calculated as follows. First, values of D, N, t, ρ_E, ρ_C, ΔT_E, ΔT_C, J, T_E, T_C, ϕ_C, V_d', V_d^*, and λ are chosen and entered into the computer program. Iterative calculations of the output power are then performed to find optimum values of H and D_E which give the maximum output power. The value N was not varied but maintained at 100 tubes for this preliminary study. For a given value of H and D_E, there is an optimum value of N. However, if all parameters are allowed to vary at once, the program finds no optimum for N, but rather increases N and reduces D_E and H until the result is a very short calandria design with an impractically large number of tubes. Factors related to fabrication feasibility, end effects, and cost which are not included in the program, would lead to an optimum N when properly considered. It is found that the optimum value of H varies with emitter temperature, the higher temperatures yielding a larger optimum heights. In all cases the optimization criterion is maximum ouput power rather than maximum efficiency.

The variation of calculated THX performance with emitter temperature can be seen in Figures I-7 and I-8. The electric power produced per THX module is shown in Figure I-7. For optimum 3rd generation performance of the overall system the THX modules functioning as superheaters and reheaters must operate

---

* Other quantities in these equations are as defined earlier in this section.

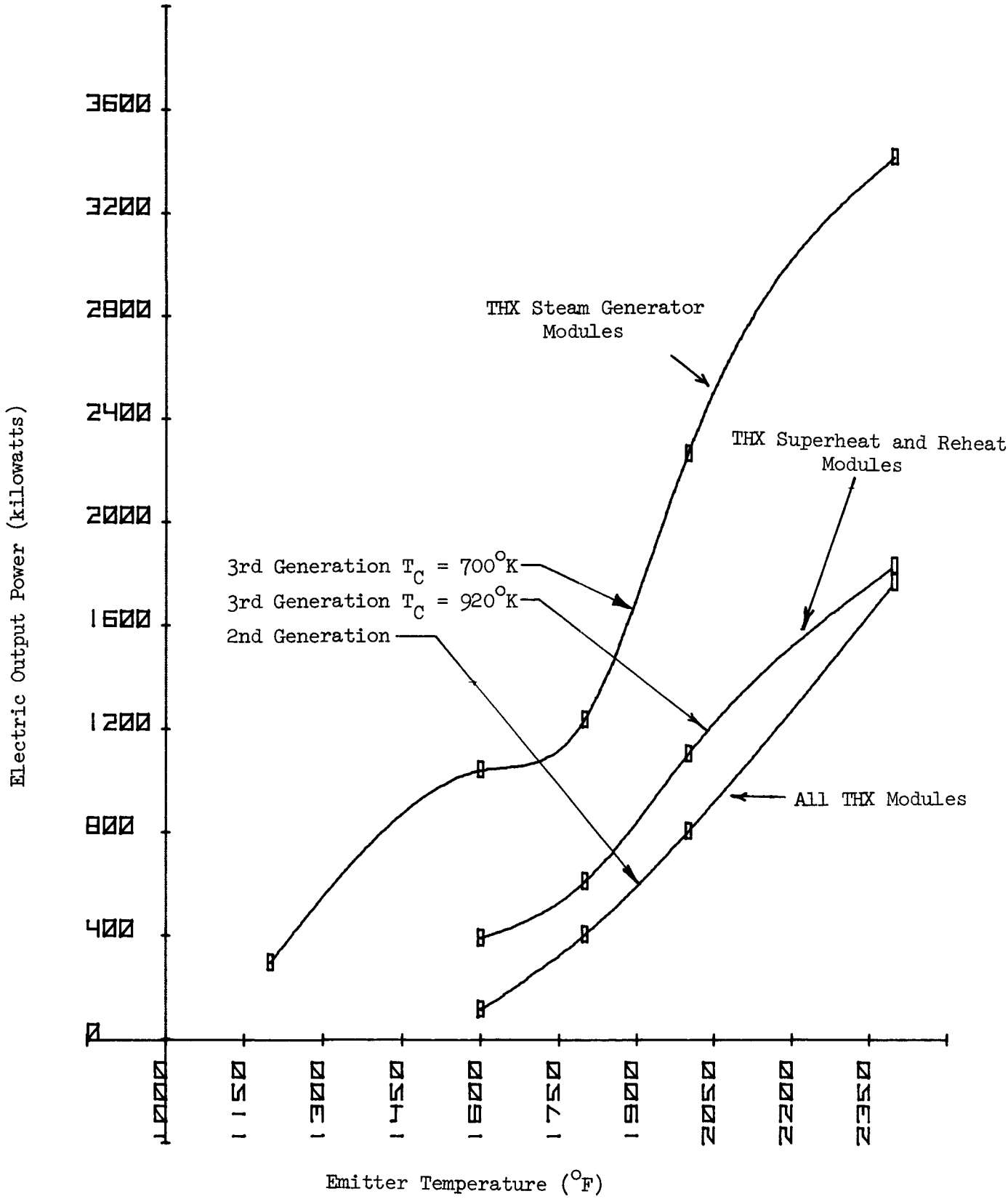

Figure I-7 Variation of Total THX Output Power with Emitter Temperature

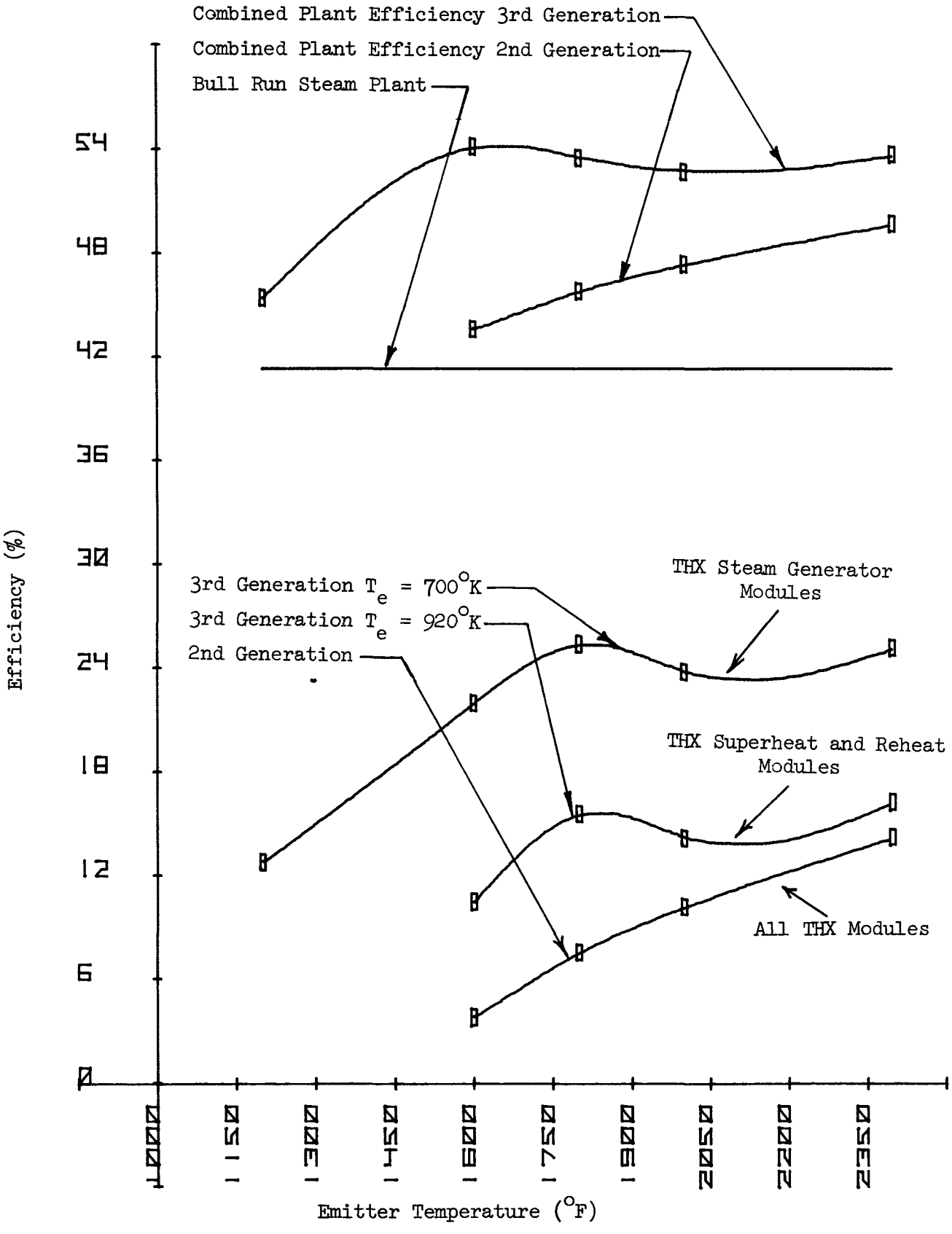

Figure I-8 Variation of Efficiency with Emitter Temperature

with T_C = 920°K, which is above the optimum collector temperature for the converters, in order to achieve the 1000°F steam conditions. However, the THX modules functioning as steam generators produce much more power since they can reject heat at 700°K, which is nearer the optimum temperature for the 1.0 ev collector work functions used. For 2nd generation performance, all modules reject heat at the same temperature because the optimum collector temperature for the 1.5 ev collector work function is near 920°K. This clearly illustrates the inherent necessity for lowering collector temperatures in order to benefit from lower collector work functions.

Thermodynamic Cycle

The steam thermodynamic cycle[11] is shown in Figure I-9. Referring to Figures I-5 and I-9 it is seen that the THX modules reject heat into the steam cycle at three places: (1) generation of supercritical steam at 725°F, (2) superheat to 1000°F, (3) reheat to 1000°F. Since the superheater and reheater are at the same temperature they can be treated schematically as a single thermionic unit with a common collector temperature. The steam part of the cycle is unchanged by the addition of the topping. Approximately 30% of the heat in the steam cycle is recirculated by turbine bleeds to the feedwater heaters.

Cycle Optimization

A decision was made to optimize the thermodynamic cycle for the maximum efficiency of the combined cycle. This was done using performance data of THX modules which were previously optimized for maximum power, as described earlier. It was originally thought that the overall efficiency might benefit from by-passing a portion of heat around the thermionic units, particularly at lower temperatures where the thermionics has a much poorer efficiency than the steam cycle. A complete heat flow network model for the system, including optional parameters to bypass heat around the various THX modules, was set up. The heat flow model also included adjustable efficiencies for the THX modules which were set to the appropriate values for each of the emitter temperatures. This model was then analyzed and iteratively optimized with the steam system constrained to match that of Bull Run Station.

5-6 FW heat from turbine bleeds
6-7 Steam generator (heat from thermionics)
7-1 Superheater (heat from thermionic converters)
2-3 Reheater (heat from thermionic converters)
1-2 HP turbine expansion
3-3A IP turbine expansion
3A-4 LP turbine expansion

PT	TEMP °F	PRESS. PSIA	ENTHALPY BTU/LB
1	1000	3515	1424
2	551.7	600	1256.7
3	1000	540	1518.6
3A	705.9	172	1378.1
4		*	1000.3
5	91.7	*	59.7
6	550.9	3715	546.3
7	725	3615	925

* PRESSURE IS 1.5" Hg

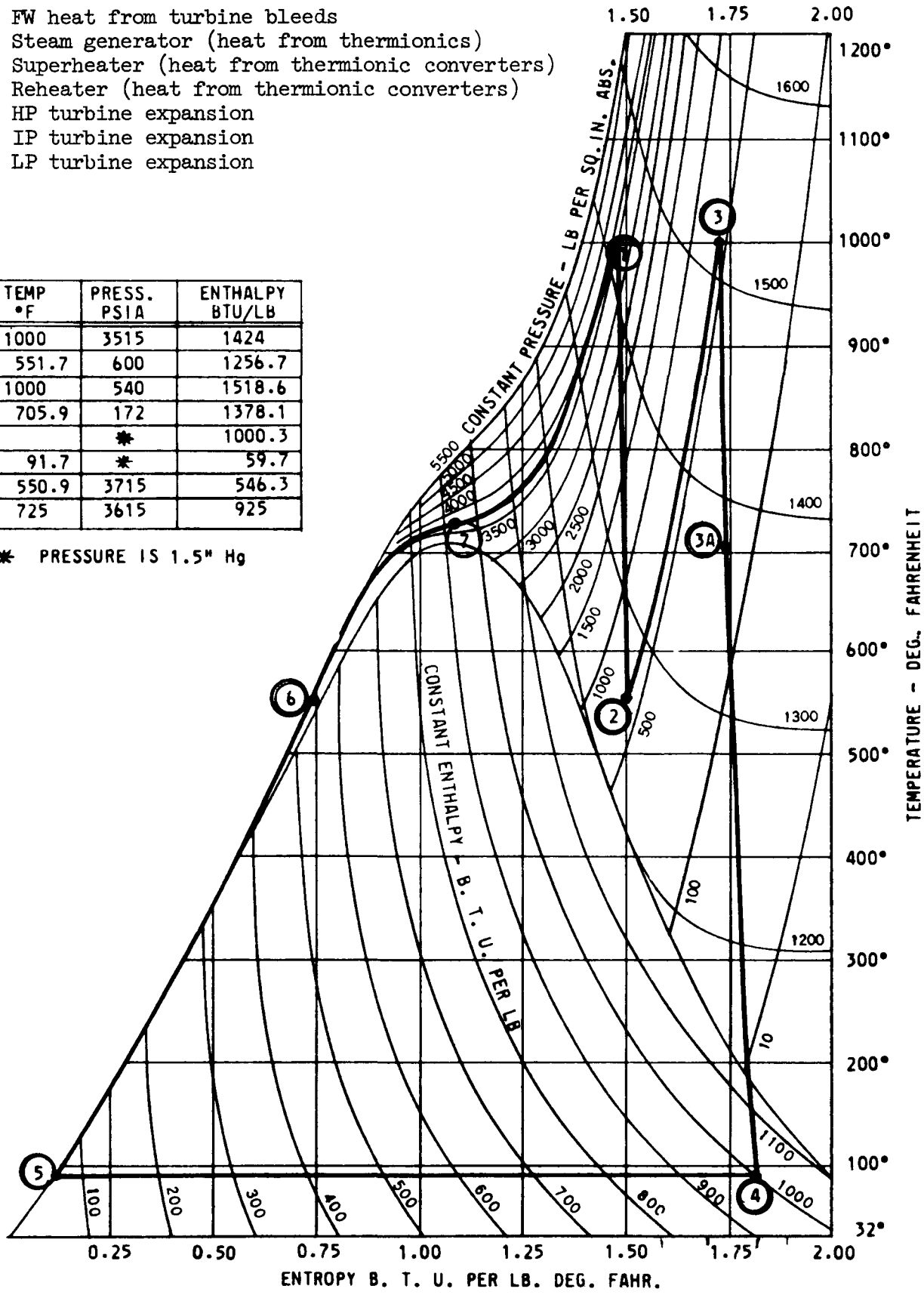

Figure I-9

I. V. A. Bull Run Temperature - Entropy Chart (with topping)

Results showed that the efficiency is never improved by bypassing heat except at a 1200°F - 3rd generation case where the thermionic reject heat was too cold to be used in a superheater and/or reheater. It was also found that the heat flow through the THX modules could replace the economizer to yield a better combined efficiency.

Calculated values of the THX module efficiencies (not to be confused with converter efficiencies) and the combined cycle efficiencies are shown in Figure I-8. A shallow minimum is seen in 3rd generation efficiencies. This results from the fact the THX parameters are optimized for maximum output power at each temperature instead of maximum efficiency. In any event, the significance of the minimum is doubtful since the variation is probably less than the accuracy of the approximations in the calculation.

The combined plant efficiencies shown for 3rd generation performance in Figure I-9 reach an approximate plateau at temperatures above 1600°F. This plateau in efficiency is related to fact that the THX modules were not optimized for efficiency. However, this point is near the economic optimum, i.e., minimum cost of electric energy, as shown below (Figure I-10).

Required Modifications to Furnace

The furnace-boiler of the steam plant must be redesigned to operate at higher temperatures with inlet air preheated to temperatures 1700°F or greater. The design case studied used heat transfer by sodium pumped through tubes inside the furnace to the THX modules. Approximately 11 cm/KWt of $1\frac{1}{2}$ in diameter tubing is required to provide the necessary heat flux. The tubing could be made of a thin-wall refractory metal such as TZM for creep strength with a bonded cladding of superalloy on the outside for oxidation resistance. A large fraction of the heat transfer to the sodium tubing occurs by radiation, hence a significant advantage is gained by using a sodium loop rather than circulation of the combustion gas through the THX. Calculations indicate that the required combustion temperatures can be achieved with coal as fuel and excessive NO_x emissions can be avoided. Slag and fly ash are not expected to be severe problems, but sulfur-containing atmospheres may be damaging to the superalloy cladding. Consequently, unless a sulfur-resistant cladding is found it may be necessary to restrict operation to the use of low sulfur fuels.

Costs Estimates:

The costs calculated in the analysis of the thermionic topped Bull Run plant are not intended to be representative of topping cycle costs in general, but rather are intended to give an idea of the feasibility of a particular design with a specific set of assumptions. Optimization of the THX design is still in its infancy, and the analysis reported here should be interpreted to provide information on cost trends, rather than absolute values. This is particularly true in light of recent fuel price increases and other inflationary factors. The costs for the thermionic system were calculated on a per module basis for a THX with a nominal 1 MWe output.

A method of cost calculation based on extrapolations of costs for existing steam plants was used to compare the costs of a thermionic system with these plants. A description of this method is given in Appendix I-1.

The assumptions incorporated in the analysis are summarized below:

- Transformers - The cost of large transformers in existing power plants is about $5/KWe. The transformers used in the THX will be more sophisticated and will require thermal insulation and cooling. Hence, they were assumed to cost 5 times as much as standard transformers, or $25/KWe.
- Jigging and assembly costs - $1000/module
- External supports - $1500/module
- Quality control and leak testing - $1200/module
- Insulators and miscellaneous - $2500/module
- Total $6200/THX module

It was necessary to assume costs for welding. Part of the structure (emitters, etc.) would be made of refractory metals which require specialized welding techniques and apparatus. However, the outer calandria can be welded with conventional TIG apparatus. These two costs are assumed to be proportional to the length of the welding seam viz:

- Costs of welding refractory metals - $1/cm
- Costs of welding ferrous alloys - $.25/cm

No estimates of the costs involved in modifying the conventional furnace, fans, preheater or power conditioning systems were made. However, the cost of sodium piping in the furnace was included in the analysis.

The calculations showed that a very large part of the cost of a calandria THX module configuration was due to the end phenums. These ends must contain a large volume of sodium to give a low-resistance electrical path around the transformers. They must also withstand the vapor pressure of sodium at emitter temperature. Hence, they must be large shell-type structures of TZM bonded to inconel, and are quite costsly. Subsequent designs have been considered which qualitatively reduce this problem significantly. Hence, it was decided to calculate two costs: one including the end plenums and another leaving them out, thereby generating a cost band which should encompass actual device cost. For the upper bound, the cost of fabricated refractory metal was taken as $30/lb, and 25% of the THX output power was assumed to be lost in the transformer. For the lower bound, the cost of refractory metal was taken as $25/lb. and only 10% transformer loss was assumed. Figure I-10 displays the results of the analysis as a plot of the ratio of the thermionic topped system construction cost to the conventional steam plant construction cost versus percentage of power produced in the topping cycle. An assumption used in the generation of the figure is that the cost of maintenance and frequency of repair is the same for both the topping cycle and the conventional steam plant. The figure is also based on the assumption that the lifetime of the thermionic system is equal to that of the steam system (methods of treating other cases are given in Appendix I-1). The cost ration of 1.0 is based on the 1972 average steam power plant cost of $144/kwe.[12] The "breakeven" line is the line below which the topping system becomes an economically attractive addition to the conventional station. Credit for the increased efficiency, reflected in low operating costs, has been included, which is why the "breakeven" line lies above 1.0. The cost calculations remain approximately valid with inflation at a later date (after 1972) so long as the construction costs of the thermionic system and the steam plant inflat at the same rate. These considerations are discussed further in Appendix I-1.

The upper and lower bounds for each performance generation represent, respectively, pessimistic and optimistic evaluations of the costs of the referance THX topping system. A complete optimization of all system variables with

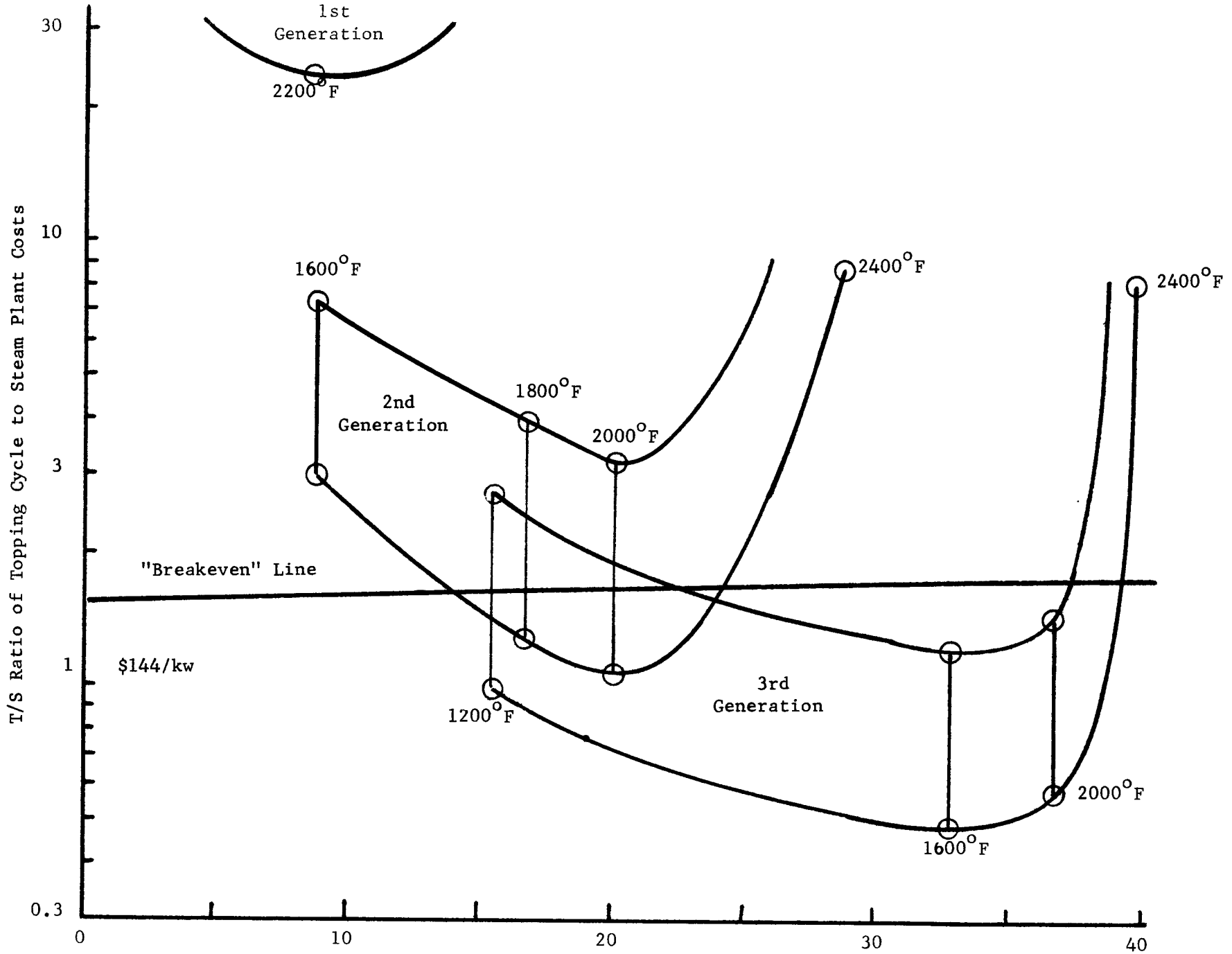

Figure I-10 Percentage of Plant Power Due to Topping Cycle

respect to costs was not feasible within the time and resources available for this study. A compromise toward achieving a complete optimization was attempted by choosing the THX dimensions for maximum output power and then optimizing the combined cycle for maximum efficiency. These two types of optimization affect different parts of the cost: the power per THX module affects the capital investment, while the efficiency affects the operating costs. However, it is felt that this approach approximates a completely cost-optimized analysis for this preliminary study.

It is seen from the graph that the lower bound of 2nd generation costs falls below the "breakeven" line, and the entire 3rd generation cost envelope falls well into this cost-advantage region. The 1st generation performance envelope falls in an entirely impractical region at the top of the graph, but it is included for comparison. The overall optimum (minimum cost) condition occurs at lower temperatures and higher proportion of thermionic power with increasing performance. The reason why the costs per KWe become large as the percentage of thermionic power goes to zero is that THX power output drops rapidly at nearly constant cost as the temperature is reduced. The rapid increase in cost near 2400°F and above is due to exponentially-increasing sodium vapor pressures and creep rates, resulting in heavier and more costly structures. Disproportionate increases in fuel costs since 1972 result in a significantly higher breakeven line than that shown in the figure.

In summary, this analysis indicates that the addition of a topping cycle to a steam power plant not only may provide an attractive increase in plant efficiency (saving of fuel resources), but may also significantly reduce electric energy production costs. Further analysis will be performed with other THX designs, and more complete system studies will be conducted to simultaneously optimize all variables with respect to costs.

ACKNOWLEDGEMENT

The assistance of two consultants in performing this study is gratefully acknowledged:

Mr. Arthur F. Mahon; Thermal Analysis, Appendix I-2.

Dr. Don W. DeMichele; Inductive Output Coupling - Eddy Current Effects, Appendix I-3.

REFERENCES FOR SYSTEMS ANALYSIS SECTION

1. Shandlin, Richard V., III, First Annual AIChE Southwestern Ohio Conference on Energy and the Environment, Oxford, Ohio (October 1973) p 72.

2. Johnson, E.O., et al, RCA Rev., 12 (1951) 163; RCA Rev. 13 (1952) 163; RCA Rev. 16 (1955) 82; RCA Rev. 16 (1955) 498.

3. Fatmi, H.A., and D. Gabor International Conference on Thermionics Power Gen., London, (1965).

4. Hernqvist, K., US Patent 3,021,472, February 13, 1962, filed December 15, 1958. Hernqvist, K., RCA Review, March , 1961.

5. Schuder, J.C., Proceedings of the National Electronics Conference 9 (1953) 626.

6. Bloss, W., Adv. Eng. Conv. (1963) 315.

7. Gabor, D., Nature, 189 (1961) 868.

8. Kaplan, C., Twenty-Second Annual Conference Physical Electronic, MIT, (1962) 105.

9. Rasor, N.S., Third International Conference on Thermionic Electronic Power Generation, Julich, Germany, (June 1972), Vol. 3, pp 1037-1038.

10. Oppen, W. R., IEEE Thermionic Conversion Specialists Conference, Gatlinburg, Tenn., (1963) 372.

11. Final Report on Thermionic Topping Converter for Coal-Fired Power Plant. Contract No. 14-01-0001-499. Prepared for Office of Coal Research by Consolidated Controls Corporation.

12. Olmstead, Leonard M., "18th Steam Station Cost Survey", Electrical World, November 1, 1973.

13. Rasor, N. S., "Thermionic Diode Converter System", US Patent No. 3,146,388 June, 1964.

14. Schock, A., J. Appl. Phys. 32, 769 (1961)

15. Britt, E. J., and N. S. Rasor, Final Technical Report Contract N00014-70-C-0252, NSR-1-4, (October 31, 1972 to June 30, 1972) Section VI.

16. Breitwieser, R., Private Communication

II BASIC CONVERTER CHARACTERIZATION

Objective and Approach

The purpose of this Task is to maintain intuitively tractable physical models and analytical descriptions of various basic modes of thermionic converter operation for use in converter inovation and diagnosis, and in system analysis.

A phenomenological approach is taken, as distinguished from a purely empirical or a classical analytical approach. The phenomenological description is a composite of elementary physical models, each of which is consistent with the experimental converter output data in a particular region of operation. The total description therefore is inherently simple and tractable since it includes only the dominant elementary processes in each region, and is inherently consistent with experimental converter data within the defined limits of that region.

The phenomenological description differs from a purely empirical (curve-fitting) description in that each adjustable parameter represents a physical quantity which can be independently measured or estimated from more basic data. It differs from the classic analytical approach, which proceeds rigorously from general equations, in that the phenomenological parameters represent "effective" or average values which absorb the second order effects that a more general treatment would include.

The phenomenological description therefore is not a substitute for either experimental data or for more detailed analysis. It is most useful as a bridge between them. Comparison with experimental data defines the regions over which each physical process is dominant. Comparison with more detailed analytical results is a sensitive test of the basic assumptions used in the detailed analysis, and immediately associates these complex results with more tractable equations and intuitive concepts for direct practical use. It is essential to recognize that the phenomenological description is valid only to the degree of approximation and only within the region for which it was originally defined. However, it is often instructive to inspect the results outside these limits in order to identify the existence and nature of features in the experimental data arising from significant processes not included in the elementary physical model.

In recent months a previously-formulated phenomenological description of elementary cesium diode operation has been explored using a programmable desk-top calculator-plotter. This formulation appears to be useful for defining the fundamental limitations of this mode of operation and for suggesting potential methods of enhancing elementary cesium diode converter performance. Only a brief outline of the formulation and results is given here. A complete description, including recent improvements in the calculator program and an extensive set of parametric results, will be issued in the near future as a separate Topical Report.

Future work will modify and extend this approach to include advanced types of converter operation. In particular, the calculator program will be generalized to include auxiliary ion sources by incorporating the results described in our previous reports NSR-1-3 and NSR-1-4.

Elementary Cesium Diode Converter Characterization

The elementary ignited diode formulation derived in NSR-1-1 has been incorporated into the program shown in Figure II-1 for the Hewlett-Packard 9820A desktop calculator. This program can be entered directly through the 9820A keyboard, or a magnetic program card will be supplied on request. The various sections of the program are labled to show the physical quantities which are calculated vs output voltage V:

ϕ_E, ϕ_C = emitter and collector work functions, respectively
J'_s = emitter saturation emission current density at zero electric field
pd = product of cesium pressure p and spacing d
T_{eE} = electron temperature at emitter side of plasma
V_c = collector sheath height
J' = output current density at transition point
V'_d = arc maintenance potential drop
V_p = plasma potential drop
V' = output voltage at transition point
ϕ_{ca} = apparent collector work function (virtual collector)
J_s = emitter saturation emission current density in sheath electric field (Schottky effect)
J = output current density in obstructed (virtual emitter) and saturation (Schottky) regions.

The output characteristics for a particular diode are fully characterized by the following input conditions:

T_E, T_C, T_R = emitter, collector, and cesium reservoir temperatures, respectively (in ^oK)

d = interelectrode spacing ("D", in mils)

O_o = effective vacuum work function of emitter ("PHI", in ev).

Constants which characterize the fundamental plasma properties for all input conditions are:

V_I = effective ionization potential (in ev)

B = ion conservation factor (in $(torr\text{-}mil)^{-1}$)

D_o = electron scattering factor (in $(torr\text{-}mil)^{-1}$).

Figure II-2 shows a calculated cesium reservoir temperature family, and Figure II-3 shows corresponding experimental data (D. Lieb and F. Rufeh, AEC Report TEE 4125-5). If a zero is entered for any of the input quantities, the program plots a family with that quantity as the family parameter. Each curve is labled with the corresponding value of the parameter and with the points at which a virtual collector ("A") and a virtual emitter ("B") appear with decreasing current. Running time is about one minute per complete J-V curve.

Programming the formulation and exploration of its results are still incomplete. However, preliminary comparison of the calculated families with experimental data over a wide range of input quantities already has provided new insight into the dominant physical processes. For example, it was found that a virtual collector probably exists in most of the data which was used in the past to compute arc drops for comparison with plasma theory; i.e., the arc drop inferred from the experimental data included both the true arc drop and the space charge barrier arising from collector emission. This required a variable effective ionization potential V_I to characterize the data (see Section III in NSR-1-2 or Section IX in NSR-1-4). With the effect of the virtual collector included, a single value of V_I (about 2.5 ev, the ionization energy of the first excited state of cesium) is now found to adequately characterize the data. Similarly the constant values of B and D_o found to characterize the data are consistent with estimates computed from fundamental atomic properties of cesium. This greatly simplifies the

analytical description and gives clearer insight into the dominant ion-production process.

Comparison of Figures II-2 and II-3 shows that the present calculator program becomes inaccurate at high current densities (>10 amp/cm^2) and high pressure-spacing products (pd >60 torr-mil). Electron-ion scattering and LTE, which become significant under these conditions, are not included in the present calculator program.

The original phenomenlogical description and related analysis are given in Section III of NSR-1-1. An updated description and its incorporation into the calculator program will be issued in the near future as a Topical Report. Elementary analytical representations of additional physical processes (e.g., the unignited mode and LTE) which have been formulated but are not included in the present calculator program, will be included in the updated program.

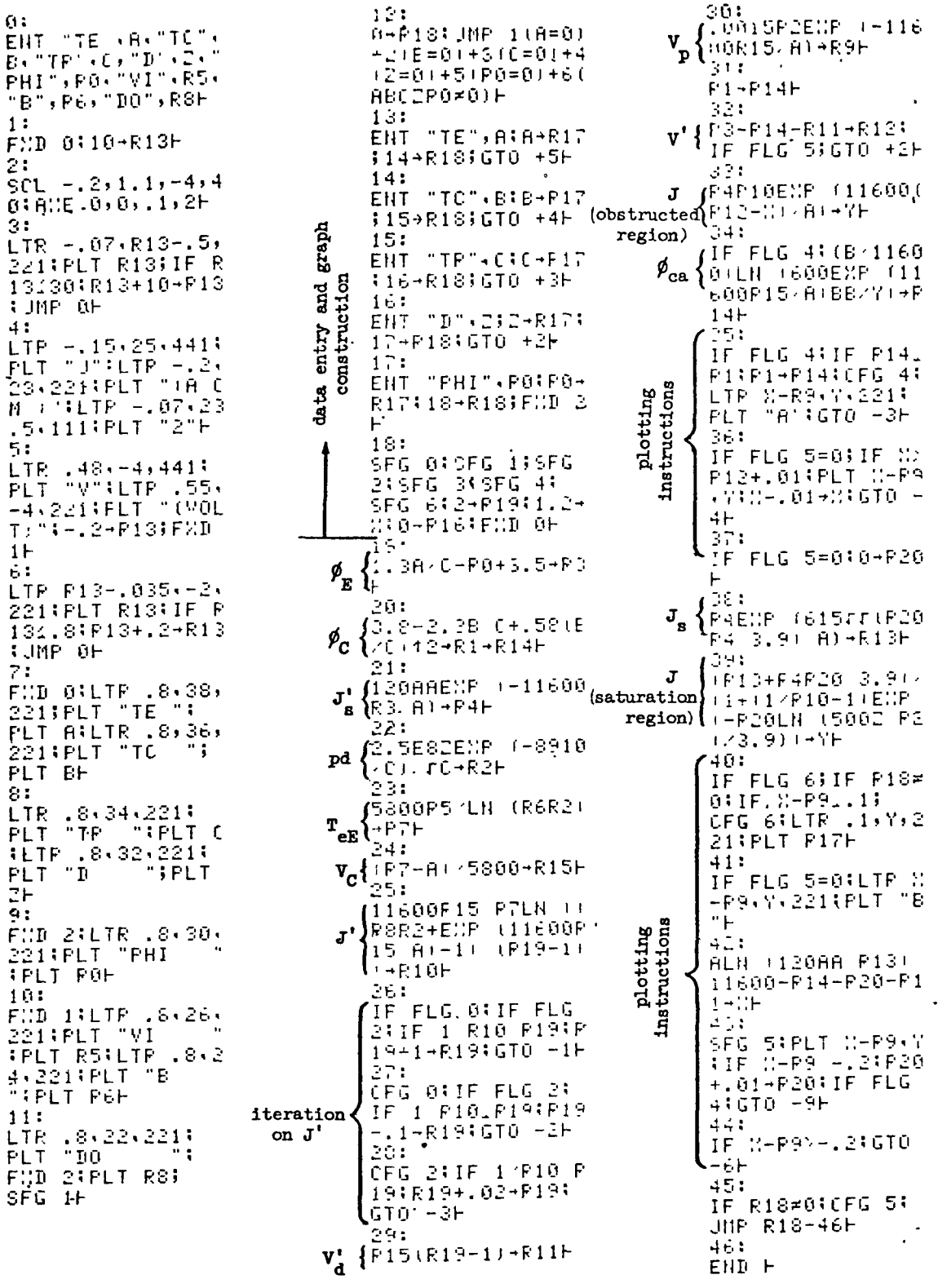

Figure II-1 Program for Ignited Cesium Diode Output Characteristics (HP 9820 Calculator with 11221A Math ROM)

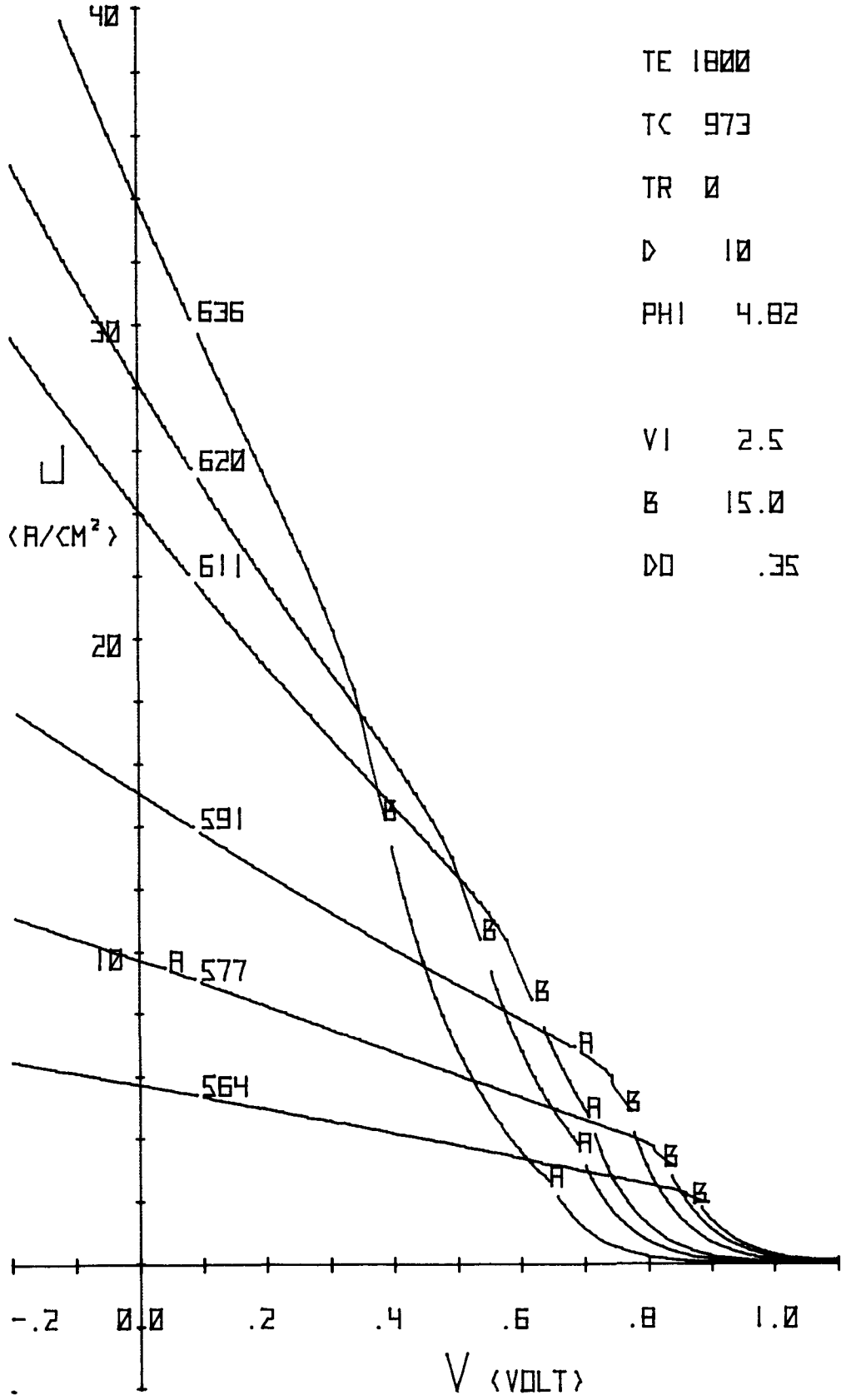

Figure II-2 Calculated Cesium Temperature Family

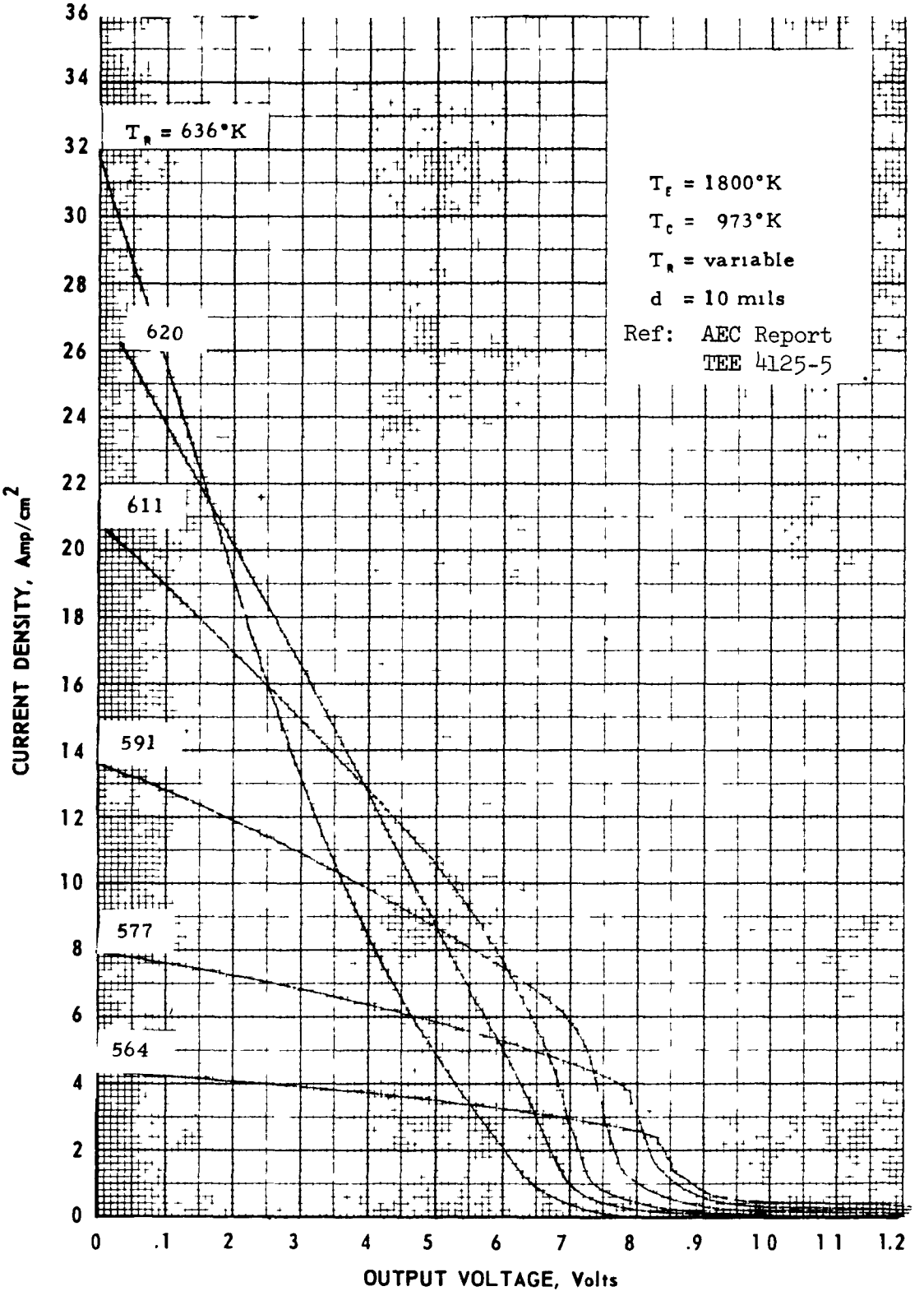

Figure II-3 Experimental Cesium Temperature Family

III ADVANCED CONVERTER RESEARCH

The purpose of the work reported in this section is to provide basic understanding for advanced converter modes which are being developed. Advanced converter configurations are conceived, analyzed, and explored experimentally in order to provide input data for the Basic Characterization and Converter Development Tasks.

Work in the past year has concentrated on demonstrating the existence of advanced operating modes and on studying the characteristics of these modes. Demountable cesium vapor systems were used which permit convenient and rapid test iterations. Three demountable converters were tested, and enhanced performance was achieved in the unignited triode, pulsed triode, and ignited triode operating modes.

A basic analysis of the general limitations of thermionic performance was initiated to provide more insight on the most effective ways to improve performance. It is pointed out that the reason for performance limiting voltage drops in the diode is primarily the loss of hot electrons from the plasma to the electrodes. This encourages the expectation of significant performance improvement in advanced mode converters, where the losses due to hot electrons can be minimized.

The basic converter considerations and demountable converter tests are described in more detail below, as is the effort presently being undertaken on the analysis of surface physics phenomenon.

A. Converter Enhancement

Introduction

Significant progress has been made in the past several years towards understanding the operation of the cesium vapor thermionic diode. Specific phenomena of the thermionic converter have been studied extensively and there has been moderate success in calculating the overall performance of the thermionic diode. These calculations make specific assumptions that relate to present unignited and ignited diode operation. The national thermionic program now includes the developement of advanced mode converters, either in diode, triode,

or hybrid configuration. Many of the same basic processes probably will be important to these new advanced modes, and the performance of these advanced modes will eventually yield ot calculation. At the present stage of understanding it seems most appropriate to begin with the basic processes that must occur in these advanced modes and to examine what limitations or opportunities these introduce to the converter. It is the purpose of the present section to begin a discussion from this point of view. The observations are applicable to the elementary cesium diode in that the discussion better defines its limitations. The observations are directed especially toward exploring possibilities for enhanced performance with the elementary diode. However, the results are also relevant for attempts to produce improved operation by employing more complex converter configurations.

Analysis

One of the most fundamental restrictions upon converter operation is that it satisfy energy balance. For a diode with positive plasma sheaths and no electron space charge barriers at the electrodes this means that the diode satisfies the following equation:[1]

$$\nu_e\, 2k\left[T_E - T_e(0)\right] + \Gamma_e(1)\left[eV_d + 2k\left(T_e(0) - T_e(1)\right)\right]$$
$$-\left[\Gamma_p(1) + \Gamma_p(0)\right]\left[eV_E + eV_i + 2k\, T_e(0)\right] - \Gamma_p(1)\, V(1) - E_r = 0$$

where ν_e is the Richardson electron flux from the emitter, k the Boltzmann constant, T_E the emitter temperature, $T_e(0)$ and $T_e(1)$ the electron temperature at the emitter and collector respectively, $\Gamma_e(1)$ the net electron flux to the collector, V_d the potential drop in the diode, $\Gamma_p(0)$ and $\Gamma_p(1)$ the ion fluxes at the emitter and collector respectively, V_E the emitter sheath drop, V_i the ionization potential of cesium, and E_r the radiation loss from the diode. This equation neglects energy exchange between the electrons and the heavy particles. It also neglects energy loss from the plasma by the diffusion of excited species. The heavy particles near the electrode are assumed to be at the same temperature as the electrodes. Some of these parameters are included in the potential diagram in Figure III-1.

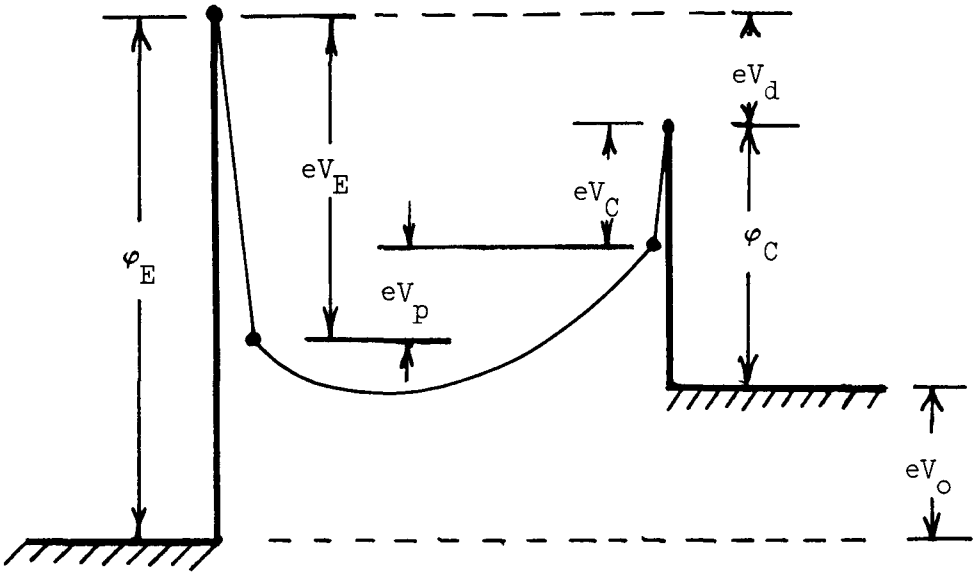

Figure III-1 Converter Potential Diagram

The energy balance equation is useful in identifying significant contributions to the voltage drop, V_d in a diode. For this purpose it can be written in the form

$$eV_d = \frac{\nu_e}{\Gamma_e(1)} \cdot 2k\left[T_e(0) - T_E\right] + \left[\frac{\Gamma_p(1) + \Gamma_p(0)}{\Gamma_e(1)}\right]\left[eV_E + eV_i + 2kT_e(0)\right]$$

$$+ \frac{\Gamma_p(1)}{\Gamma_e(1)} V(1) - 2k\left[T_e(0) - T_e(1)\right] + \frac{E_r}{\Gamma_e(1)} \qquad (2)$$

The last term, E_r, the radiation loss from the diode can be estimated using the work of Norcross and Stone.[2] These authors calculated the radiation loss from a cesium plasma, giving their results for non-resonance radiation in the following form:

$$R_{\text{non-resonance}} = A\, n_e^2 + B\, n(1) \quad \frac{\text{watt}}{\text{cm}^3} \qquad (3)$$

where n_e is the plasma density, $n(1)$ the density of the ground state and A and B are tabulated coefficients[3] dependent upon the plasma density and electron temperature. $n(1)$ is also a function of n_e and T_e through the Saha equation so this result can be given intirely in terms of these variables. Some calculated results are given in Table 1. The corresponding pressure also is given for these results. This value of pressure is only a crude estimate; to avoid bringing in the gas temperature complete equilibrium is assumed. (This approximation for the pressure is not involved in the radiation result.) From these results it can be seen that for moderate diode pressures (<3 torr), and for plasma densities and electron temperatures that are usually encountered in thermionic converters, the radiation loss should be at worst the order of 10 watt/cm^3, or less than 1 watt/cm^2 at typical diode converter spacings. In other words, for a diode carrying 10 amp/cm^2, this would require a voltage drop much less than 0.1 volt. Therefore, loss of non-resonance radiation should not be a major contribution to the cesium diode voltage drop.

TABLE 1

NON-RESONANCE RADIATION LOSS

	log n_e = 15		14		13	
T_e [^oK]	R [watt/cm^3]	P' [torr]	R [watt/cm^3]	P' [torr]	R [watt/cm^3]	P' [torr]
2000	434	6400	5.33	88.2	.17	4.24
2200	154	800	1.84	10.8	.053	5.0×10^{-1}
2400	66.9	139	.78	1.90	.02	8.6×10^{-2}
2600	33.9	31.6	.38	.47	8.8×10^{-3}	2.3×10^{-2}
2800	19.3	9.16	.21	.17	4.5×10^{-3}	1.05×10^{-2}
3000	12.1	3.41	.13	.099	2.5×10^{-3}	7.7×10^{-3}
3200	8.16	1.70	.088	7.97×10^{-2}	1.5×10^{-3}	7.2×10^{-3}
3400	5.81	1.14	.063	7.6×10^{-2}	1.0×10^{-3}	7.3×10^{-3}
3600	4.32	.94	.046	7.7×10^{-2}	7.2×10^{-4}	7.6×10^{-3}
3800	3.32	.88	.036	8.0×10^{-2}	5.4×10^{-4}	7.9×10^{-3}
4000	2.63	.88	.028	8.35×10^{-2}	4.2×10^{-4}	8.3×10^{-3}

Resonance radiation loss from a cesium diode also has been calculated by Norcross and Stone. For a planar diode this result is given approximately by

$$R_{resonance} = 1.7 \times 10^{-14} \; N_2 \frac{\epsilon}{\sqrt{d}} \quad \frac{watt}{cm^3} \tag{4}$$

where N_2 is the 6P population density, ϵ the emissivity of the electrodes and d the converter spacing. N_2 is proportional to gas density, therefore the result is proportional to the gas pressure and inversely proportional to gas temperature.

$$R_{resonance} \sim \frac{P}{T_g} \frac{\epsilon}{\sqrt{d}} \tag{5}$$

The results as a function of pressure and electron temperature are plotted in Figure III-2 for a nominal reference case. From this figure it is evident that for typical converters (p = 1-2 torr, T_e = 3200 - 3600°K) again the loss is the order of 10 watts/cm^3. Therefore, this loss also is not a major effect in present optimized diodes, involving the order of 0.1 volt drop in output at 10 amp/cm^2. As spacing is decreased (with other parameters constant) this loss per cm^2 diminishes as the square root of spacing. However, in practice, an increased ion production probability is needed as spacing decreased, so the electron temperature must increase to maintain the plasma. Therefore, the ion production rate per unit volume must increase inversely with spacing as will also the resonance excitation since these are tied together. The net effect is that for small spacings the voltage drop due to the resonance radiation escape increases with reduced spacing. Therefore, any modification of the converter, e.g., through addition of new atomic species or treatment of the electrodes, that reduces this radiation loss, will improve the performance of the elementary ignited diode.

The third term from the last in equation 2 is negligible compared to the preceding term since V(1) for any significant device must of necessity be negligible compared to $\left[eV_E + eV_i + 2k\,T_e(0)\right]$. The second term in equation 2 is an important one for consideration. It is a measure of the energy required to produce the ions for space charge neutralization in the ignited converter. This term will now be examined to identify some of its fundamental limitations.

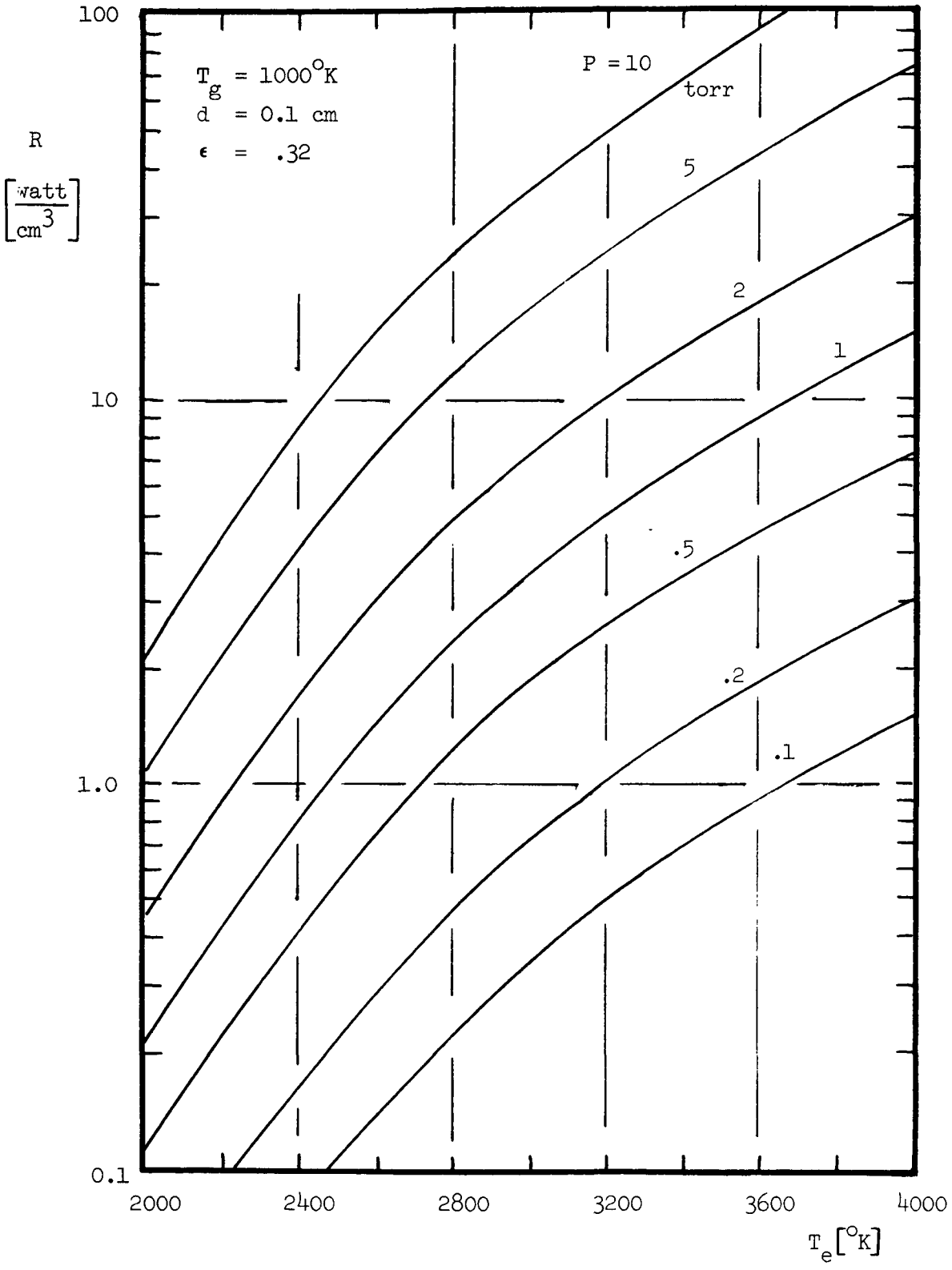

Figure III-2 Resonance Radiation Loss

If the ion currents from the plasma to the electrodes diminished, a space charge imbalance first appears as a negative space charge barrier at the electrodes. These barriers limit the electron flow from the emitter and increase the effective work function at the collector. Both these effects diminish converter performance. The onset of a space charge barrier at the emitter can be calculated using the condition for zero sheath field at the emitter:[4]

$$2\Gamma_p\left(\frac{MV_E}{2e}\right)^{\frac{1}{2}} - \frac{kT_e}{e}\, n\left[1 - \exp\left(-\frac{eV_E}{kT_E}\right)\right] - 2\nu_e\left(\frac{mV_E}{2e}\right)^{\frac{1}{2}} = 0 \qquad (6)$$

where n is the plasma density and, M and m the ion and electron masses respectively. To eliminate the plasma density in this equation the ion flux boundary condition for the plasma-sheath interface can be used.

$$\Gamma_p(0) = \frac{n(0)}{2}\, v_p(0) \qquad (7)$$

where v_p is the mean ion velocity. A result is obtained in the form

$$\frac{\nu_e}{\Gamma_p} = \sqrt{\frac{M}{m}}\ \Psi_{VE} \qquad (8)$$

where Ψ_{VE} is plotted in Figure III-3. (for $T_e/T_p = 1$) and in Figure III-4 (for $T_e/T_p = 2$) as the curves separating the regions of dashed curves. T_p is the ion temperature ($T_p \approx T_E$) and $\sqrt{\frac{M}{m}}$ is about 492 for cesium. A virtual emitter with reduced electron emission is expected above these plots of Ψ_{VE}. This means that ion currents in excess of 2-5 times $\nu_e\sqrt{\frac{m}{M}}$ are required at the emitter if its full emission capacity is to be utilized.

An additional constraint is imposed at the emitter by the interdependence of the ion and electron fluxes and the sheath height. This is found by combining equation 7 with the electron flux boundary condition for the plasma-sheath interface near the emitter, that is,

$$\Gamma_e = \nu_e - \left[\frac{n(0)\ v_e(0)}{4} - \frac{\Gamma_e(0)}{2}\right] \exp\left[-\frac{eV_E}{kT_e(0)}\right] \qquad (9)$$

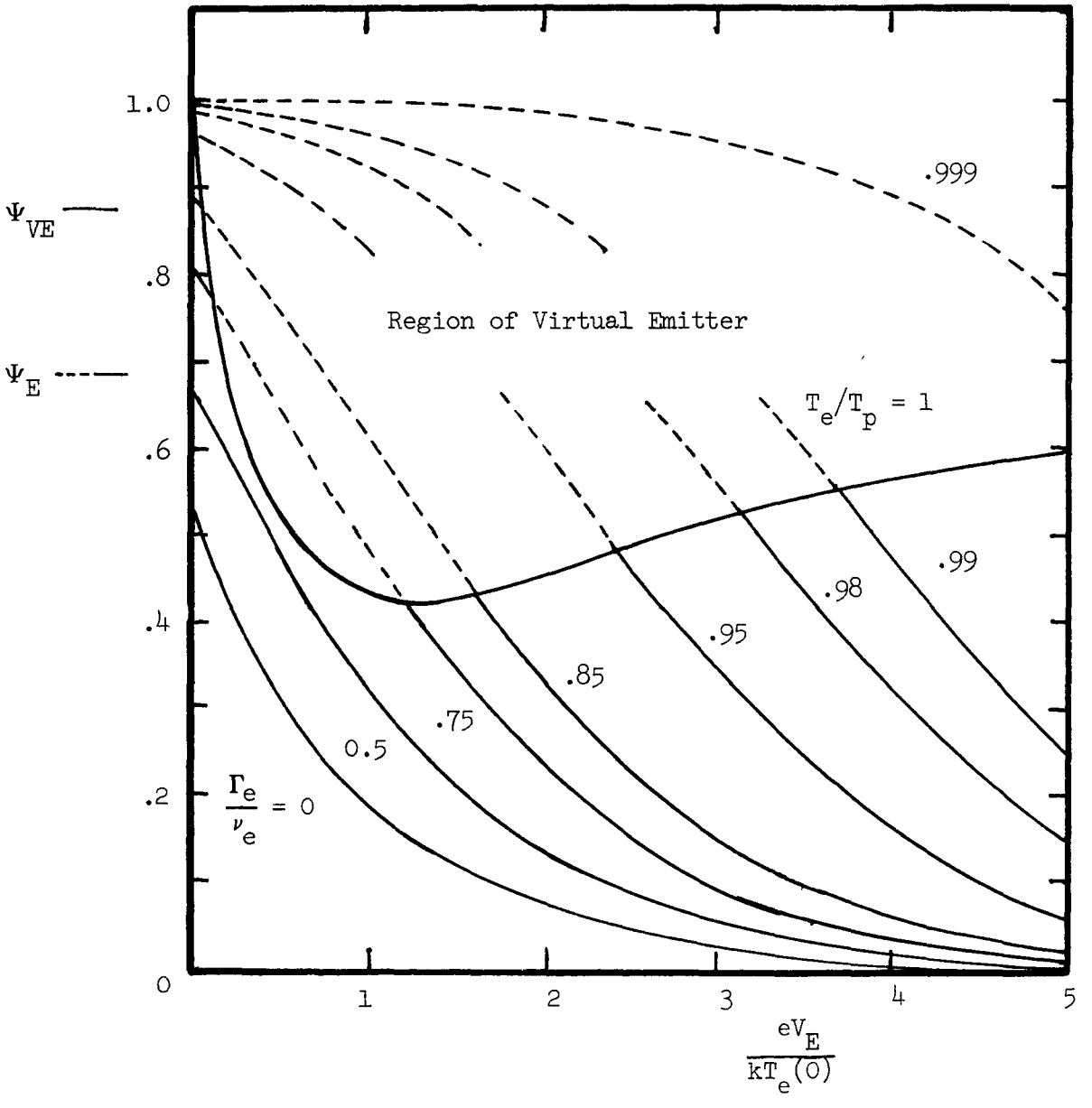

Figure III-3 Emitter Sheath Parameters of $(T_e/T_p = 1)$

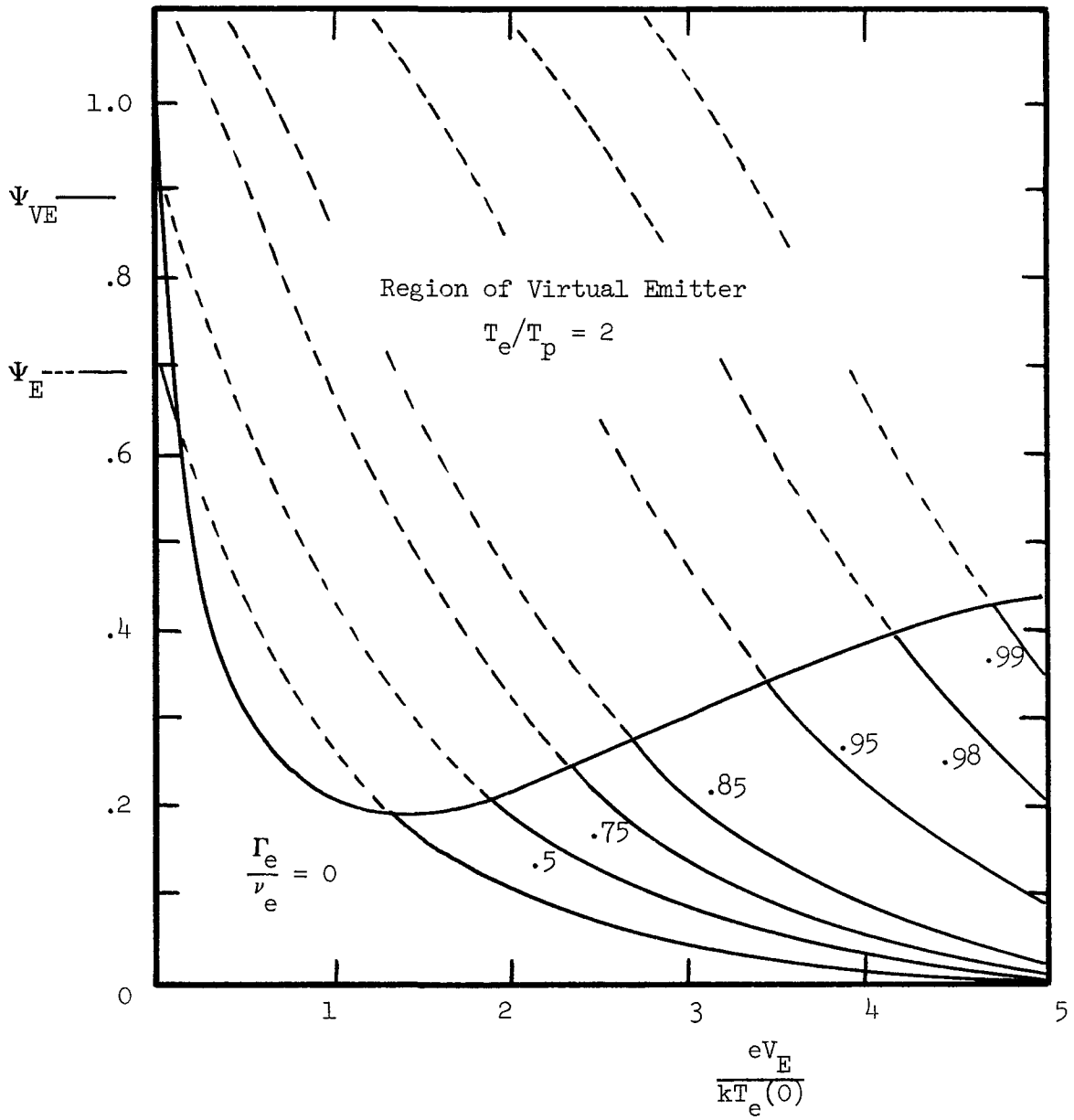

Figure III-4 Emitter Sheath Parameters for ($T_e/T_p = 2$)

The result can again be put in the form

$$\frac{\nu_e}{\Gamma_p} = \sqrt{\frac{M}{m}}\cdot\sqrt{\frac{T_e}{T_p}}\cdot\Psi_E \qquad (10)$$

where the factor Ψ_E is plotted as the family of curves in Figure III-3 for the case of $T_e/T_p = 1$ and in Figure III-4 for the case of $T_e/T_p = 2$. These two sets of curves show how diode current can be maintained with diminished sheath heights as the electron temperature of the device goes down. At present converter operating conditions ($T_e/T_p \approx 2$), a sheath height at the emitter the order of $2kT_e$, or about .5 - .6 ev., is required for Γ_e/ν_e the order of 0.5. This means that the contribution, of ion flow to the emitter, to the converter voltage drop should be

$$\frac{\Gamma_p(0)}{\nu_e}\cdot\frac{\nu_e}{\Gamma_e(1)}\left[eV_E + eV_i + 2kT_e(0)\right] \approx \frac{2(5)}{(.2)492\sqrt{2}} \approx .07 \text{ volts} \qquad (11)$$

This is only a small contribution to the voltage drop observed. Therefore, this fundamental requirement of converter operation is not the feature of the converter <u>directly</u> limiting its performance.

A similar contribution to voltage drop occurs due to ion flow to the collector. There the plasma is approximately in thermodynamic equilibrium. The ion flow to the collector for various electron temperatures and cesium pressure (using this equilibrium assumption) is shown in Figure III-5. The result shows, for observed electron temperatures at the collector ($T_e \approx T_E$) and typical cesium pressures ($p = 1$ torr) the ion currents are the order of 0.2 amp/cm^2. Thus, in a 10 amp/cm^2 device a contribution to the voltage drop of

$$\frac{\Gamma_p(1)}{\Gamma_e(1)}\left[eV_E + eV_i + 2kT_e(0)\right] \approx \frac{.02}{10}(5) = .01 \text{ volts} \qquad (12)$$

is estimated. Although this ion flux is a critical requirement for device operation, it also does not contribute significantly to the diode voltage drop, and therefore its <u>generation</u> does not impose a significant basic performance limitation.

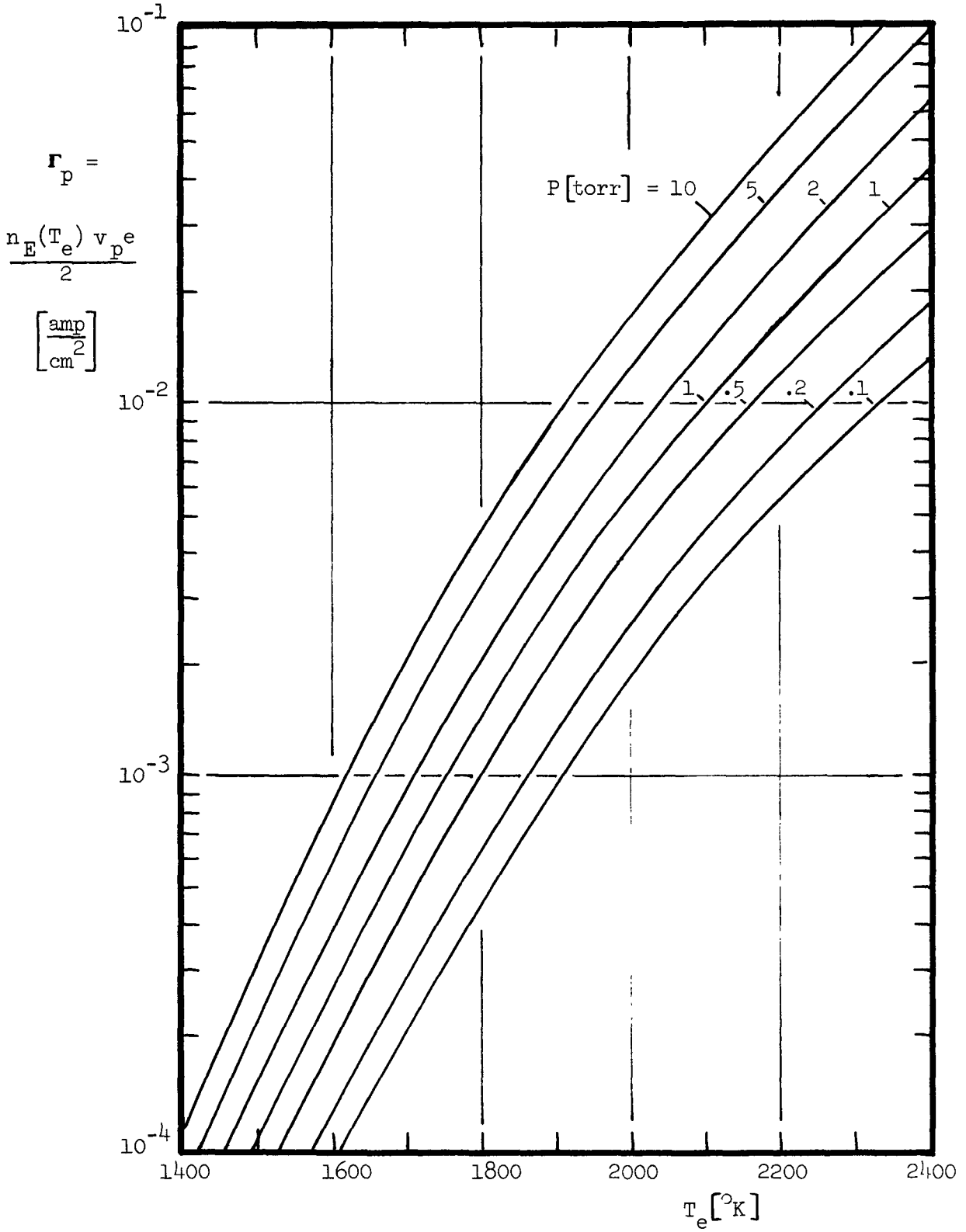

Figure III-5 Plasma Ion Current to Collector

The required magnitude of this can affect the converter performance in another way, however. If the zero field condition, equation 6, is applied to the collector and combined with equation 12, the conditions for the onset of a virtual collector are obtained in the form

$$\frac{\Gamma_e}{\Gamma_p} = \sqrt{\frac{M}{m}}\,\Psi_{VC} \tag{13}$$

which are plotted in Figure III-6 as the solid curves. General parameters of the collector sheath (independent of the existence of a virtual collector) can be obtained by combining the ion and electron boundary conditions at the collector:

$$\Gamma_p(1) = \frac{n(1)\, v_p(1)}{2} \tag{14}$$

$$\Gamma_e(1) = \left[\frac{n(1)\, v_e(1)}{4} + \frac{\Gamma_e(1)}{2}\right] \exp\left(-\frac{eV_c}{kT_e(1)}\right) - \nu_c \tag{15}$$

where $\Gamma_e(1)$ is the electron mean velocity near the collector, and ν_c the Richardson back emission from the collector. Equations 11 and 12 can be put into the form

$$\frac{\Gamma_e(1)}{\Gamma_p(1)} = \sqrt{\frac{M}{m}}\,\Psi_C \tag{16}$$

The factor Ψ_C also is plotted in Figure III-6, as the dashed curves. The position of these curves relative to the virtual collector onset curves suggests that a virtual collector exists under some practical operating conditions of the elementary, ignited-mode, cesium diode converter as back emission increases. The performance loss in such a case is not that the ion flux to the collector is a significant expenditure of energy, but that a virtual collector gives a direct reduction in converter output voltage by increasing the effective collector work function. Clarification of the practical significance of this potentially important result therefore deserves detailed attention in future work.

The major contributions to the voltage drop in the elementary ignited diode converter are the first and second-to-last terms in the energy balance equation, equation 2. The ration ν_e/Γ_e in an optimized diode is the order of 2, and

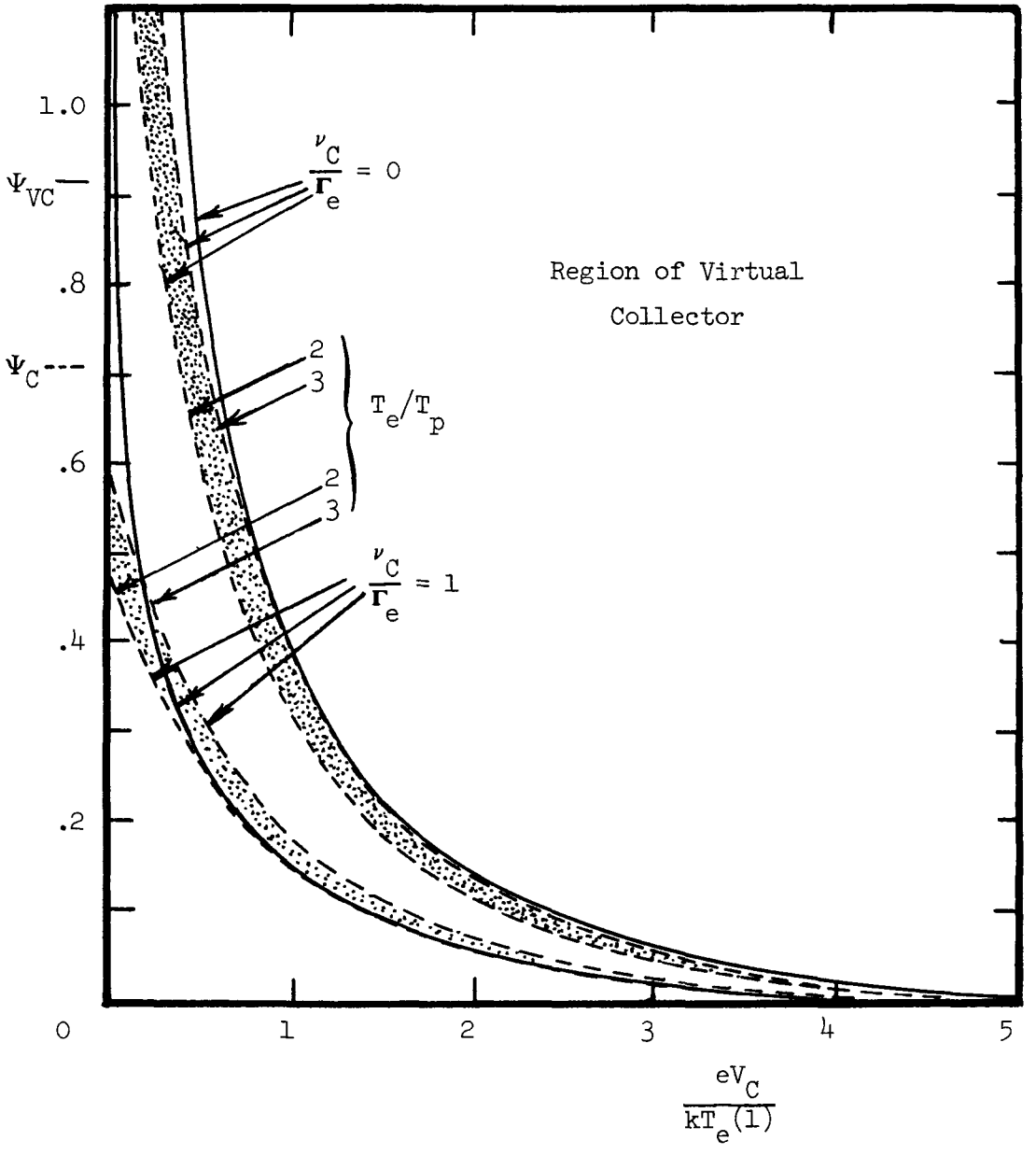

Figure III-6 Collector Sheath Parameters

$2k[T_e(0) - T_E]$ is the order of .6 volt. $2k[T_e(0) - T_e(1)]$ is also the order of .6 volt. Thus, the contribution of these two terms is the order of 0.6 volts. This means that the major voltage loss in a converter presently limiting its performance is not the energy required to produce the required ions, or necessarily the radiation loss that accompanies this ion production. Rather the most important loss is the loss of hot electrons out of the diode at the emitter and collector. If the required ionization could be produced at a lower electron temperature, there would be a corresponding improvement in this voltage loss.

Conclusion

General statements about energy balance, sheath boundary conditions and cesium plasma radiation have been used to point out some general limitations to thermionic converter performance. To summarize, it can be said:

1. In the present optimized, ignited, cesium diode, the main source of the performance-limiting voltage drop is the loss of hot electrons from the plasma to the electrodes.

2. These hot electrons are presently a necessary condition for production of the ion currents to the electrodes which in turn are needed for space charge neutralization, but the production of ions does not of itself constitute a significant energy loss in present diodes compared to the hot electron loss. Therefore, any increase in ionization efficiency would allow the reduction of electron temperature and therefore the improvement of diode performance.

3. In present optimized diodes, radiation loss does not contribute significantly to diode voltage drop. Yet, the extent to which a diminished radiation loss would allow a reoptimization leading to improved performance merits further study.

4. General considerations of the collector sheath imply the possible existence of a virtual collector in practical converters. This could be causing reduced converter voltage output by increasing the effective collector work function. This effect merits careful study.

5. The fact that hot electron loss is the major loss in present elementary diode converters leads one to expect significant performance improvement through the use of advanced mode converters. If the ions were produced by surface ionization, as in the unignited triode, or produced in restricted regions, as in the ignited triode and hybrid mode, this hot electron loss could be made small in comparison to other converter losses. This would lead to improved performance.

B. Demountable Converter Tests

Introduction

As shown in the Project Strategy (Figure 2), the purpose of this Task is the primary exploration of various advanced converter configurations and operating modes. Advanced electrode configurations and components are assembled "bread-board" fashion on a Varian ultra-high vacuum flange and are then tested in the cesium vapor chamber described in Section IV of NSR-2-1. Direct heating of the electrodes is typically but not exclusively used. The cesium chamber has a sapphire window which permits optical pyrometer temperature measurements and visual observation of the discharge. Such observations are very helpful for basic interpretation of the electrical and thermal characteristics of a particular converter concept, and assuring that no significant spurious discharges are occuring elsewhere in the assembly.

Three converter assemblies have been constructed which are designated DC-1, DC-2, and DC-3 in the order of their initiation. DC-1 and DC-3 have been operated in the cesium chamber. DC-2 has been completed but, because of its greater complexity, was preceded by DC-3 in the test program. In order to permit parallel evaluation of future assemblies, a second cesium chamber has been constructed and will be placed in operation within the next few months.

1. First Exploratory Triode (DC-1)

The primary purpose of DC-1 was to check out operation of the cesium chamber, the instrumentation and the diagnostic techniques to be used with succeeding converter assemblies. It was a simple triode assembly, consisting of a single

directly-heated tungsten ribbon used as the main emitter, a nickel collector, and five directly-heated parallel tantalum wires used as auxiliary emitters in the interelectrode gap, as shown in Figure III-7.

DC-1 was operated successfully in the ignited and unignited triode modes. Its output characteristics were in accord with previously-reported data on these modes. These data will not be described in detail here because they have been superceeded by the more extensive data acquired with DC-3, described below.

DC-1 eventually failed because a small leak apparently existed in the cesium reservoir assembly. This caused oxidation and failure of the tantalum auxiliary emitters. This leak was eliminated, and there has been no difficulty maintaining ultrahigh vacuum conditions in the cesium chamber after many hours of subsequent high temperature operation with cesium.

2. Hybrid Mode Triode (DC-2)

The hybrid mode triode is designed to simulate the experimental geometry in which the hybrid mode apparently occured in a cylindrical converter (see Section IV-A). A cross section of this device is shown in Figure III-8. An important feature of this geometry is that there are two emitters, electrically separated. The first emitter is the central electrode labeled "ionizer". It simulates the bottom of the cylindrical emitter in the previous tests. Ions can be generated with this electrode by operating an ignited auxiliary discharge between the ionizer and the collector. The second emitter, labeled "main emitter", will provide emission current for the main unignited discharge in the annular gap between it and the collector. The volt-ampere characteristic of this portion of the converter will be sensitive to ions produced by the auxiliary discharge.

The ionizer will be heated indirectly by electron bombardment. The main emitter will be heated by driving a discharge between the two emitters during half of the 60 cycle JV sweep. Data will be taken during the other half cycle when this discharge is not being driven. If this electrode heating technique works as anticipated, it will be valuable for further studies with multiple electrode systems.

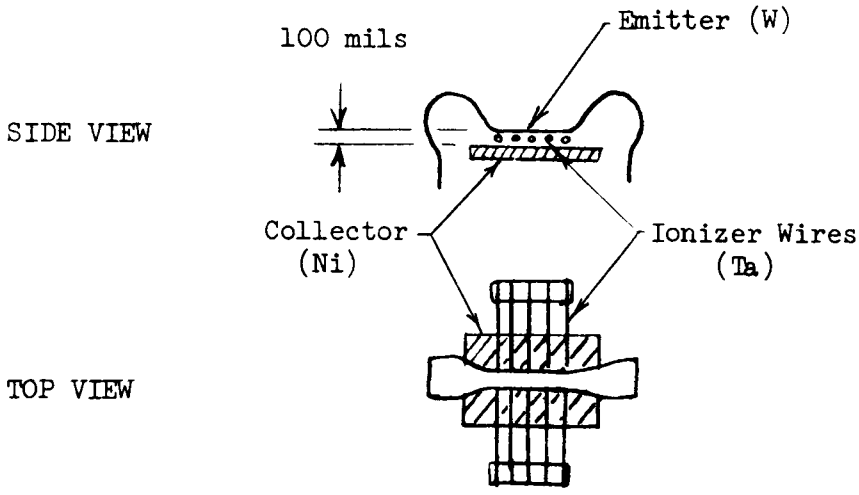

Figure III-7 Demountable Converter #1 (DC-1)
Electrode Configuration

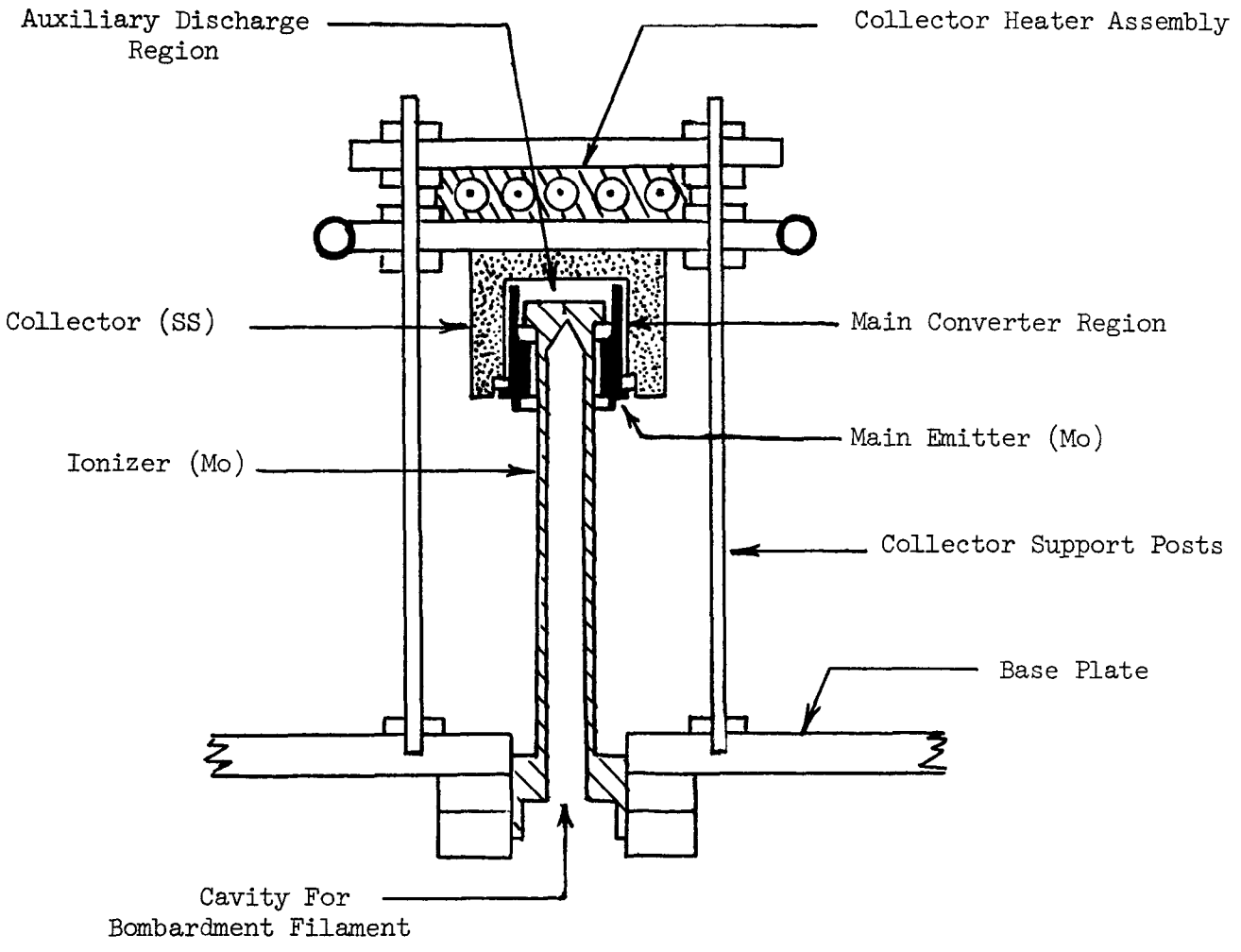

Figure III-8 Cross Section of the Hybrid Mode Triode DC-2

Previous experiments which led to the hybrid mode being postulated showed great sensitivity to the gap where ions leave the ionizer region. The interpretation presently given is that there is a delicate balance between generation and loss of ions, to allow the mode to exist by virtue of the contact potential difference between the emitters. The gap connecting the ionizer cavity with the space charge limited section of the converter is adjustable in the present device. However, the existence of a sensitive balance should not be a problem. Since the emitter is in two insulated sections, the strength of the auxiliary discharge can be varied at will, ensuring the existence of the auxiliary arc and permitting the optimum conditions to be defined.

The construction of hybrid mode triode (DC-2) is essentially complete. A test stand is presently being prepared for operating the device.

3. Second Exploratory Triode (DC-3)

DC-3 was constructed to overcome some of the inadequacies observed during operation of DC-1, and to obtain more detailed preliminary data needed for design of subsequent demountable converter assemblies and instrumentation. Figure III-9 shows the essential elements of the DC-3 assembly. Three parallel, coplanar, independently-heated 1-mil thick tungsten ribbon emitter pass centrally-spaced through a nickel collector block. The emitter-collector gap is about 45 mils throughout and the inter-emitter separation is about 30 mils. Two of the emitters are about 125 mils wide (about 0.80 cm^2 total area each within the collector) and one of the end emitters is about 100 mils wide (about 0.65 cm^2 total area within the collector).

The ribbons are tensioned individually by springs, and are stretched over high purity alumina thermocouple tubing about 100 mils after emerging from each end of the collector block. This tubing support technique serves two valuable purposes: First, it maintains the ribbons accurately coplanar and accurately spaced relative to the collector block over a wide range of temperatures. Second, it tends to flatten the temperature profile within the block, and to sharply define the high temperature region of the ribbon. The reason for this latter observed and desirable behavior is not known, but may arise from a temperature-dependent thermal conductance of the tungsten-alumina interface.

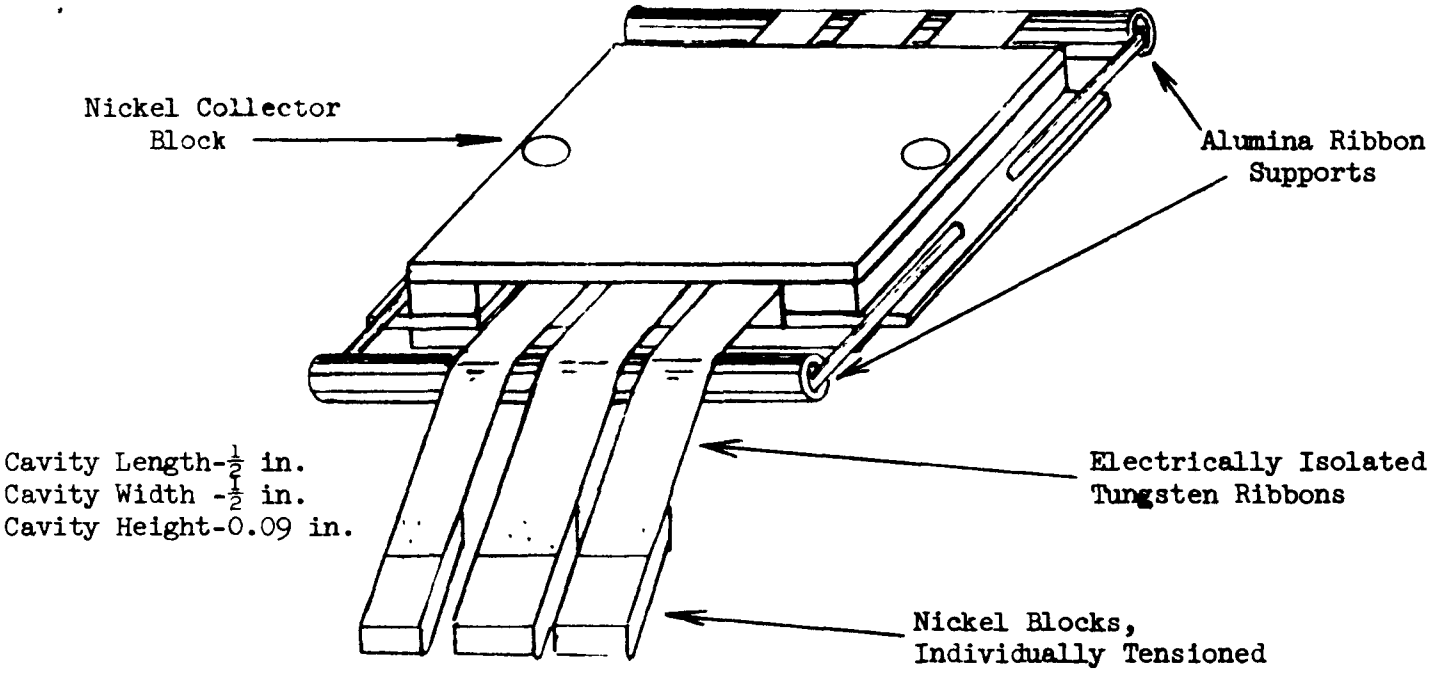

Figure III-9 Demountable Converter DC-3

This electrode structure has remained stable through over two hundred hours of operations and is otherwise completely satisfactory. The only significant addition which might have improved its basic usefulness would have been collector guard section at the ends of the collector. However, no effects were observed which could be attributed to end affects per se.

Various combinations of the three heated tungsten ribbons have been tried as main emitters and as auxiliary ion sources. It should be realized that the use of ordinary tungsten emitters in DC-3 permits operation in the advanced modes only at relatively low emission currents. Similarly, the open structure of this assembly may not allow the most efficient utilization of ions. The purpose of this device is to establish the basic plasma characateristics of various advanced modes of operation before less familiar advanced emitter materials and more complex structures are employed for operation in the practical output regime.

Unignited Triode Tests

Based on prior basic understanding of unignited triode operation,[5-7] the following operating point was estimated as beging near optimum for a cesium unignited triode with ordinary tungsten ion and electron emitters:

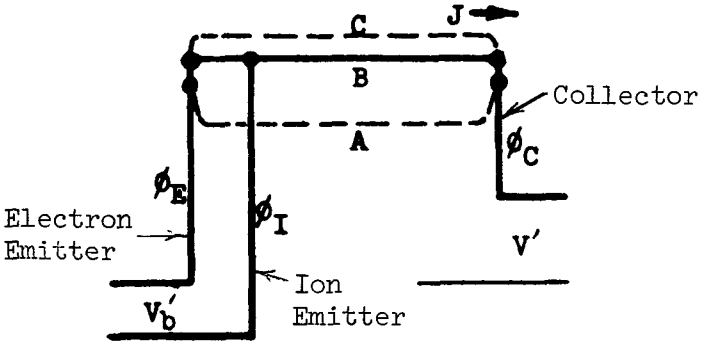

ϕ_E = 2.0 ev T_E = 1200°K

ϕ_I = 2.6 ev T_I = 1410°K

ϕ_C = 1.6 ev T_C = 760°K

V_b' = 0.6 v T_R = 470°K

V' = 0.4 v J = 0.3 amp/cm^3

Figure III-10 Motive diagram of Unignited Triode at Optimum Output Voltage.

where ϕ_E, ϕ_I, and ϕ_C are the work functions of the electron emitter, the ion emitter and the collector respectively, and T_E, T_I, and T_C are their respective temperatures; V' and V_b' are the zero field output and bias voltage respectively;

J is the output current density, and T_R is the cesium reservoir temperatures. Figure III-11 shows a current-voltage characteristic taken with the outer ribbons operating in parallel as electron emitters and the central ribbon operated as an ion emitter. Figure III-12 is a current-time characteristic under the same conditions. A one-microsecond wide pulse, sufficient to ignite the auxiliary discharge, was applied to the ion emitter every 0.5 millisecond for diagnostic purposes. The qualitative interpretation of the data is as follows:

- Immediately after the pulse, the discharge is strongly ion rich at condition A (envelope A in Figures III-11 and III-12 and curve A in Figure III-10). High emission currents typical of ignited mode operation are obtained due to the Schottky effect in the strong sheath electric field. Ions are rapidly lost from the plasma, which therefore decays to condition B within 10-20 microseconds.
- Zero electric field occurs at the emitter at condition B; ϕ_E is higher and emission current is much reduced without the Schottky effect.
- Between conditions B and C the plasma decays much slower (~200 microsecond time constant) due to formation of ion-containing sheaths.
- At condition C the rate of the ion loss equals the rate of ion supply from the ion emitter.

Figure III-13 shows how the (unpulsed) unignited triode output characteristic depends on the bias voltage V_b. It can be seen that increasing V_b increases the output current significantly for output voltage $V < V'$, but that it has relatively little effect near the optimum (zero field) condition at V' corresponding to the condition in Figure III-10. Furthermore, increasing V_b actually decreases the collector current for output voltage $V > V'$. This behavior is understandable when it is considered that increasing V_b increases the ion emission current via the ion Schottky effect. Furthermore, the ion emitter collects only a small fraction of the resulting increased electron current if its potential is below that of the collector, i.e., for $V < \phi_I - \phi_C - V_b$. However, when the ion emitter potential is above that of the collector (i.e., $V > \phi_I - \phi_C - V_b$), the ion emitter begins to collect most of the electron current and therefore significantly reduces the output (collector) current.

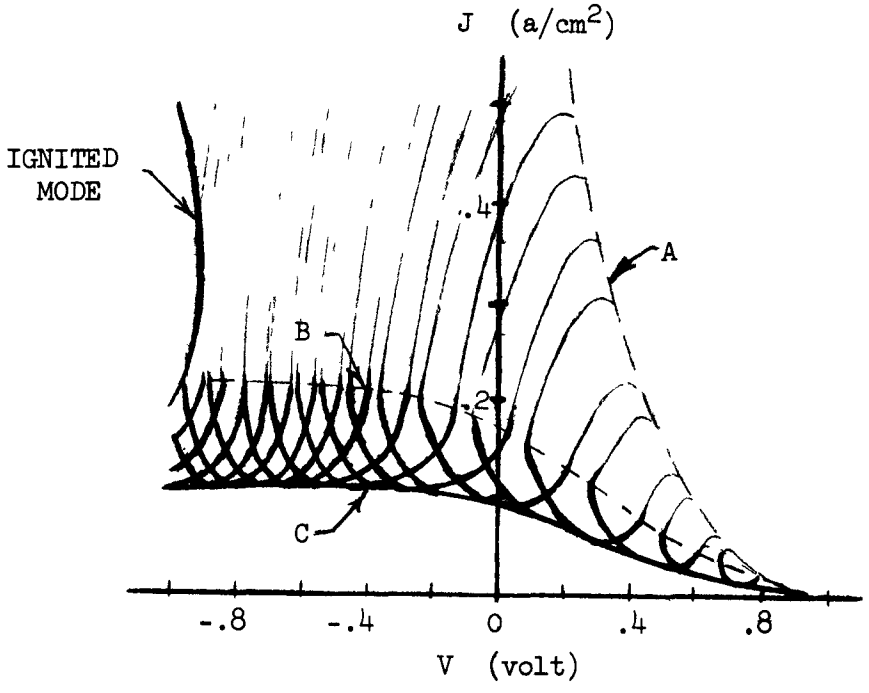

Figure III-11 J-V Characteristic for Pulsed Triode Near Optimum Condition for Unignited Triode Mode.

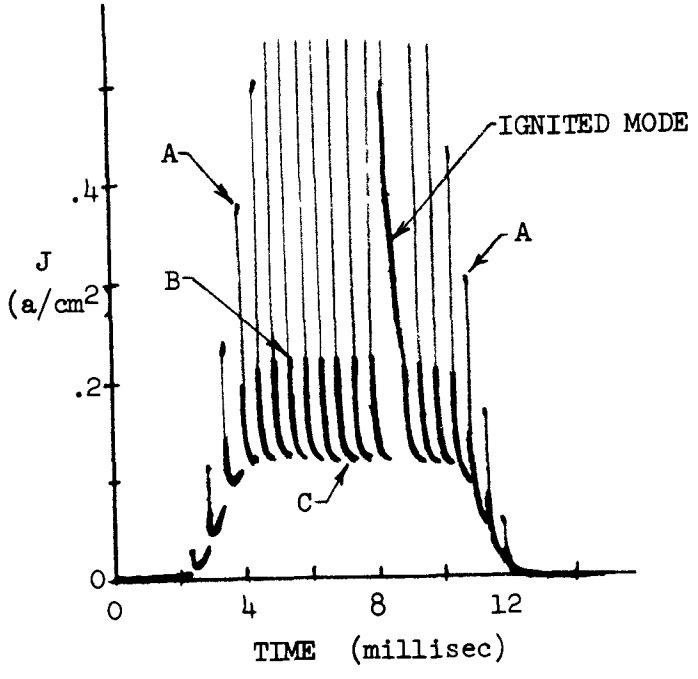

Figure III-12 Time-base Sweep Corresponding to Preceeding Figure.

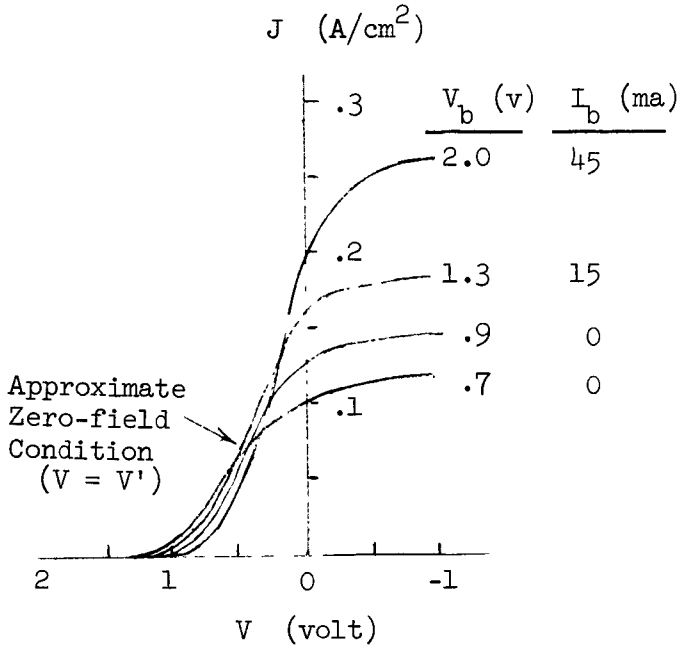

Figure III-13 Dependence of Unignited Triode Output Characteristics on Bias Voltage V_b near Optimum Condition.

I_b is Bias Current.

It can be seen that the bias current is essentially zero near the bias voltage for maximum power output and increases rapidly for $V_b > V_b'$. Since this bias current represents a severe parasitic energy loss in the system, it is clear that the optimum practical value for V_b is near V_b' and therefore near zero bias current. This is of considerable practical significance since it suggests that an isolated ion emitter will "float" in the plasma at the optimum potential, i.e., the ion emitter must be electrically insulated from the emitter but it is not necessary to connect it to any point in the circuit. It is puzzling that this fact was not reported by Hernqvist in view of its apparent practical significance. The optimum operating point observed and inferred experimentally was approximately:

	Condition	J (a/cm^2)
$T_E = 1200^oK$		
$T_I = 1500^oK$	A	0.30
$T_C = 765^oK$	B	0.08
$T_R = 465^oK$	C	0.04
$V_b' = 0.8$ v		
$V' = 0.4$ v		

It may be seen that, except for a slightly higher optimum ionizer temperature and much lower output current, the observed values are near those expected from basic understanding.

One of the end emitters was operated as the ion emitter with the center emitter and the opposite end emitter connected in parallel as electron emitters. The output current characteristics of the electron emitter adjacent to the ionizer were found to be essentially identical to those in the arrangment discussed above. However, the output current of the other (far) emitter was found to be about 1/3 that of the adjacent emitter, indicating that the electron current is ion-transport limited. The conclusion is that much higher currents can be expected in a configuration which minimizes ion transport distance and has sufficiently low cesium pressure to minimize the ion density gradient.

Strong RF oscillations occurred when the temperature of the far emitter exceeded that giving maximum output current. The oscillations were coherent with a period of about 4 microseconds. This is approximately equal to the ion transit time from the ionizer to the far emitter.

In summary, the following significant observations and conclusions relative to the unignited triode have been drawn from the results thus far:

- Except for the low output currents obtained, the results agree substantially with those expected from basic theory of the unignited triode and with those of Hernqvist.[5]
- An outstanding difference from Hernqvist's results is that initial pulsing was not required in the present device to initiate the unignited triode mode (i.e., to destroy Hernqvist's "Z-state").
- Another important new result is that optimum bias voltage for the ion emitter V_b occurred at the floating potential, i.e., at zero bias current and therefore at zero auxiliary power input.
- The unexpectedly low output currents and higher required ion emitter temperature probably result, at least in part, from the fact that available cesiated tungsten work function data were obtained in the presence of a strong ion-rich emitter sheath (as in condition A), and an electron-rich sheath (as in condition C) probably is required to confine the ions while they are transported efficiently to the main discharge in this configuration. Highly non-uniform (patchy) electrode surface could also contribute to these effects.

Pulsed Triode Tests

Figures III-14a and III-14b are completely analogous to Figure III-11 and III-12 respectively, except that the central emitter is being operated at much lower temperature (below visible incandescense), and the pulse period is about 120 microseconds instead of 500 microseconds. It can be seen that it is possible to maintain the discharge continuously above condition B by virtue of the ions which persist after the 1 microsecond pulses. This behavior is analogous to pulsed diode operation, which is well-understood from our previous work (see Ref. 3, NSR-1-3, and NSR-1-4). Figure III-15, which is the same as Figure III-14 but with an extended time base, shows the current decay waveform after a pulse.

Of particular importance is that the high-current ion-rich plasma (condition A) persists for more than 10 microseconds. Therefore, it is possible to hold the output in this condition continuously if a pulse if applied every 10 microseconds.

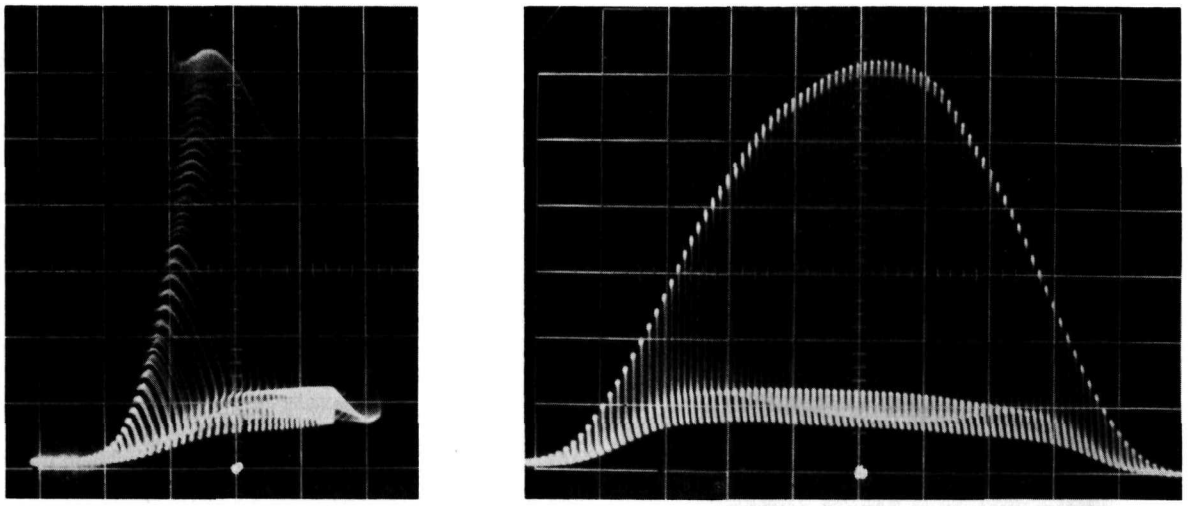

(a) (b)

Figure III-14 Output Characteristics of DC-3 as Pulsed Triode (center emitter pulsed positive at low temperature).

(a) JV Characteristic (.05 a/cm^2 per div. and .5 v per div.)

(b) Current v/s time (same current scale and 1 msec. per div.)

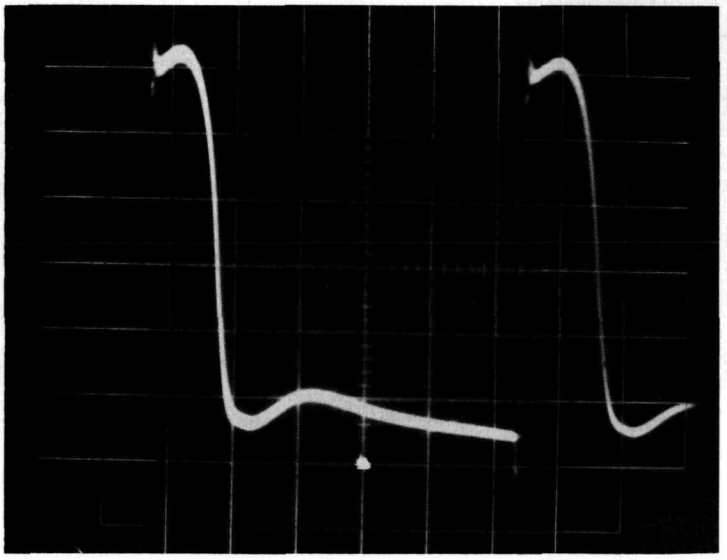

Figure III-15 Same as Figure III-14b with 20 sec. per division.

Because of the non-ideal configuration of DC-3 and difficulty in efficiently coupling and measuring the input pulse, it is difficult to evaluate the input power to the pulsed third electrode. However, pulse measurements under these conditions indicate that the total pulse power input to maintain the main discharge in the high-current, ion rich condition is no more than the total output under that condition. In an improved configuration, it is expected that the pulse input power might be made negligibly small for the pulsed triode. It is concluded, therefore, that the pulsed triode concept may have considerable practical potential and should be explored further. The present results show that ions from a pulsed third electrode can be effectively utilized to suppress the arc drop. The pulsed triode could be superior to the pulsed diode because:

a) the pulse circuitry is inherently isolated from the main load

b) it should be possible to pulse small-area auxiliary electrodes much more efficiently than the large main electrodes (less capacitance and eddy current effects)

c) the pulse (auxiliary electrode) current density can be independently optimized

d) the main electrodes need not withstand the ion bombardment associated with the high pulse voltage.

Ignited Triode Tests (DC-3)

Another mode of DC-3 operation studied used an outside ribbon as the main emitter and each of the other two ribbons successively as the auxiliary emitter for ignited triode operation.[7] As expected, the ribbon immediately adjacent to the main emitter is much more effective as an auxiliary emitter than the farther ribbon. Other operating arrangements used the center ribbon as the auxiliary emitter with the outer two as main emitters and vice versa. The results were similar to the single ribbon arrangement except that it was possible to get farther into the power quadrant. A further observation is that the auxiliary discharge power required for enhanced performance using the center ribbon as the auxiliary emitter is independent of whether one or both outside ribbons are used as main emitters. This indicates that only a small fraction of the ions produced in the auxiliary discharge reach the main discharge.

Figure III-16 shows a family of I-V curves taken with both outside ribbons operating in parallel as main emitters and the central ribbon as the auxiliary emitter at the same temperature. As expected, the optimum cesium temperature for a 1300°K emitter temperature is seen to be 475°K, which corresponds to a cesium pressure giving an electron mean free path about equal to the inter-electrode spacing. The enhanced output at the optimum is slightly less than second generation performance at this temperature (i.e., $\phi_C' = 1.5$ ev).

Although Figure III-16 shows nearly complete suppression of converter arc drop through use of an auxiliary discharge, these data are not in a practical operating region since the auxiliary discharge current is comparable to the main discharge current. This large auxiliary current is thought to occur because the auxiliary discharge is not isolated from the main discharge in this device, i.e., as occurred in the end region of the previously reported hybrid mode diode. In future ignited triodes, various structures will be interposed successively between the two discharges to establish the configurational parameters for minimizing the auxiliary current requirements.

C. Surface Physics

This Task has two aspects. One is to provide satisfactory electrodes for operating the test devices of the Advanced Converter Research and Converter Developement Tasks. The other aspect is to develop the basic characterization of electrode surfaces which have potential for use in advanced converters.

In general, advanced converter operating modes require emitters which give adequate electron emission at cesium pressures corresponding to an electron mean free path about equal to the electrode spacing. The conditions under which known emitter sufaces can satisfy this requirement were outlined in Section VII of the preceeding annual report (NSR-2-1). During this past year this requirement was fulfilled in the demountable converters by operating them in a low-current, low-temperature regime which was adequate for exploration of the plasma processes, and for which ordinary tungsten is an adequate emitter in cesium vapor. Platinum emitters satisfactorily fulfilled the requirements of the fixed configuration converters operating in the practical output current regime. While platinum may not be satisfactory for practical applications because of its high cost, it has been a convenient and stable high-performance ($\phi_o \sim 5.5$ ev) emitter during the transition from research into more applied technology.

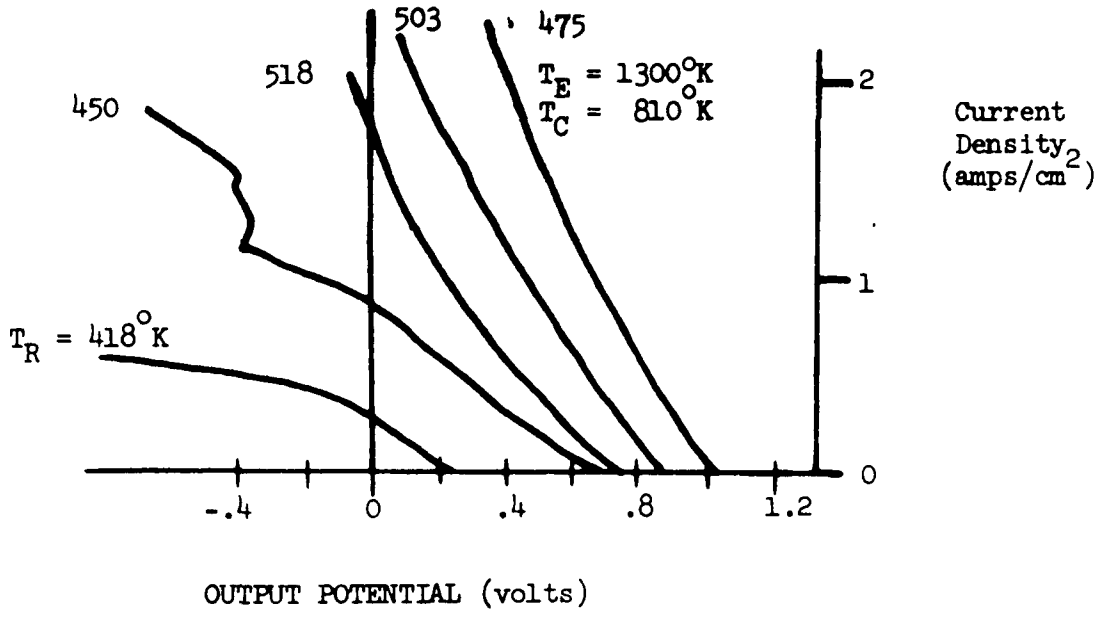

Figure III-16 Cesium family of volt ampere curves for DC-3 operating in the ignited triode mode.

It is expected that future work will progressively utilize alternate emitters with similar performance but lower potential cost (e.g., oxidized tungsten). It is not a primary purpose of this Task, however, to conduct extensive experimentation on or development of these surfaces. It is intended primarily to utilize the substantial data and technology developed by other groups active in this area. In particular, Thermo Electron has made substantial progress toward reducing the cesium-oxygen-tungsten emitter to engineering practice using an oxygen-dispensing collector approach. In addition to their data and technology, which is developed intensively within the region of practical importance, the French group at Saclay has obtained extensive emission data for Cs-O-W and Sr-O-W emitters over a wide range of temperatures and partial pressures. To date, however, there is not a comprehensive basic analytical characterization of these highly complex coabsortion sytems, which limits our understanding of them and therefore inhibits their confident and general use. An anologous situation exists for collector technology.

The second aspect of this Task is to develop the basic characterization of such surfaces. A physical model and analytical formalism for the Cs-O-W emitter has been developed, as outlined in Section VII of NSR-2-1. It was intended this year to incorporate this formalism in computer program for direct comparison with the available extensive data. Such comparison requires a detailed familiarity with the data and the conditions under which it was obtained. Accordingly, arrangements were made for Dr. Desplat of the Saclay laboratories to visit us and participate jointly in programming our formalism for comparison with his data. Administrative difficulties prevented this visit from occuring this past year. These difficulties now appear to be resolved, and it is expected that the visit and its objective will be accomplished within the next few months.

REFERENCES FOR SECTION III

1. Hansen, L. K., J.A.P. 38, 4345 (1967).

2. Norcross, D. W., Report on 27th Annual Conference on Physical Electronics, M.I.T. (1967) p. 332.

3. See reference 2

4. See reference 1

5. Hernqvist, Karl, U.S. Patent 3,021,472, Feb. 13, 1962; filed Dec. 15, 1958, Also RCA Review, March, 1961.

6. Rasor, N. S., Advanced Energy Conversion 2, 545 (1963).

7. Rasor, N. S., Paper presented at 3rd International Conference on Thermionic Electrical Power Generation, Julich, Germany, June 1972; Vol. 3, p 1027. Also Section IX in NSR-1-4.

IV ADVANCED CONVERTER DEVELOPMENT

The purpose of this work is to develop advanced thermionic converters in geometries more closely resembling those necessary for systems application. A primary goal is to demonstrate on a more realistic scale the efficient utilization of the advanced performance modes of operation which have been developed in the demountable converter program. To this end, work in the past year has concentrated in three areas. The first was the verification of the advanced "hybrid" mode of performance observed in the cylindrical converter described in our last annual report. The second was the design of a fixed configuration converter amenable to a variety of advanced modes of operation and capable of producing on the order of 100 watts of power. The third was the design and initiation of the construction of a processing station to significantly reduce the iteration time required for construction, test, and disassembly or repair of cesiated converters. The results of the first two efforts are summarized in subsection IV-A and the third is summarized in Section IV-B.

A. Fixed Configuration Converters

1. Hybrid Mode

During pulse testing of a cylindrical converter last year an anomalous increase in output performance was observed. This was tentatively explained by the existence of an ignited mode discharge at the bottom of the emitter which was feeding cesium ions to the converter's interelectrode space, allowing the rest of the device to operate with very little arc drop. Post test inspection indicated the platinum sleeve used to clad the niobium emitter substrate had slipped down during operation, forming a cavity beneath the emitter. Figure IV-1 illustrates the converter geometry. The details of the device's operation were reported in last years annual report.[1]

During this year the converter was reassembled and further tests were performed. Initially there was no evidence of advanced performance, although the curves did show two distinct ignited regions of operation. (Figure IV-2) Both forward and reversed pulse testing were conducted to ascertain whether

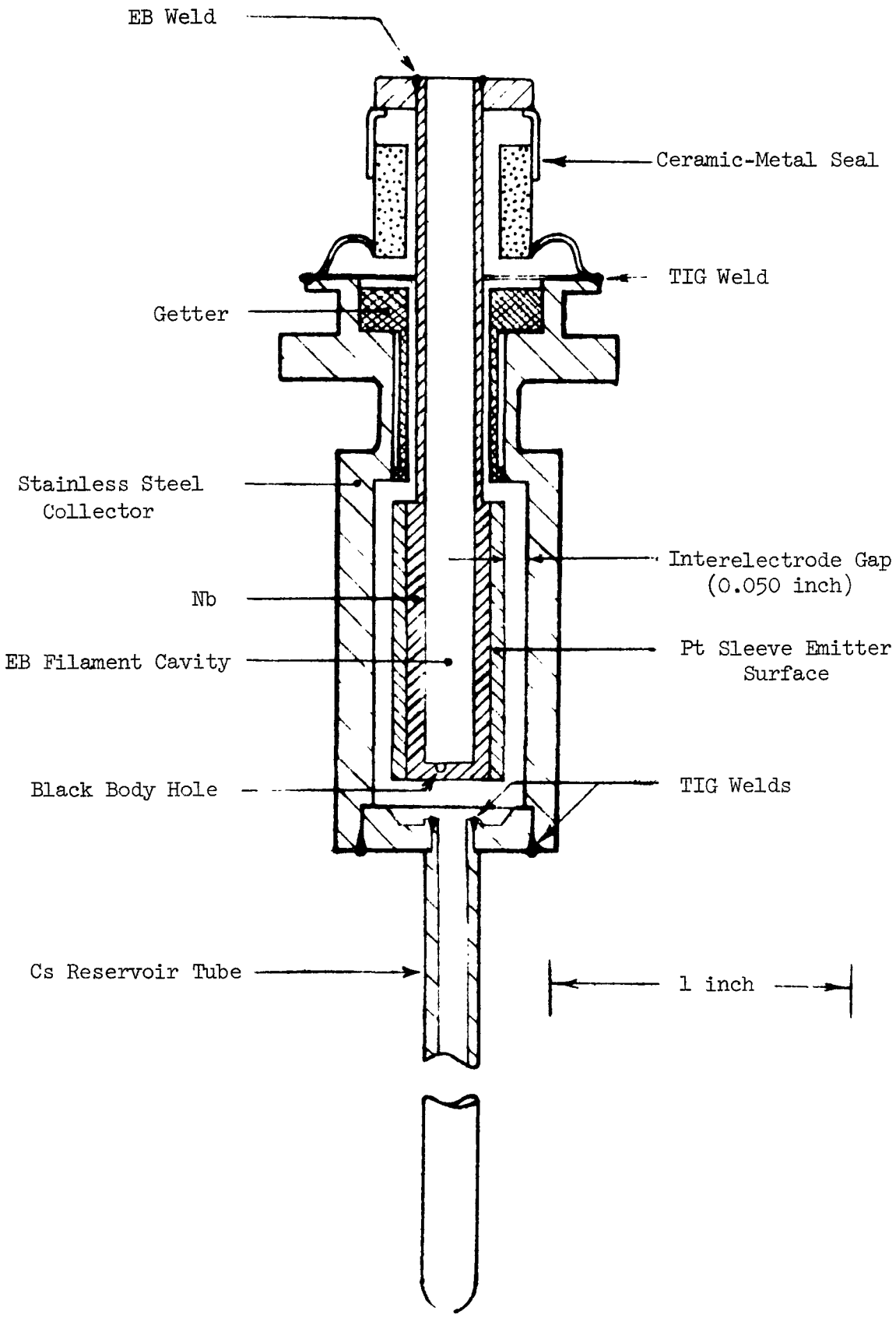

Figure IV-1 Cylindrical Converter Used in Hybrid Operating Mode Tests

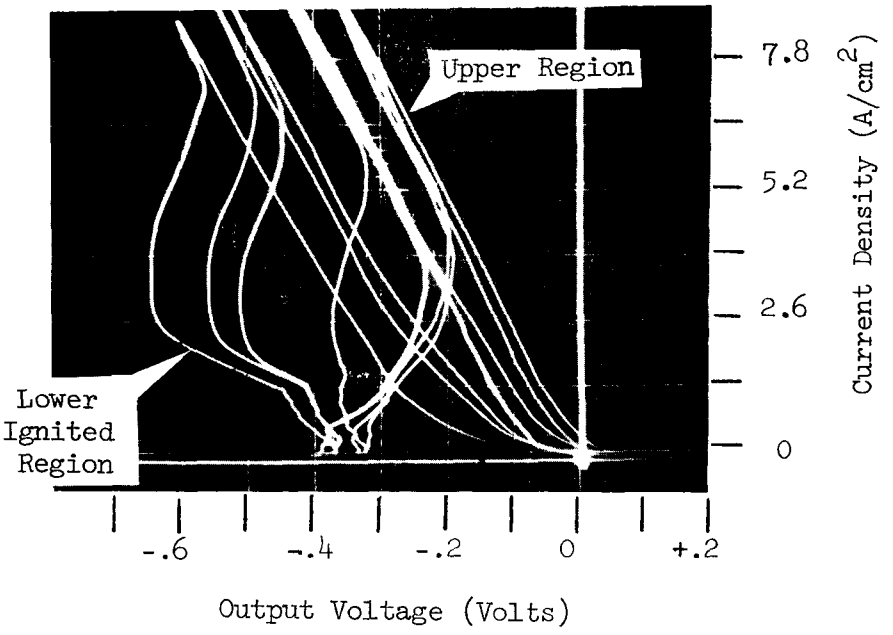

Figure IV-2

Before "push" at $T_E = 1400^{\circ}K$; Family of output characteristics of Pt-Nb diode for sleeve-collector distance of about 2 mils. ($T_C = 860^{\circ}K$, and $450 < T_R < 520^{\circ}K$).

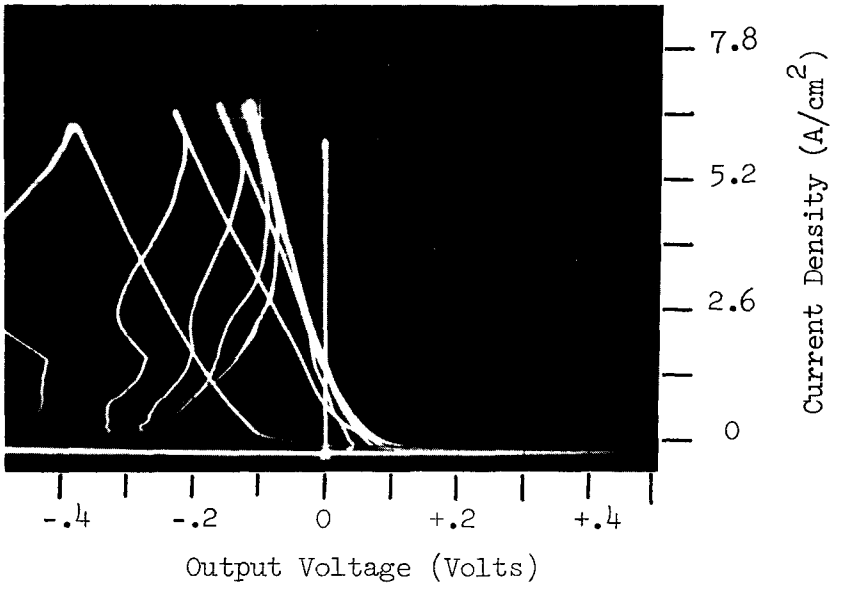

Figure IV-3

After "push" at $T_E = 1400^{\circ}K$; Output characteristics for sleeve-collector distance of about 10 mils ($T_{Co} = 860^{\circ}K$, and $460 < T_R < 560^{\circ}K$).

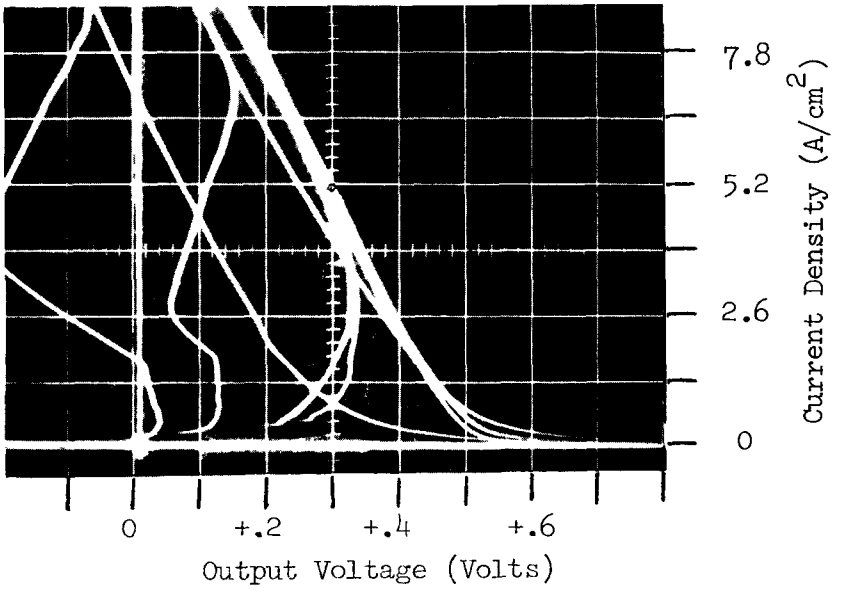

Figure IV-4

After "push" at $T_E = 1500^{\circ}K$; Output characteristics for 10 mils distance. ($T_C = 930^{\circ}K$, and $450 < T_R < 516^{\circ}K$).

such testing earlier might have resulted in special electrode surface conditions which might have generated the improved performance. No change in performance was observed.

Based on the mechanism postulated for the observed performance improvement, it was felt that the distance between the platinum sleeve and the bottom of the diode could be crucial, and that an optimum value should exist. It was decided to alter this distance and observe the effect.

During the initial testing period after reassembly, the sleeve-collector distance remained constant at about 2 mils. This value was computed from the differential thermal expansion required to obtain short-circuit (zero distance) when the emitter temperature was increased or the collector temperature was decreased from the operating point. The differential expansion was then extended beyond the short-circuit condition to "push" the Pt sleeve further up the Nb emitter substrate and thereby increase the sleeve-collector gap. This procedure succeeded in increasing the gap to about 10 mils, and enhanced performance was obtained upon returning to the normal operating temperatures. This performance enhancement corresponded to about 0.2 volt decrease in arc drop, whereas previously about a 0.4 volt decrease has been observed. Subsequent attempts to push the sleeve further resulted in gaps of about 11 and 12 mils, which caused progressive losses in performance corresponding to increases of about 0.1 volt in arc drop. These results suggest that the initial 2 mil gap was too small to permit efficient passage of ions from the end-arc into the main interelectrode space. Furthermore, the increase in arc drop as the the gap increased from 10 to 12 mils suggests that this distance is so large that ion loss from the end-arc is beginning to extinguish it. The minimum arc drop appears to occur with a sleeve-collector spacing in the vicinity of 5 mils.

Figure IV-2 shows the performance obtained prior to raising the sleeve (i.e., sleeve-collector spacing about 2 mils). In this figure the two distinct ignited regions of operation mentioned above are apparent. They presumably arise from the separate existence of arcs in the bottom cavity and main electrode gap under this condition. The characteristics of the converter after "pushing" the sleeve to produce a gap of about 10 mils are shown in Figures IV-3 and IV-4. Only slight enhancement was obtained at 1400°K. However, substantial enhancement was

obtained at 1500°K. A similar emitter temperature "threshold" for enhancement was observed in the earlier data (at 1300°K rather then 1400°K). Figure IV-5 from the earlier data illustrates this threshold behavior. The threshold condition could arise from the requirement for a sufficient contact potential or emission current difference to support the hybrid-mode of operation.

These results are significant because they confirm the previous observation of enhanced performance in this device. They show conclusively that the observed enhanced performance is associated with the position of the Pt sleeve, and does not arise solely from emission (surface)effects. Work is planned in the advanced converter research task to further study this mode of operation.

2. Fixed Configuration Converter Design

There are two primary purposes for the fixed configuration converters which have been designed. The first is to evaluate the engineering credibility of the advanced modes of operation. The second is to study the operating parameter envelope of a device having a practical geometry. Operation of these devices will allow better estimates of attainable performance, particularly efficiency, to be made, and should reveal unexpected geometry-dependent phenomena which have not been predicted.

The ground rules for the design of the fixed configuration converter were as follows:

1. It must allow operation in a variety of advanced operating modes.
2. It must be amenible to electrode alteration in the processing station.
3. It should allow operation in the ignited mode in a practical operating regime to facilitate comparison with previous devices.
4. It should be strongly based on the extensive prior experience in the field.

A variety of conceptual designs of both plane and cylindrical geometries were considered. A cylindrical geometry was selected for the first converters to be made for the following reasons:

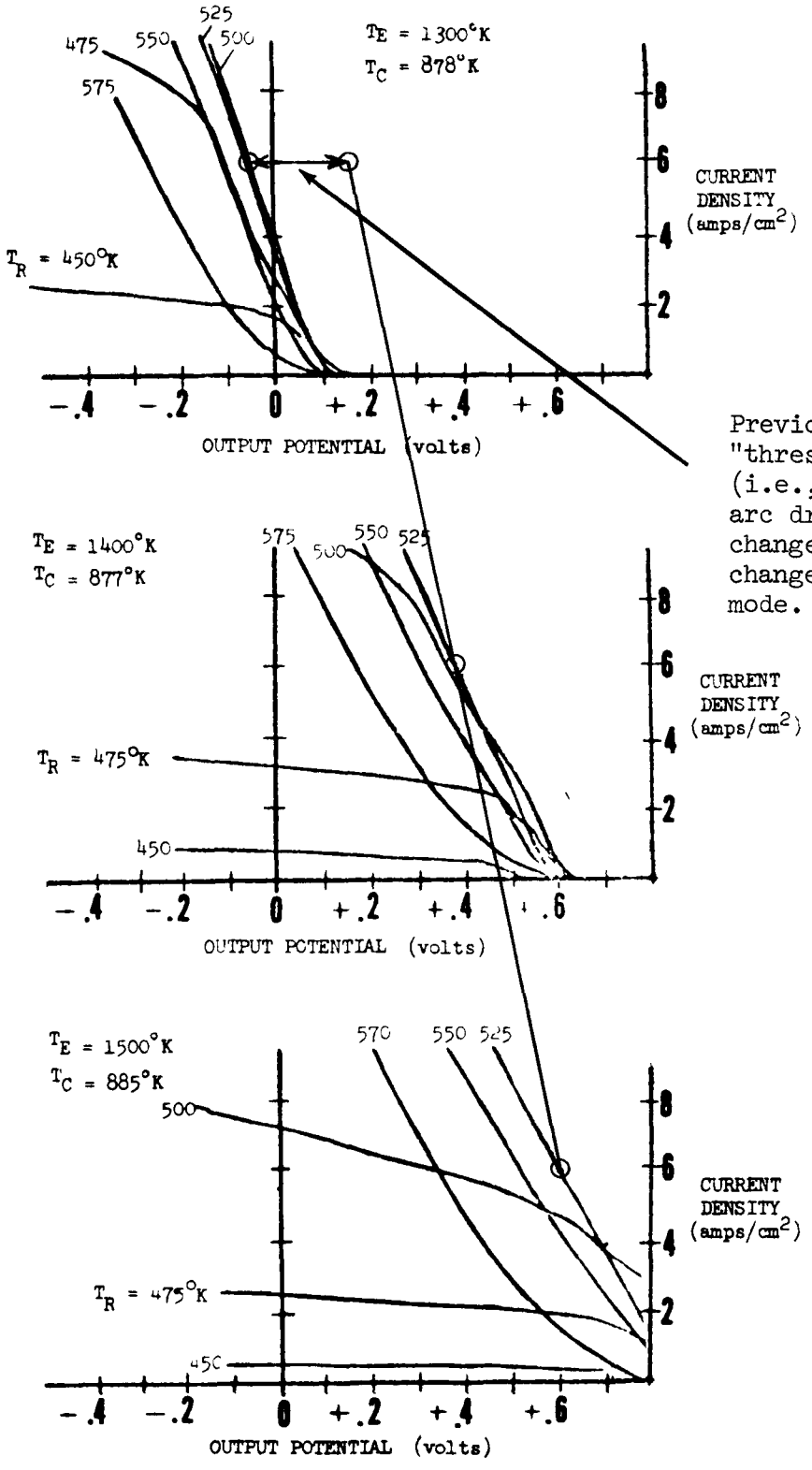

Previously observed emitter temperature "threshold" for hybrid mode operation (i.e., anomalous large dependence of arc drop on T_E). Voltage should only change by about 0.2 volt per 100°K change in T_E for conventional ignited mode.

Figure IV-5 Emitter Temperature "Threshold"-Hybrid Mode

1. This geometry has been most frequently used in the past for devices with large output powers. Consequently the design problems have been thoroughly explored and it therefore has the highest probability of successful operation with a minimum of basic development effort. Previously existing hardware and hardware designs may be easily adapted to the new configuration.

2. Present system designs accentuate the cylindrical geometry.

3. The cylindrical geometry provides a better opportunity for studying magnetic field effects resulting from high cell currents.

The converter design which has resulted from this work is shown in Figure IV-6. A unique feature of the design is the introduction of a third electrode lead in the insulator seal region of the converter. This lead is not intended to generate ions itself, but rather is a means for providing electrical connections to the special third electrode structures which will be devised as a result of the knowledge gained during the demountable converter tests. This same circumferential lead has been designed to permit multiple opening and resealing operations on the converter, thus enabling us to meet both ground rules 1 and 2.

An emitter area of 25 cm^2 was selected so that a total power output of 100 watts could be anticipated. The collector/collector-heat-sink structure was designed to provide a broad range of collector temperatures at any anticipated converter operating point.

The converter test stands are unusual in that they incorporate the converter cesium reservoir system. Final bakeout and cesiation of each converter tested will thus occur following instrumentation, rather than before, as has been the custom in the past. This approach has been selected since it allows the repeated use of cesium of known purity, and it minimizes the instrumentation required when installing a converter in its test stand.

Specifics of the emitter assembly, collector/collector-heat-sink assembly, insulator-seal assembly, and third-electrode designs are discussed separately below, as is the analysis of expected thermionic performance.

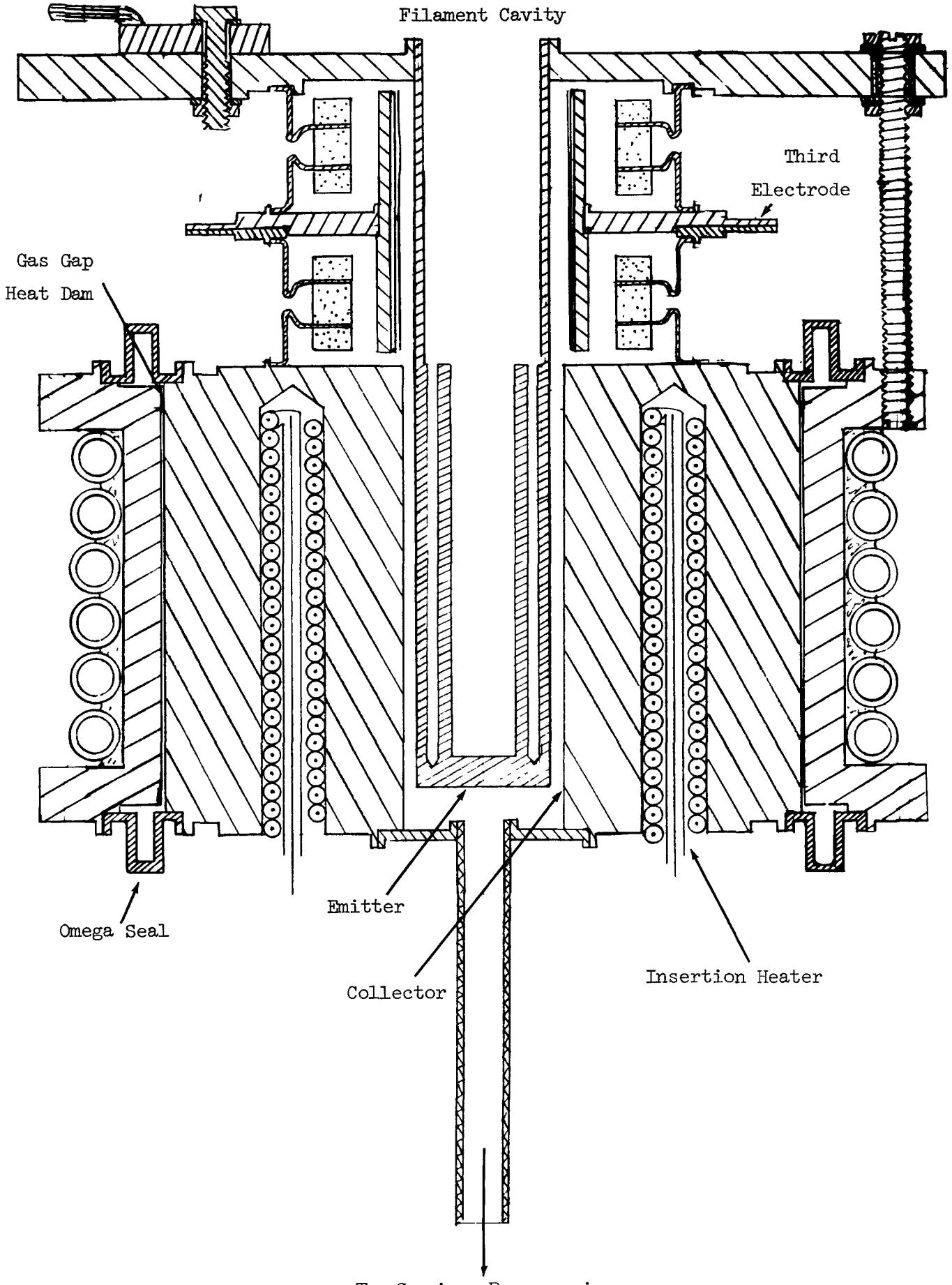

Figure IV-6 Fixed Configuration Converter Design

Thermionic Performance

The design of the converters was based on projected efficient operation with near second generation performance. An effective collector work function ϕ_C' of 1.6 ev was assumed. The analysis used is summarized below.

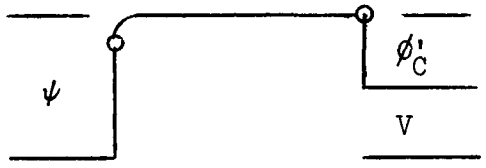

Electron Motive Diagram
At Maximum Output Power

The output current, including the effect of scattering, is given by

$$J = (J_E - J_C) / \left[1 + 3/4\ (d/\lambda)\right]$$

with $J_E = AT_E^2 \exp\left[-\psi/kT_E\right]$ = emitter emission into plasma

$J_C = AT_C^2 \exp\left[-\phi_C'/kT_C\right]$ = collector emission into plasma

$\psi = \phi_C' + V$ = condition for maximum power output

Solving these equations for V gives

$$V = kT_E \ln\left\{AT_E^2 / \left\{J\left[1 + 3/4\ (d/\lambda)\right] + J_C\right\}\right\} - \phi_C'$$

where
T_E = emitter temperature (^oK)
T_C = collector temperature (^oK)
d = interelectrode spacing (mm)
λ = cesium mean free path (mm) .063/p for pressure p in torr
ϕ_C' = effective collector work function (ev)
J = output current density (A/cm^2)
V = output voltage at electrodes (volts)
A = 120 $amp/cm^3 - {}^oK^2$
k = 8.6×10^{-5} $ev/{}^oK$

Thus, for given values of ϕ_C, T_E, T_C, and J, the output voltage V and output power, JV, may be obtained.

The required input power is approximated by[4]

$$Q_E = J(\psi + 2\ kT_E - 0.25) + 1.5\ \ (T_E/1000)^4 - (T_C/1000)^4\ + 1.5\ \ w/cm^2$$

In the design of a converter, a plot of the projected performance as a function of emitter temperature and electrode input power is very useful. Figure IV-7 illustrates such a plot for second generation performance with an interelectrode spacing of 1 mm and a cesium reservoir temperature of 440°K. This cesium temperature corresponds to a mean free path nearly equal to the interelectrode space, a condition which should be near optimum for high performanc emitter materials.

Emitter/Emitter-Stem Assembly

A cylindrical emitter nominally 1.6 cm in diameter and 5 cm long will be used in the fixed configuration converters. This will result in a surface area of 25 cm^2, which should provide an electrode power of 100 watts with e.g., an emitter temperature of 1500°K and a current density of 6A/cm^2. The availability of existing electron bombardment filament assemblies and bombardment heating technology resulting from the GGA Thermionic program made these dimensions particuarly attractive.

In addition to the electron bombardment filament cavity, each emitter will have four thermocouple holes. These will allow emitter temperature profile estimates to be made, and may serve to establish the location and nature of localized discharges which may occur in some advanced operating modes.

The optimum lead area-to-length ratio[2] as a function of emitter temperature and current density is shown in Figure IV-8. These curves are approximately valid for any material which closely follows the Lorentz ratio between electrical and thermal conductivity. The emitter stem for this design was selected to provide optimum performance at an emitter temperature of 1500°K and a current density of 6A/cm^2.

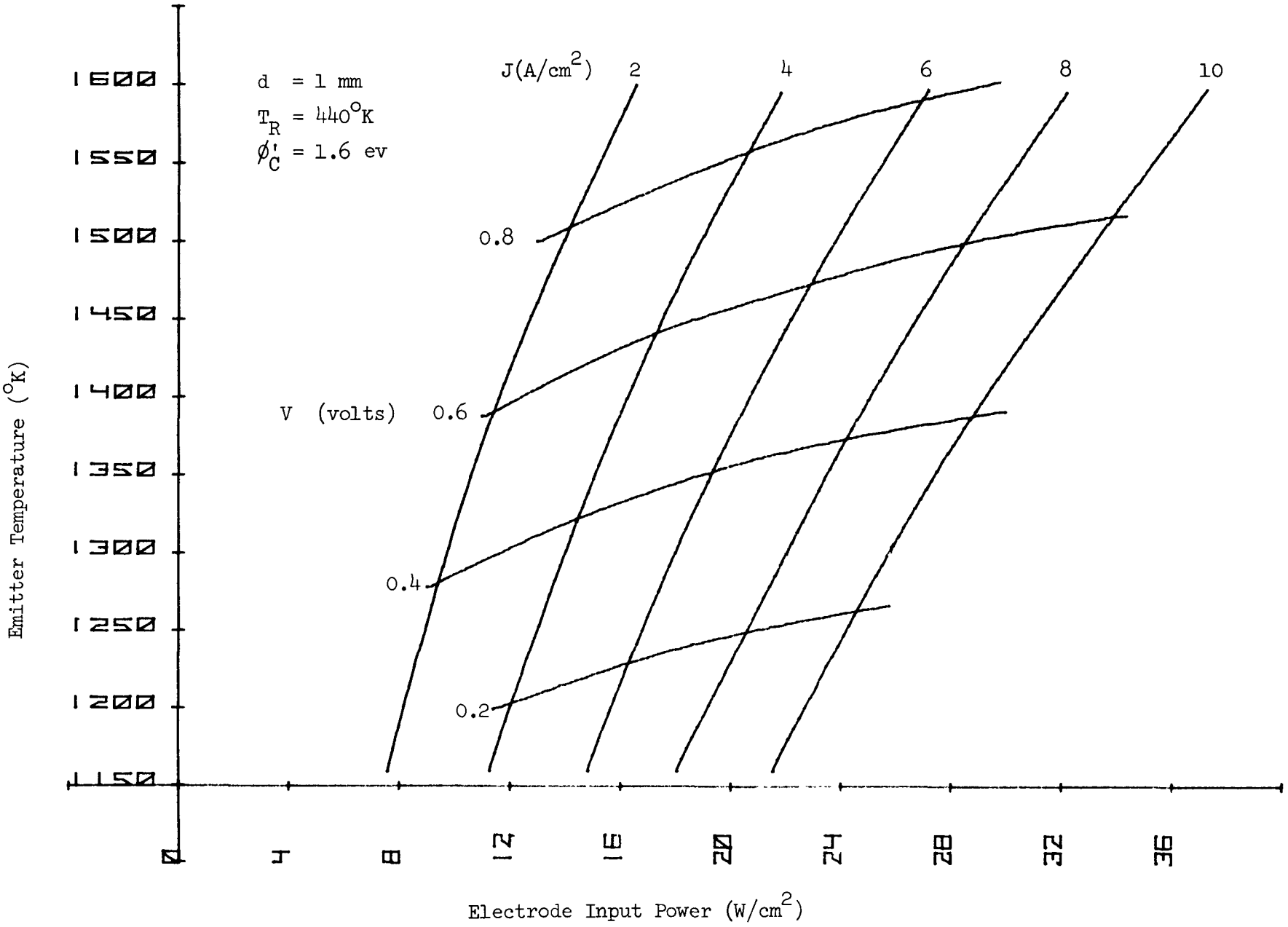

Figure IV-7 Second Generation Performance Projection

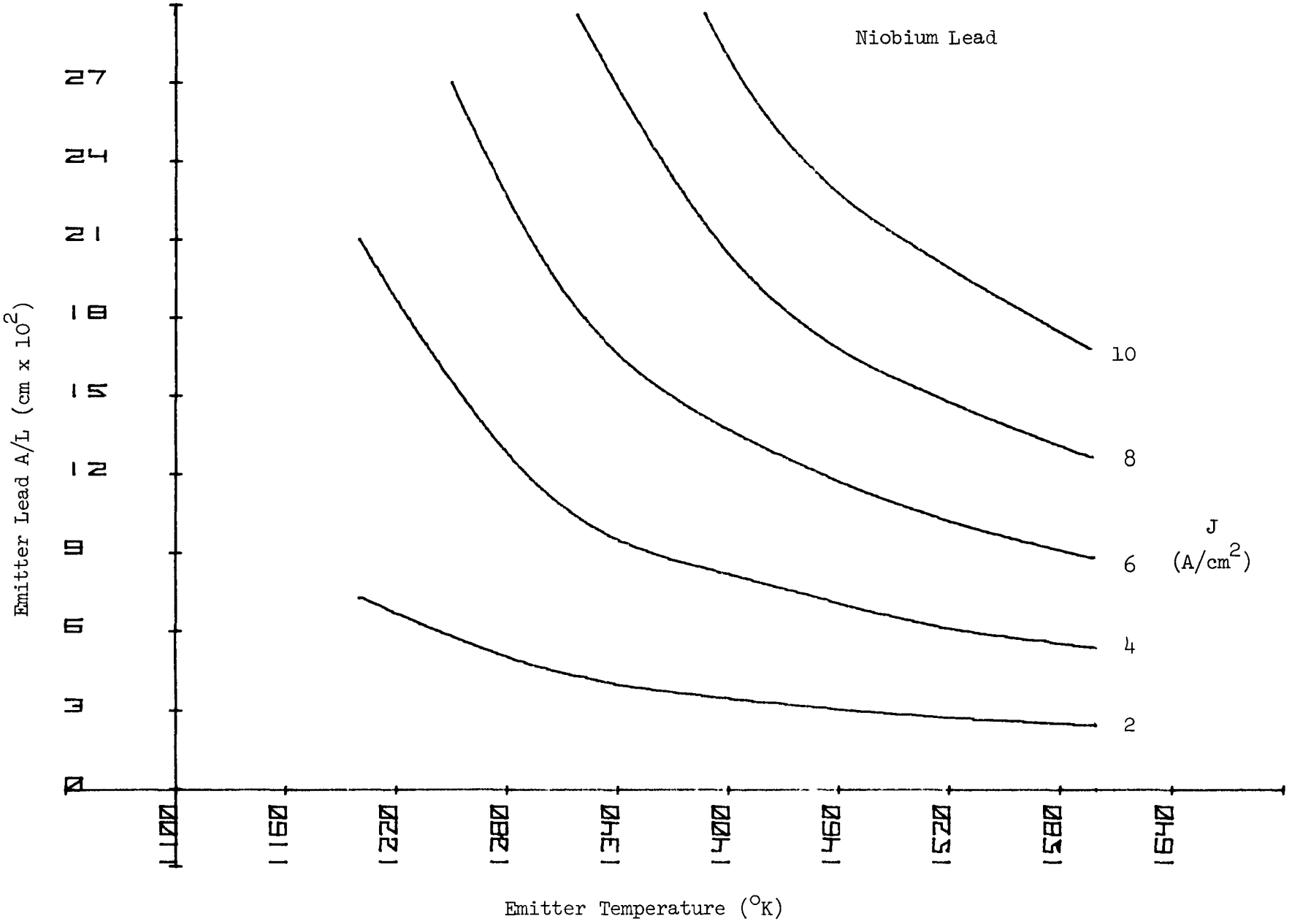

Figure IV-8 Optimum Emitter Lead Area/Length Ratios

Niobium is tentatively selected for an emitter material because of its refractor nature, and its close match to platium alumina with respect to thermal expansion. These expansion matches will allow the possibility of operation with a high bare work function surface (platinum), operation in the hybrid mode (platinum and niobium surfaces exposed), and with triode geometries requiring insulated electrodes at emitter temperatures. The ability of niobium to operate at high emitter temperatures will allow comparisons between these converters and past devices operating in the ignited (first generation) mode.

Collector/Collector-Heat-Sink Assembly

The most important factor in the design of the converter-heat-sink assembly was the ability to provide a broad range of collector temperatures at a variety of cell operating points. Secondarily, the design emphasizes reliability through the use of redundent components and proven techniques.

As can be seen in Figure IV-6, the heat sink incorporates the converter collector. Nickel was selected for this electrode. Ten insertion heaters have been provided to allow collector temperature control. Insertion heaters were selected over wrapped and brazed sheathed heater wires since they may be more readily removed and replaced. The use of ten heaters not only serves to reduce the heater wire surface temperatures, but also increases the heat sink reliability through redundancy.

Outside the ring of insertion heaters is a 0.015" gap which serves as a heat dam. A variety of gases or vacuum may be used in this gap to vary its thermal conductance. The gap is bridged by an omega seal which provides sufficient flexure to accommodate the large temperature gradient which will occur across the gap. Outside of the gap there will be a stainless steel cylinder, cooled to near room temperature by water flow in attached stainless tubes.

For purposes of the heat transfer analysis the collector/collector-heat-sink structure was divided into four regions. They correspond to the nickel collector block, stainless steel heat sink, gas gap, and omega seal.

The heat conducted through each of the first three regions was approximately related to the temperature drop across it by the relationship

$$q_i = \frac{2\pi k_i \, h\Delta T_i}{\ln (Rl_i/R2_i)}$$

where q_i = heat flux across the region

k_i = thermal conductivity of the material

ΔT_i = radial temperature drop across the region

$R1_i$ = inner radius of the region

$R2_i$ = outer radius of the regions

The heat flux across the omega seal was approximated by the relationship:

$$q = \frac{2\pi R t k_i \Delta T_i}{w}$$

where R = average radius of the seal

t = thickness of the material used

w = the distance traveled through the seal by heat flowing radially

The thermal conductivity, as a function of temperature of helium, argon, and a mixture of helium and argon in the gas gap was obtained from the experimental data reported by W. R. Lloyd.[3] The radiative transfer across the gas gap was approximated by radiation from a surface having an emissivity of 1, operating at the hot side temperature. Initially this may be a poor approximation, but as the gap sides oxidize it will become increasingly correct.

The calculated thermal characteristics of the collector-heat sink assembly are shown in Figure IV-9.

Insulator Seal Assembly

The insulator seal assembly makes use of existing high purity alumina/copper-brazed seals recovered from the thermionics program at Atomics International. The flanges on these seals are Kovar, and consequently a support assembly has been designed to maintain structual rigidity. This assembly and representative seals will be tested in cesium prior to incorporation in a converter to establish their ability to perform in the test environment. The extended flanges incorporated between insulator seals provide a circumferential weld which is relatively easily accessible, and which may be used to repeatedly assemble and disassemble a converter.

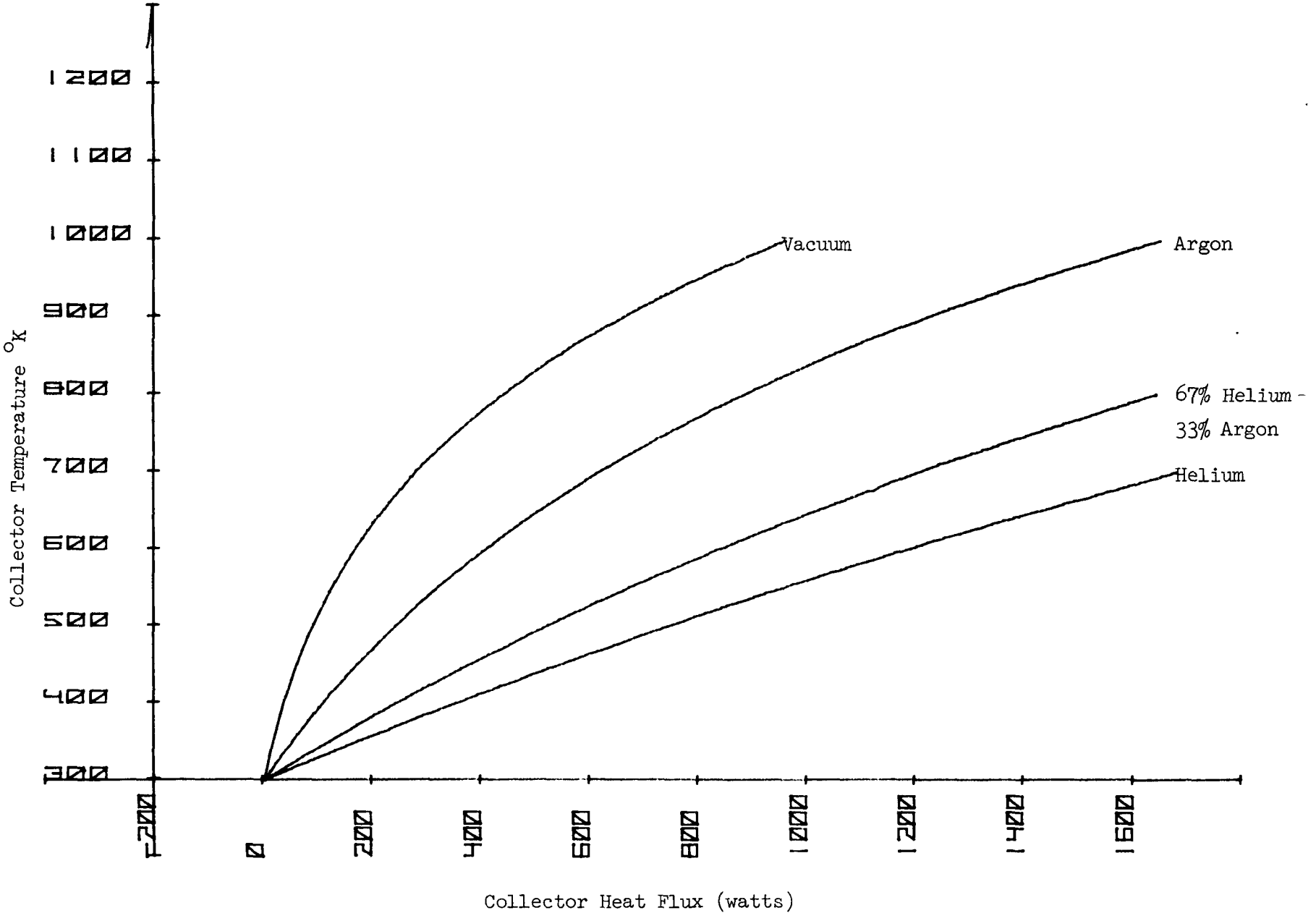

Figure IV-9 Collector Heat Sink Thermal Characteristics

Third Electrode Designs

A variety of third electrode configurations are presently under study, and Figure IV-10 illustrates those which are most interesting based on the experiments and analysis which have been conducted to date. While the actual configurations used will vary in detail from those shown, depending on the results of the demountable converter tests which will be performed during this coming year, these designs will be developed early in the year to provide a base of experience for the designs actually tested.

B. Processing Station

The purpose of this work was to design and initiate construction of a facility for fabrication, disassembly, reassembly and processing of converter assemblies in a purified inert gas atmosphere without intermediate exposure to air.

In the past converters have normally been fabricated in air, then outgased and cesiated under vacuum, transferred in air to a vacuum test station, instrumented, and operated under vacuum. The occurence of a leak while the device was exposed to air generally resulted in sufficient background gas pressure and contamination of the electrodes to put the following test results in question, and even to result in the converter's loss. For these reasons modification of assembled devices was also rarely attempted. As a result a new converter was normally fabricated to test each new concept, and either development iteration times were very long (several months) or testing was quite expensive due to the need to build backup devices and perform tests based on premature results. The processing station has been designed to obviate the leak and concurrent contamination problem by never allowing exposure of a device to an impure atmosphere. This will permit repeated use of basic converter components, and should greatly reduce test costs and iteration time.

Figure IV-11 shows the station schematically. Figures IV-12 and IV-13 show the equipment layout which will be used. The two essential elements of the facility are an argon glove box and a vacuum glove box, connected by a vacuum interlock. To these are appended the equipment needed to fabricate, instrument, pretest and repair converter assemblies.

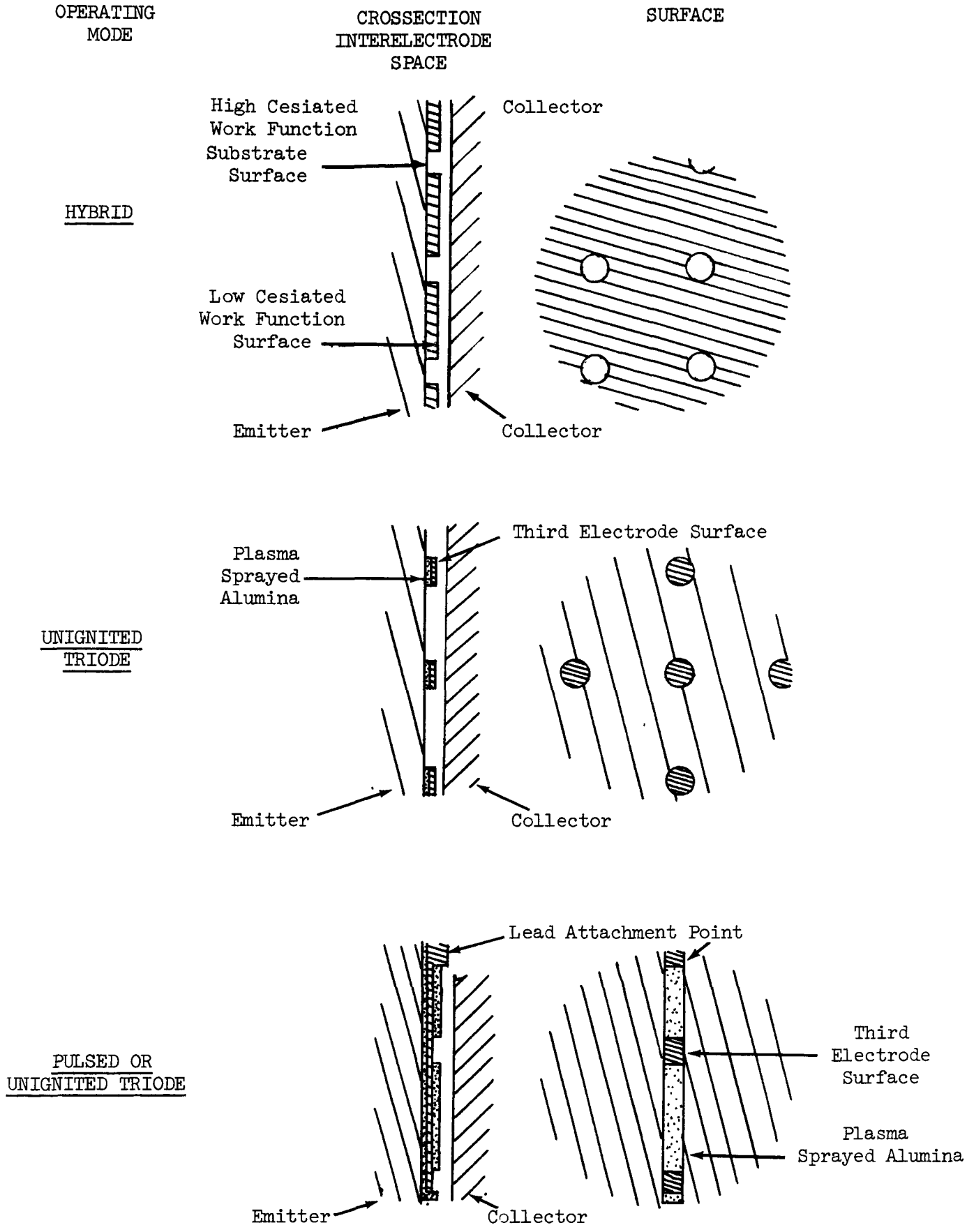

Figure IV-10 Possible Third Electrode Configurations

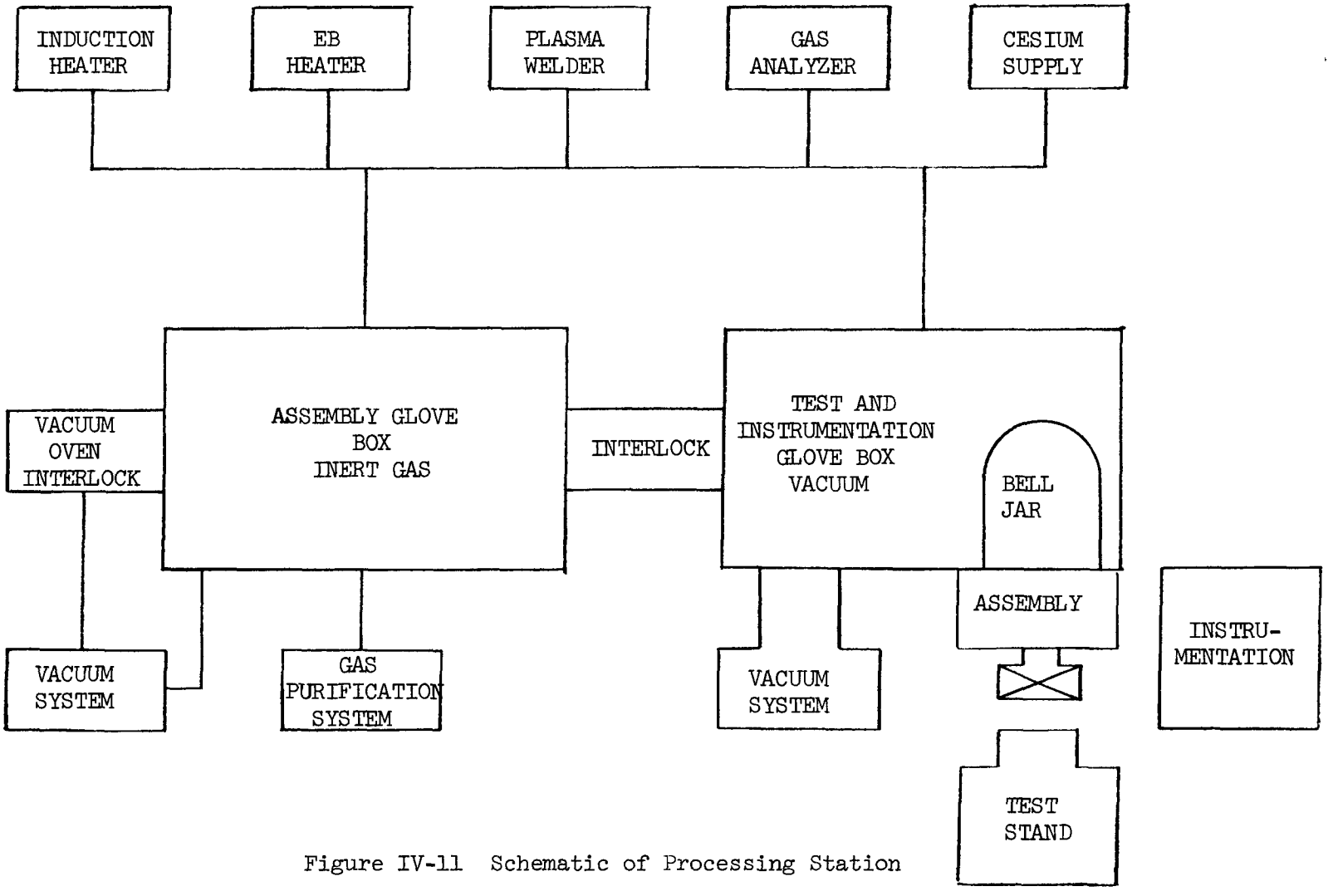

Figure IV-11 Schematic of Processing Station

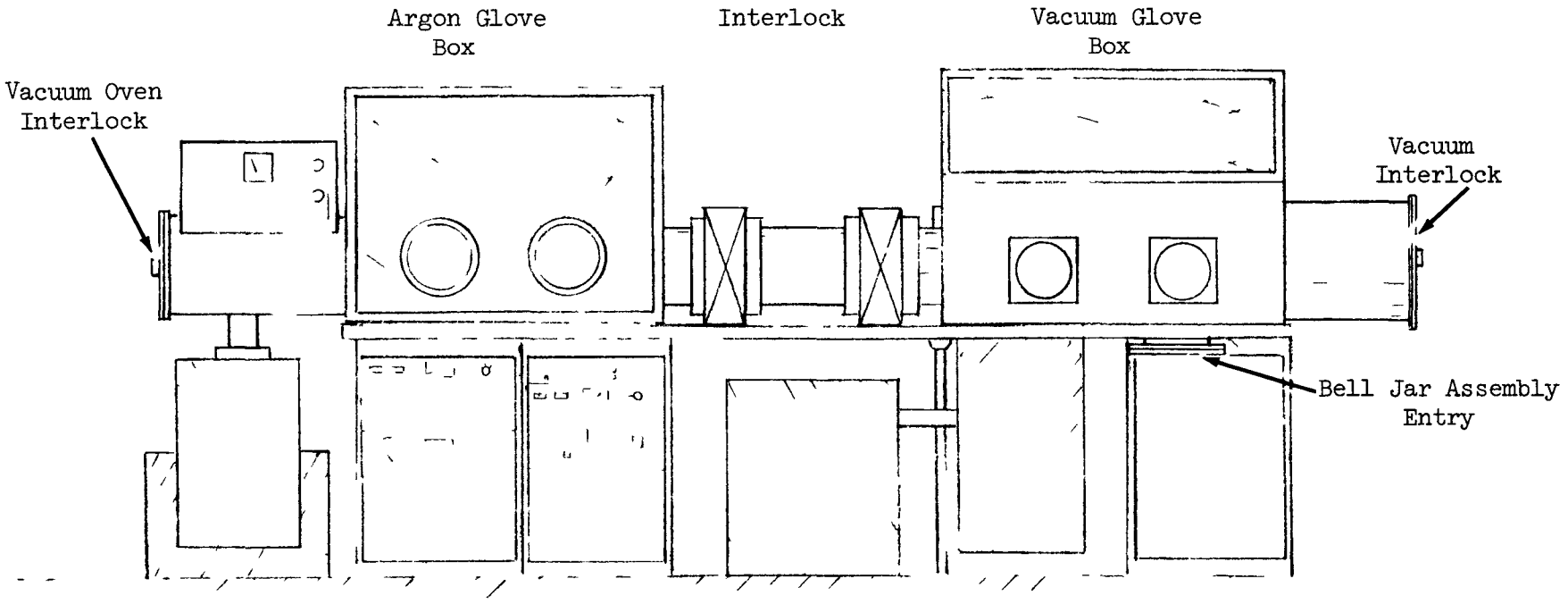

Figure IV-12 Processing Station - Front View

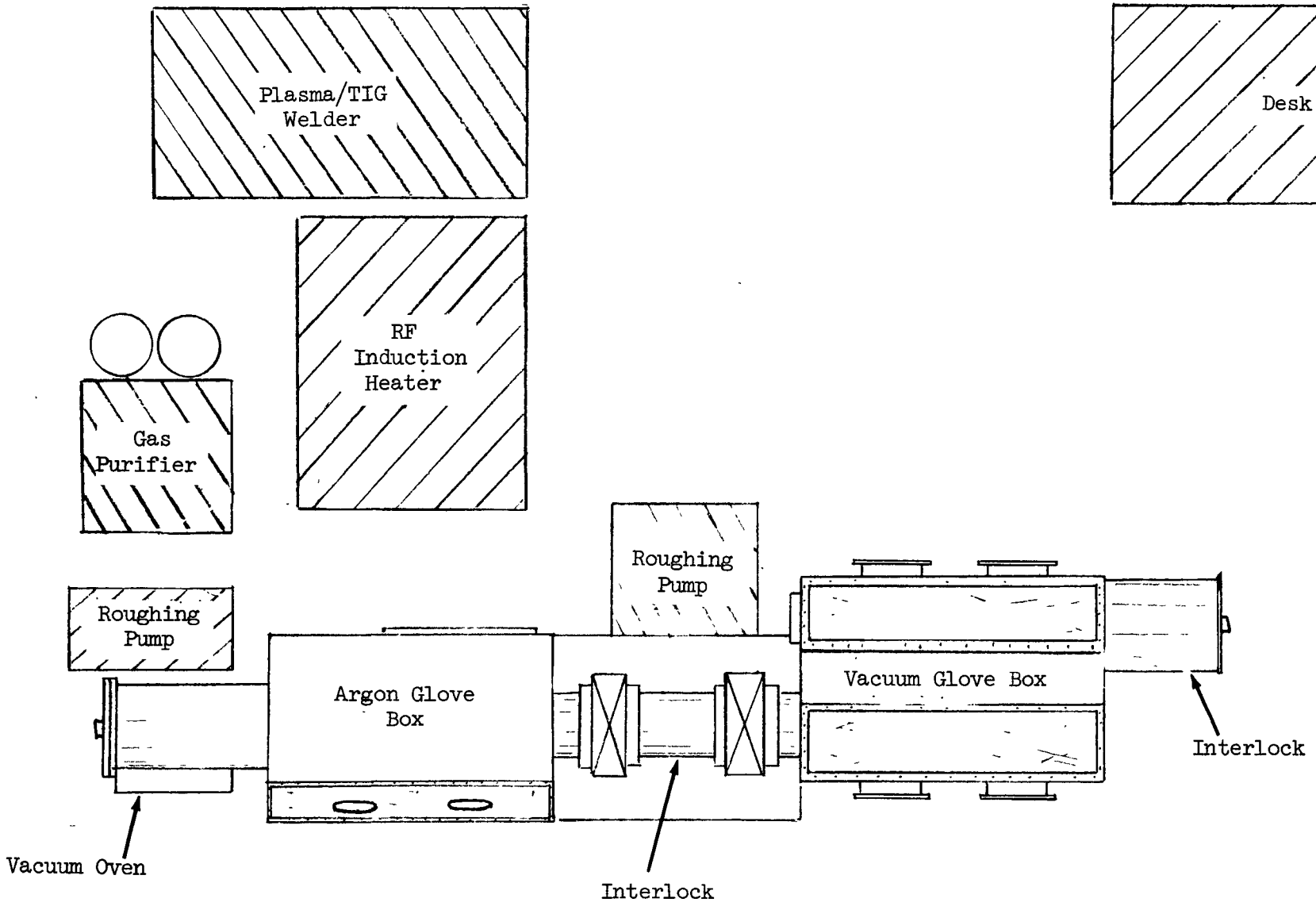

Figure IV-13 Processing Station - Top View

Converter components will be degassed in a vacuum oven prior to entry into the argon glove box, where they will be assembled, joined, outgassed, and possibly loaded with cesium. This box can also be used for converter disassembly following testing, and possible repair and modification. The converter will then be passed to the vacuum glove box under an argon atmosphere. There it will be installed in a test station, instrumented for test, and covered with a bell jar. The vacuum glove box will then be evacuated and the converter pretested. If unsatisfactory the system may again be let up to argon and repairs made. Following a successful pre-test, the glove box will be backfilled with argon and the evacuated bell jar/converter assembly will be removed to a test stand where the experiment will be conducted.

The glove boxes were obtained from NASA Lewis Research Center, where they had been in storage as excess equipment. The long lead time items such as the vacuum system components, controls, argon purification system, etc., have been ordered. The fabrication of special parts, such as the interlocks, feedthrough panels, control system, etc., has been initiated.

The assistance of Dr. R. Breitweiser and Mr. Arthur Mahon in designing this station and acquiring the necessary equipment is gratefully acknowledged.

REFERENCES FOR SECTION IV

1. Rasor, N. S., and E. J. Britt, "Practical Aspects of Fundamental Research in Thermionic Conversion" Progress Report, COO-2263-1, NSR-2-1 (Julyl, 1972 to August 31, 1974).

2. Shock, Alfred, "Optimization of Emission-Limited Thermionic Generators", J. Appl. Phys. 32, 1564 (1961).

3. Lloyd, W. R., D. R. Wilkins, P. R. Hill, "Heat Transfer in Multicomponent Monatomic Gases in the Low, Intermediate, and High Pressure Regime", Thermionic Conversion Specialists Conference, Framingham, Massachusetts, (Oct., 1968).

4. Breitweiser, R., Private Communication

V MINI SYSTEM

Introduction

The purpose of this Task is to construct and maintain operational a small but fully self-contained system in which advanced converter and systems innovations are initially reduced to engineering practice on a small and relatively inexpensive scale. Such a system satisfies the following needs in this project: First, in the absence of a full scale development activity, there is a need to encounter unique systems integration problems of advanced converters at an early enough stage to include and satisfactorily resolve them in future work. Second, there is a need to gain early experience with unique converter input coupling techniques in order to assure the practical reality of advanced system designs incorporating them. Third, there is a need for an operational system which credibly demonstrates what can be reduced to practice at a given time, without relying entirely on analytical estimates.

To satisfy these needs a "mini-system"was designed using small cylindrical converters capable of operation in air. The converters are designed to be modular and can be quickly exchanged in the system. Thus, as advanced converters become available they can readily be incorporated in the mini-system. The first converter used in the mini-system will be operated in the ignited mode. The design incorporates a wide interelectrode gap and a high bare work function emitter (which allows the use of low cesium vapor pressures) so that it will be suitable for use in the pulsed diode mode if such operation looks attractive in the future. Although the first converter will use electron bombardment heating and direct heat rejection to air, later mini-system devices may incorporate heat input and heat rejection techniques (heat pipe, sodium loops, steam generator, etc.) which are selected for emphasis in the system design task.

The converter is connected to its load through an inductive output coupling circuit which acts as a power conditioning unit to obtain the desired output voltage. Two methods of inductive output coupling, the push-pull and flux-reset techniques, are being considered for THX design. The mini-system will explore and evaluate these methods in support of the systems design work.

Converter Design and Fabrication

The design of the first mini-system converter is shown in Figure V-1. The emitter area is $7\frac{1}{2}$ cm^2. The converters have been designed to operate at temperatures as low as $1500^{\circ}K$ with emission currents as high as 10 amps/cm^2. An interelectrode spacing of 0.050" was selected to allow the possibility of operation in the pulse enhanced mode. This wide spacing implies the use of low cesium pressures and to obtain good performance at these low temperatures and low cesium pressures a platinum emitter is used. While the emission requirements can be met through the use of additives or other techniques, the use of platinum presently provides the most reliable high performance emitter surface. The platinum is in the form of a cladding sleeve with 0.040" thick walls. It is machined from solid platinum bar stock, then mechanically swaged onto the emitter substrate and finish machined.

Niobium emitter substrates support the platinum sleeves. Niobium was selected because of its good thermal expansion match to platinum. Fabrication of these substrates was delayed because of casting flaws discovered in the niobium bar stock. The flaw, which had the form of lonitudinal porosity in the center of the bar extending throughout its length,was not dicovered until after the parts had been fabricated. A second piece of stock was ordered, and the suppliers made a special mill run to supply it. The second piece of niobium was defective in the same manner. The porosity was sealed successfully by electron beam melting platinum over the porous regions. This process results in the formation of a very hard alloy of platinum and niobium which has a higher melting point than the platinum itself.

A niobium transition piece is brazed on top of the insulator seal. The emitter stem is then electron beam welded to the transition piece. The emitter current lead is a flexible copper braid brazed into a molybdenum ring which, in turn, is electron beam welded to the transition piece.

The converter collector is made from stainless steel and is designed to allow cooling by air convection. It incorporates a heat dam which allows the insulator seal to run at temperatures lower then the collector. A titanium getter is used to maintain low residual gas pressures in the interelectrode space.

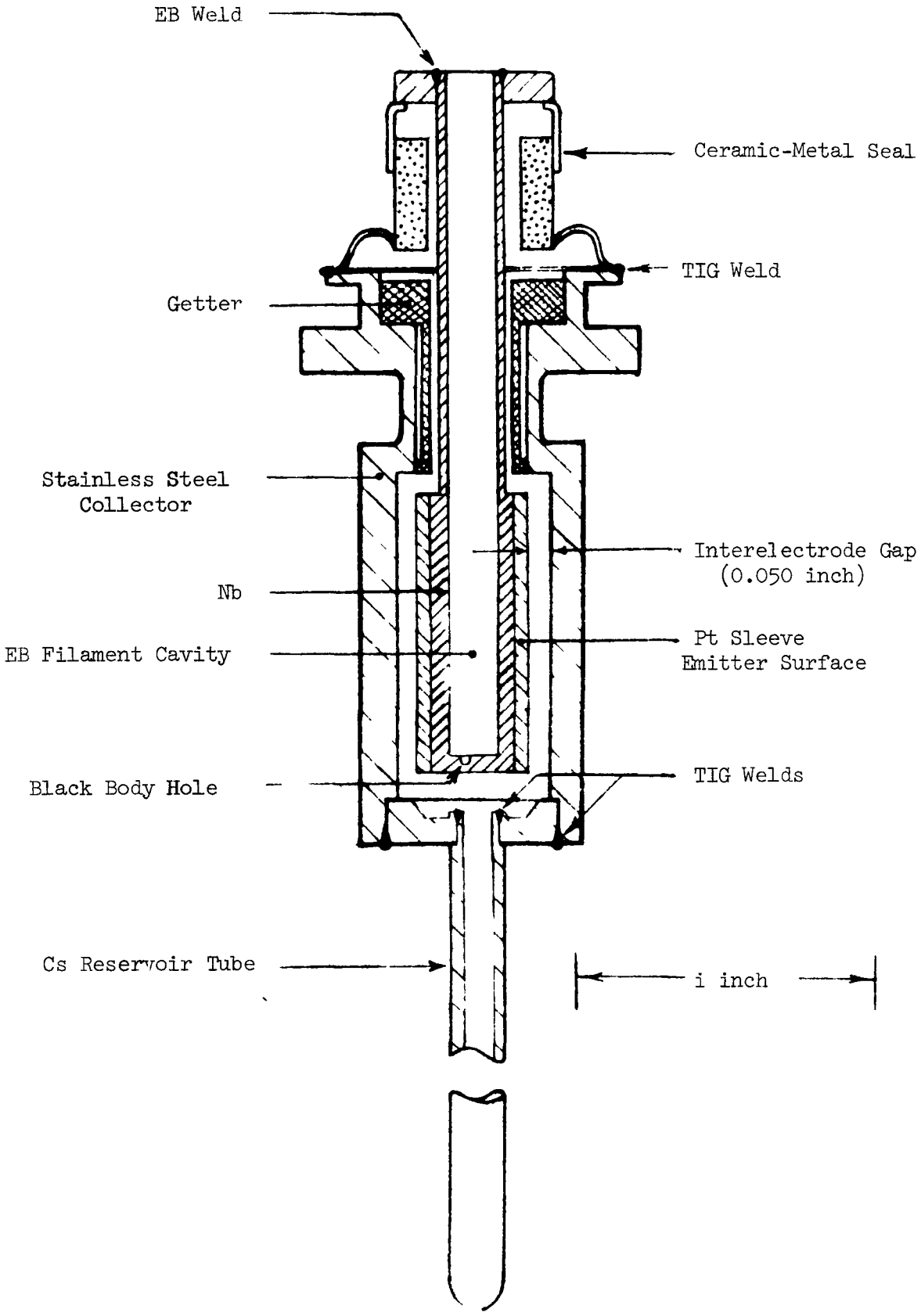

Figure V-1 Mini-System Converter Designs

A closed chamber is welded on top of the converter to form an evacuated volume for the electron bombardment filament. This chamber has two small feed-throughs mounted in its side for the electron bombardment filament. A third large feed-through in the top of the chamber introduces the emitter current lead. A drawing of the entire converter assembly is shown in Figure V-2.

Inductive Output Coupling

Two methods of coupling converters to their load inductively are presently under development. Both methods make use of the fact that thermionic converters have two stable operating states: high current (low-impedance) mode, and a low current (high-impedance) mode. In the elementary cesium diode these correspond to the ignited and unignited modes of operation. In advanced converters the two modes may be produced by turning the auxiliary ion generator on and off. Figure V-3 shows the schematic circuits for the two methods.

In the flux reset method,[2] a single converter drives the primary of a transformer. The converter is alternately switched between tis low-impedance power-producing state and its high-impedance state. A small amount of energy, supplied by a self-powered pulse generator in the secondary circuit, is used to reverse the flux in the transformer core while the converter is in its high impedance mode and while the load is switched out of the circuit. The load is then reconnected, and the flux in the core again rises after the converter is placed in its power-producing state. The output from the transformer secondary is interrupted DC with a high duty cycle (80-90%). The output voltage is determined by the turns ratio used in the transformer.

In the second method,[3] two converters are connected in push-pull across the primary of the output transformer. While one converter is producing power, the other is operating in its high inpedance state. They are switched simultaneously between operating states by means of a self-powered pulse generator in the secondary circuit. The output on the secondary side of the transformer is in the form of square-wave AC, with a voltage determined by the transformer turns ratio.

The push-pull circuit has the advantage of not requiring a switch in the load circuit, but the converters are individually operated with a 50% duty cycle, which tends to reduce system efficiency and increase its cost. Both approaches are

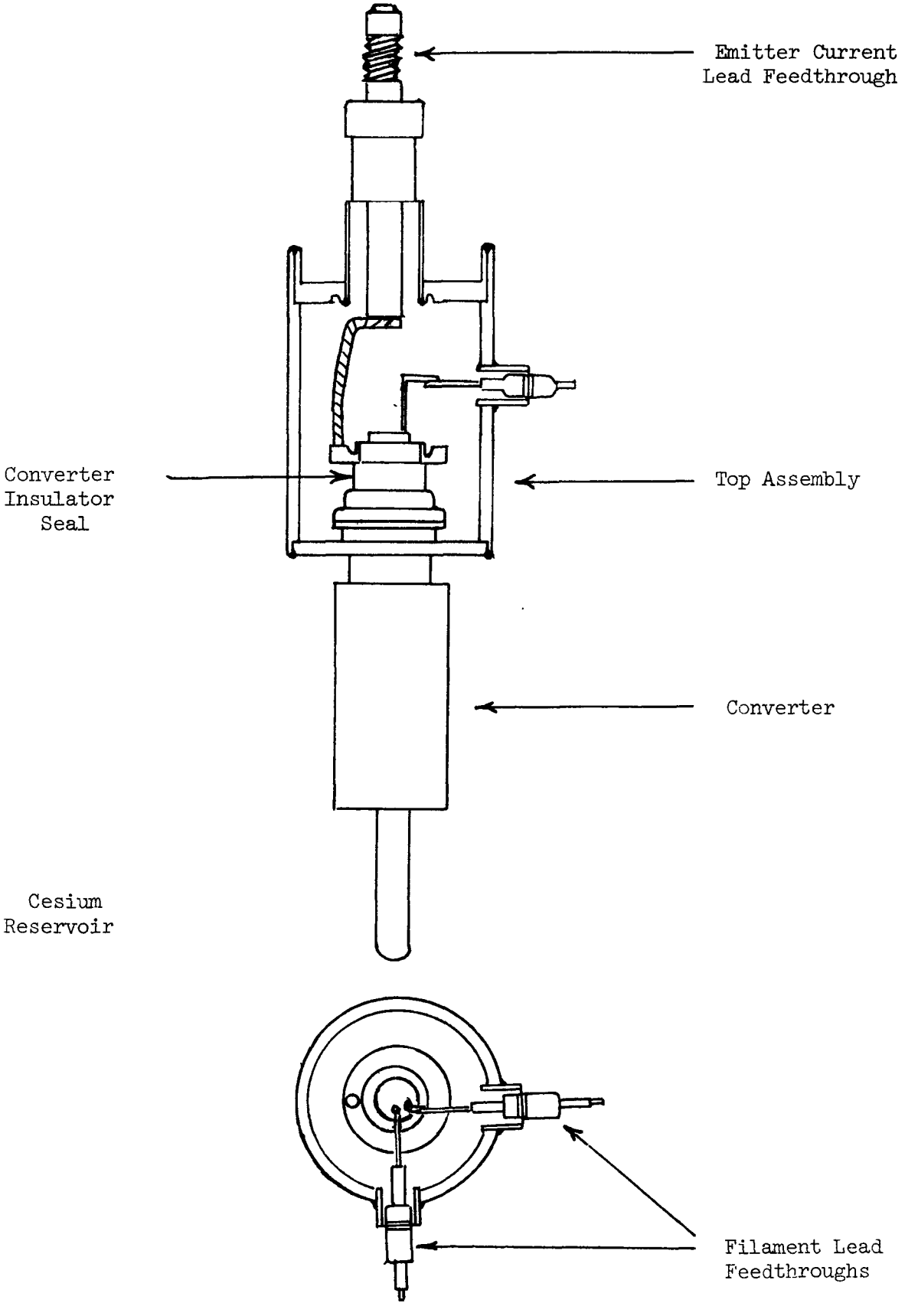

Figure V-2 Mini-System Converter-Top Assembly

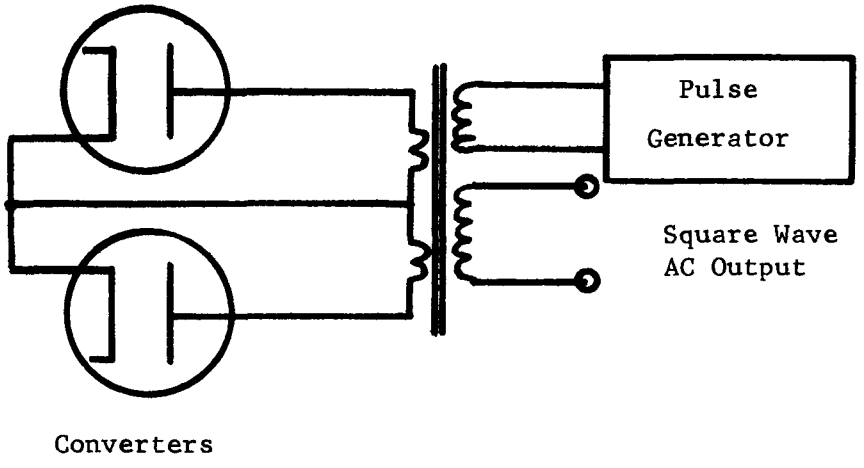

Pushpull Operation

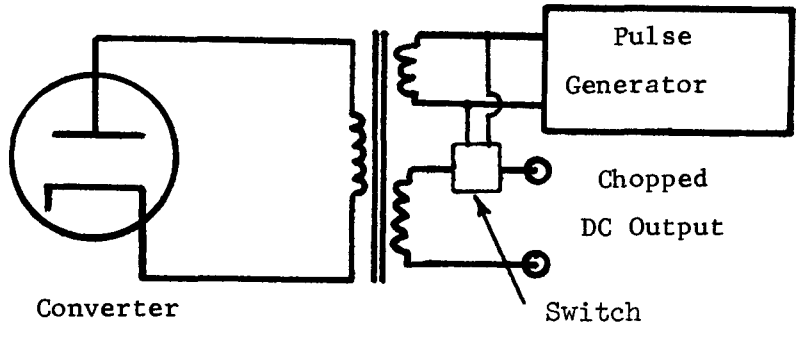

Flux Reset Operation

Figure V-3 Converter Configurations For Inductive Output Coupling

of interest in systems studies. For the first min-system the flux reset method has been selected, since it requires only one converter.

Flux Reset Circuitry

The flux reset circuit developed for the mini-system essentially consists of three pulse generators and some solid state switching circuits connected to the secondary windings of the converter output transformer. The mini-system converter is connected to the primary of this transformer. A block diagram of the arrangement is shown in Figure V-4. Pulses are successively generated to turn off the converter, reset the flux, and fire (ignite) the converter. A portion of the output power is fed back from the load to drive the pulse generators and the switching logic. The largest inefficiency in the system is the power lost in the iron in the transformer core. Since all switching circuitry is located on the secondary side of the transformer, no voltage drops associated with switches are placed in series with the low voltage converter output. The circuit has a Ni-Cd battery which is used to run the switching logic during startup. Once in operation the battery can be switched out of the circuit and/or recharged with the output of the system.

Schematic diagrams of the circuit used are shown in Figure V-5 and V-6. It was fabricated by Applied Research and Development in Olmsted Falls, Ohio. Two models will be used. The first circuit is a variable parameter "breadboard" model to be used for system integration tests. A second model of the circuit will be built with components chosen for best possible performance as determined by the integration tests. The second circuit will be installed in the finished cabinet of the min-system.

Measurements of the operating characteristics of the variable-parameter model of the flux reset circuit were made with a simulated converter power source. Figure V-7 shows a schematic of the converter simulator used. The simulator produces an output which has 1/20th the current of a converter and 20 times the voltage. By using a suitable turns ratio on the transformer it makes an entirely adequate analog of a real device. As shown in Figure V-8, its I-V characteristic has two branches, analogous to the unignited and ignited modes,

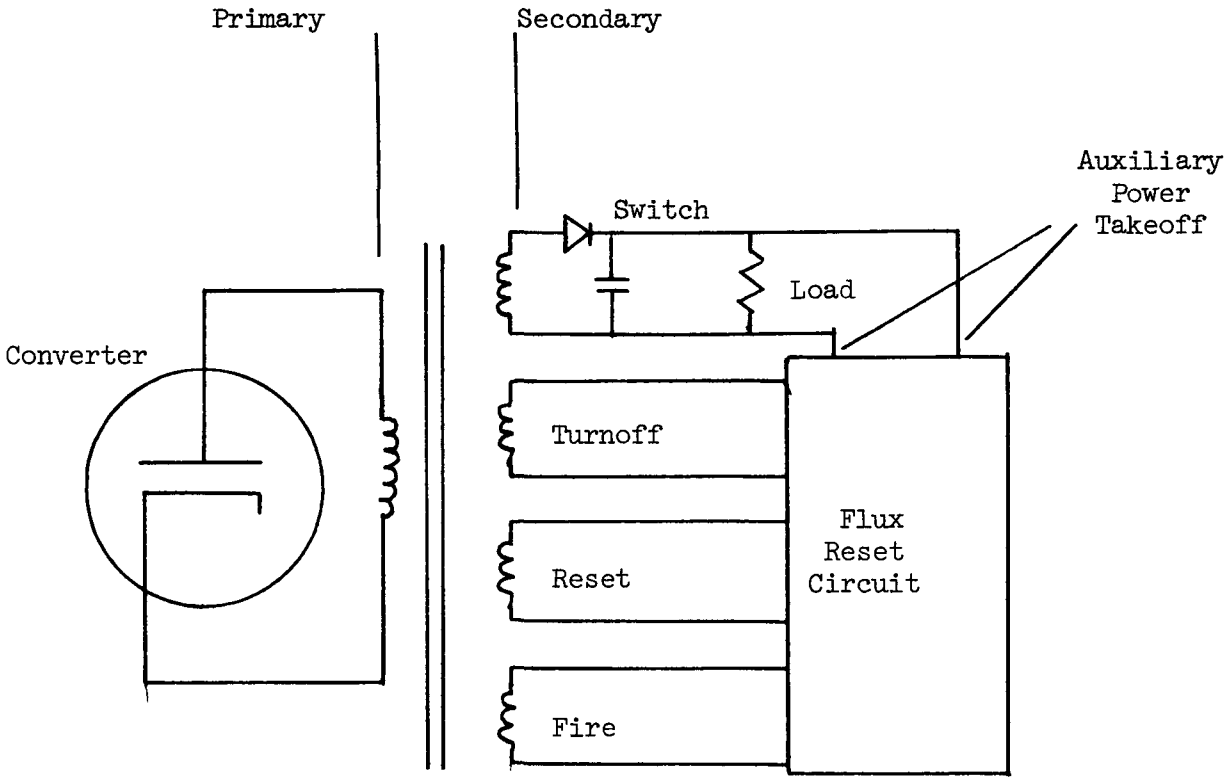

Figure V-4 Block Diagram of Mini-System Circuitry

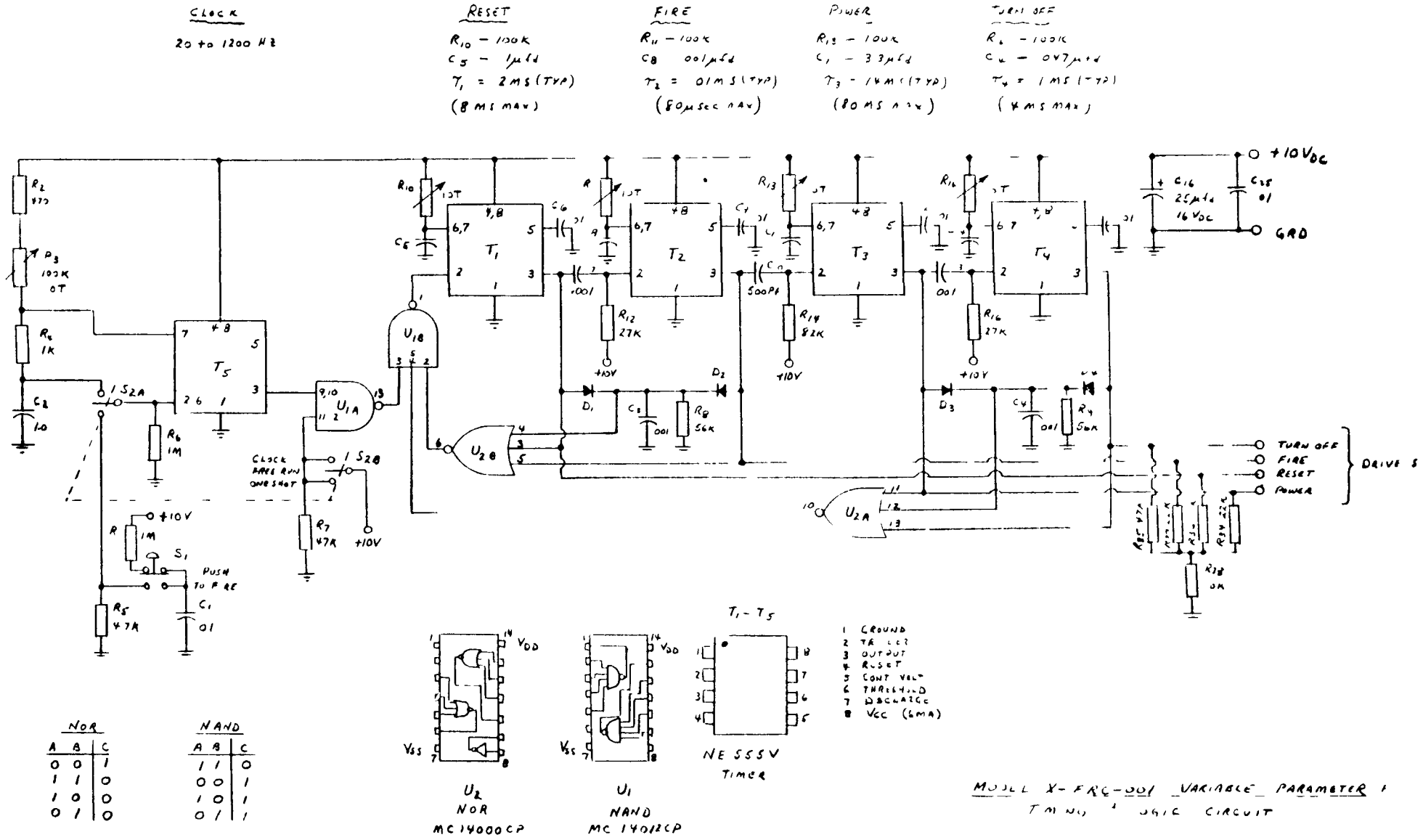

Figure V-5 Flux Reset Timing and Logic Circuit

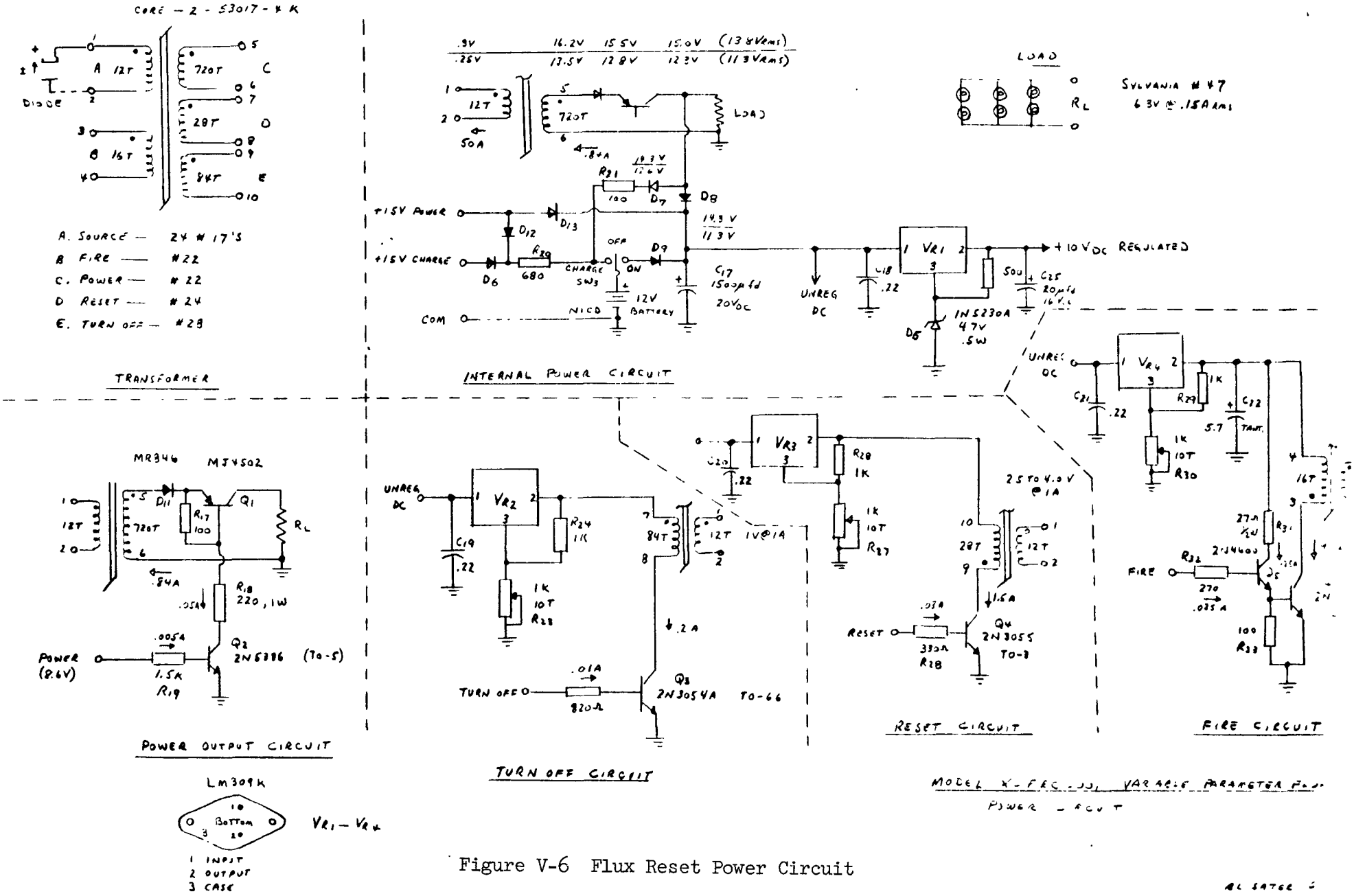

Figure V-6 Flux Reset Power Circuit

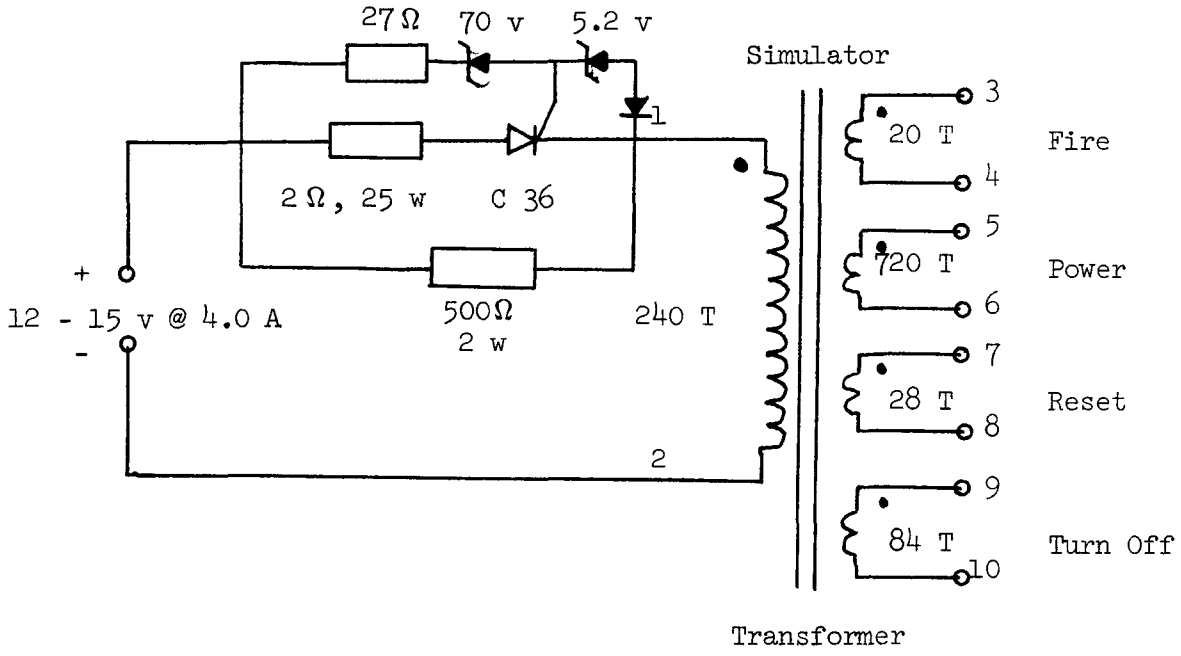

Figure V-7 Thermionic Diode Simulator Circuit

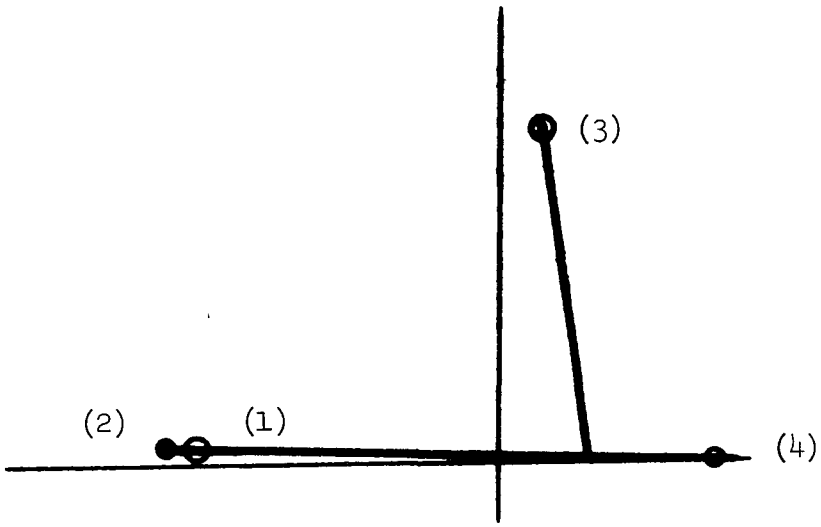

Figure V-8 Volt-Ampere Curve of Simulated Converter (oscilloscope tracing)

(1) - Reset
(2) - Ignition
(3) - Power
(4) - Turn-off

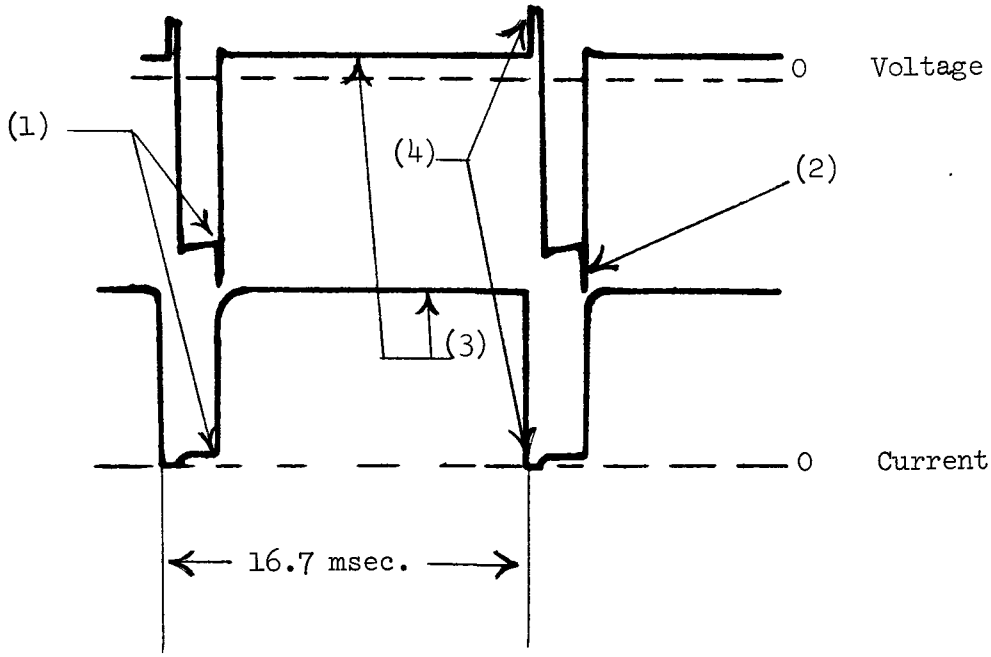

Figure V-9 Voltage and Current Waveforms for Flux Reset Circuit (oscilloscope tracing)

consisting of straight line segments with different impedances. It transfers from the lower mode to the higher mode (ignites) in a manner completely analogous to actual converter behavior.

The variable-parameter model of the flux reset circuit was successfully operated with the simulated converter power source. Results show that the circuit concept is viable, and stable operation is easily maintained with no problems in startup. The transformer core losses are somewhat greater than expected; subsequent models will use a different core material to suppress these losses. Figure V-9 is a tracing of oscilloscope voltage and current waveforms measured on the primary side of the output transformer. The sequence of operating points are shown in their order of occurrence in Figures V-8 and V-9. The flux in the transformer core is first reset by a pulse in the secondary while the converter is de-ignited and the load switched out of the circuit. Second, the converter is ignited with another pulse and the load reconnected. Third, power is delivered to the load until the transformer core begins to saturate. Finally, fourth, a pulse is used to turn-off or de-ignite the converter in preparation for the next reset.

Summary and Conclusion

Fabrication of the components for the min-system converters has been completed and they are awaiting cesiation. Initial operation will be with flux-reset inductive output coupling. The circuit which provides the switching pulses and logic necessary to flux reset operation has been built and successfully tested with a simulated converter.

REFERENCES FOR SECTION V

1. Britt, E. J., and N. S. Rasor, NSR-1-3 and NSR-1-4.

2. Oppen, W. R., IEEE Thermionic Conversion Specialish Conference, Gatlinburg, Tenn., (1963) 372.

3. Rasor, N. S., "Thermionic Diode Converter System", US Patent No. 3,146,388, June, 1964.

APPENDIX I-1 TOPPING SYSTEM COST ANALYSIS

Introduction

Considerable confusion is prevalent regarding the evaluation of trade-offs between performance gains and additional costs incurred when a topping cycle is added to a steam cycle electric generating station. If the proposed topping cycle has a lower capital cost than the main plant, a longer lifetime, increases the overall efficiency, and costs less to repair and maintain than the main plant, then the modification is clearly beneficial. However, in most design concepts the increase of performance must be traded off against possible differences in capital costs, lifetimes, and/or maintenance costs between the main plant and the topping section. A method for quantitative comparison between the costs of the modified and the conventional plants is needed. In principle the comparison is simple: viz, the total of all fixed charges and operating costs incurred during the life of each plant (topping-cycle-and-steam, and steam only) are computed. These total costs are then divided by total amounts of electric energy produced by each respective plant (i.e., output power times working lifetime). If the total cost per unit of energy thus computed is less for the topping cycle than for the steam plant, then a savings is realized and the topping cycle should be added to the system. However, in practice, the procedure just described is undesirably complicated, if not impossible, in the face of design uncertainties for many topping cycle concepts and unknown inflationary factors. Hence a method is described below which allows cost comparison between a modified and a conventional plant using an approach analogous to perturbation techniques applied to existing plant energy costs. Since all plant, fuel, and maintenance costs are treated as dimensionless ratios in this analysis most uncertainties common to both plants (e.g., inflationary factors, etc.) are cancelled out.

Cost Analysis

To begin, it is assumed that the modification to include a topping cycle is performed as an "add-on" and the output power of the steam cycle plant remains unchanged. Under these conditions it is impossible to increase the overall cycle

efficiency without a minimum accompanying increase of electric output.* If the efficiency of the conventional plant is η and its electric power output is P, the topping cycle + steam plant has an increased efficiency $\eta + \Delta\eta$ and increased electric power output P + ΔP.

It can be shown that

$$\Delta P/P \geq \frac{\Delta\eta/\eta}{1 - (\eta + \Delta\eta)} \qquad (1)$$

It will be shown later that the minimum amount of power increase possible P is the economic optimum for a given efficiency increase $\Delta\eta$. The topping portion of the plant may be used to produce a greater power increase but a smaller cost savings is available.

Fixed Charges

Assume that the annual fixed costs incurred by the station are directly proportional to the capital investment and inversely proportional to the useful lifetime. Realizing that various parts of the plant have different lifetimes, the concept of an overall plant life as used here means actually an amortization time over which the fixed cost can be distributed. These costs would include the costs of financing, taxes, depreciation, and insurance as well as capital investment. Let the annual fixed charges per kw be denoted by

$$C_{fxd} = \frac{\gamma M}{t_s P}$$

where

M = the total money invested in constructing the plant

P = the electric output in kw

t_s = plant lifetime in years

γ = an amortizing multiplier to include all the proportional fixed costs

* Cases where the total electric output is unchanged can be analyzed by merely reducing the output of the original plant by the amount of power produced in the topping cycle. The costs of the original plant are then reduced proportionately. Identical results are obtained by this approach.

The fixed charges for a modified topping + steam plant are defined as

$$C_{fxd} - \Delta C_{fxd} = \frac{\frac{M}{t_s} + \frac{N}{t_T}}{P + \Delta P} \qquad (3)$$

where N = the total money invested in constructing the topping cycle modification

t_T = lifetime of the topping cycle section of the plant

t'_s = lifetime of the steam section of the plant when used in conjunction with the topping cycle. (in most cases $t'_s \approx t_s$)

It is convenient to define two quantities

$$S = \frac{M}{P} = \$/kw \text{ of capital investment in the conventional steam plant}$$

$$T = \frac{N}{\Delta P} = \$/kw \text{ of capital investment of the topping cycle}$$

Then eliminating between Equations 1 and 2 yields

$$\Delta C_{fxd} = C_{fxd} \frac{P(1 - t_s/t'_s) + \Delta P \left[1 - (t_s/t_T)(T/S)\right]}{P + \Delta P} \qquad (4)$$

Fuel Costs

The fuel cost is inversely proportional to efficiency. If C_F denotes the annual cost per kw for the conventional steam plant, then

$$C_F = \frac{f}{\eta} \qquad (5)$$

where f is the fuel cost to supply 1 thermal kw of heat to the plant for a period of 1 year. For the topping + steam plant the fuel cost is calculated similarly. The fuel cost in the modified plant is

$$C_f - \Delta C_F = \frac{f}{\eta + \Delta\eta} \qquad (6)$$

Eliminating f between Equations 5 & 6 yield

$$\Delta C_F = F_F(\Delta\eta/\eta) \qquad (7)$$

Maintenance, Supervision and Repair Costs

These costs are less easily determined than fixed charges and the fuel costs. The procedure used here was to take the maintenance costs as the difference between the total operating costs and the fuel costs. Let the annual maintenance cost per kw be denoted by C_m. For the topping + steam system the maintenance cost is denoted $C_m + \Delta C_m$. The modified system repair cost is

$$C_m + \Delta C_m = \frac{C_m P + r C_m \Delta P}{P + \Delta P} \tag{8}$$

where r is the cost-weighted ratio of the frequency of repair for the topping section of the plant to the frequency of repair for the steam part of the plant.

Equation 8 can be solved for ΔC_m to give

$$\Delta C_m = C_m (r - 1)(\Delta P / P + \Delta P) \tag{9}$$

Cost Condition Required for the Topping System

All of the changes in annual costs have now been expressed in terms of the costs of the conventional plant, along with the fractional changes in power output and/or efficiency (Eqs. 4, 7, & 9). The condition that must be met before the topping system should be built is that the sum of costs for the topping + steam plant is less than the sum of the costs of the conventional steam plant, i.e.,

$$C_{fxd} - \Delta C_{fxd} + C_F - \Delta C_F + C_m + \Delta C_m < C_{fxd} + C_F + C_m \tag{10}$$

or that annual savings

$$\Delta C_{fxd} + \Delta C_F - \Delta C_m > 0 \tag{11}$$

substituting the previous equations into Eq. 11 and rearranging:

$$T/S \leq \frac{t_T}{t_s} \left[\frac{CF}{C_{fxd}} \left(\frac{\Delta \eta}{\eta} \right) \left(\frac{\Delta P}{P + \Delta P} \right) + \left(1 + t_s / t'_s \right) - \frac{C_m}{C_{fxd}} (r - 1) \right] \tag{12}$$

subject to

$$\frac{\Delta P}{P} \geq \frac{\Delta\eta/\eta}{1 - (\eta + \Delta\eta)} > 0$$

This gives the maximum economically favorable value of the ratio of the capital investment in the topping cycle to the capital investment in the conventional steam plant.

Numerical Values of the Cost Parameters

The results of biannual surveys of bus bar energy costs in steam power stations are given in Table I.[1] The values of C_{fxd}, C_F, and C_m can be computed from the data presented there. To convert from bus bar energy costs (mils/kwhr) to annual costs per kw, multiply by the number of hours in a year (8766) and the annual plant factor. The values of $C_{fxd} + C_F$ can be thus directly converted, but C_m must first be computed by subtracting the fuel cost from the total operating cost. The values calculated for C_{fxd}, C_F, and C_m are shown in Table II along with the ratios of costs that appear in Inequality 12.

Summary

Equation 12 relates the proportionate increase in capital investment and additional maintenance which may be justified in building a topping system of any given efficiency. This expression allows the generation of a meaningful "breakeven line" when looking at the performance of a topping cycle for a particular application. Some of the necessary data for calculating such a line for a steam plant system has been given.

TABLE 1 STEAM PLANT POWER COST RISE OVER 10-YEAR PERIOD

	1972	1970	1968	1966	1964	1962
Total busbar energy cost, Mills/net kwhr	7.99	7.20	6.04	5.84	6.82	6.78
Construction cost excluding switchyard, $/kw . .	144.33	125.57	117.94	118.81	126.80	145.95
Fixed charges, Mills/net kwhr.	3.78	3.72	3.12	2.59	3.32	3.42
Operating costs, Mills/net kwhr	4.21	3.48	2.92	3.25	3.50	3.36
Fuel cost, Mills/net kwhr	3.49	2.83	2.40	2.73	2.93	2.78
Fuel cost portion of operating costs, %	82.6	81.8	82.8	84.7	82.6	83.5
Fuel cost, $\phi/10^6$ Btu	35.86	28.36	24.12	26.24	26.26	27.24
Manpower, operating and maint. employees/Mw . .	0.172	0.144	0.160	0.174	0.206	0.271
Station net heat rate, average Btu/net kwhr . .	10,115	9,927	9,980	9,713	10,347	10,098
Annual plant factor, average, %	57.86	62.80	62.65	65.00	62.51	65.38
Utilization factor, average, %	98.60	98.02	99.68	98.50	96.67	99.57

TABLE II CALCULATED PARAMETERS FOR STEAM POWER PLANTS OVER 10-YEAR PERIOD

	1972	1970	1968	1966	1964	1962
Total annual cost $/kw	$40.52	39.64	33.17	33.28	37.37	38.86
Annual Fixed Charges C_{fxd} $/kw	$19.72	20.48	17.14	14.76	18.19	19.60
Annual Fuel Cost C_F $/kw	$17.70	15.58	13.18	15.56	16.06	15.93
Annual Maintenance Cost, C_m $/kw	$3.65	3.60	2.86	2.96	3.12	3.32
Ratio C_F/C_{fxd}	.923	.76	.77	1.054	.883	.813
Ratio C_m/C_{fxd}	.19	.175	.167	.201	.172	.17

APPENDIX I-2 INDUCTIVE OUTPUT COUPLING - EDDY CURRENT EFFECTS

Introduction

One of the difficulties encountered in the design of a THX module involves the conversion of the low voltage, high current output of a thermionic diode to higher voltages and lower currents. This is necessary to prevent resistive power losses in the current-carrying bus bars, as well as to provide a better match to user requirements.

One possible way to step up the THX output voltage is to inductively couple the THX to its load. The use of an appropriate transformer turns ratio then permits the desired voltages to be obtained. The purpose of the work reported here was to ascertain the nature of possible eddy current losses in the THX current conductors which result from the alternating magnetic fields created with inductive output coupling. This scoping study will provide input for more detailed THX designs, particularly with respect to the need for current path isolation, the number of transformer loops required per THX module, etc.

Analytical Approach

The general diode-transformer structure may be prepresented by a single driven loop conductor with a diode completing the loop.

Figure 1

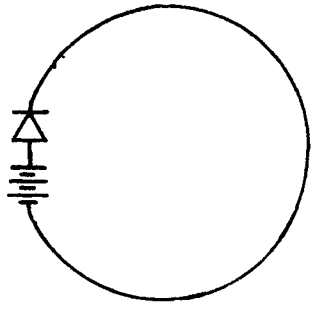

The problem considered here is the generation of eddy currents in the conductor due to the alternating magnetic field generated when the diode current is switched on and off. Because of the high currents necessary the conductor is expected to have a large cross sectional area. Since the design of the diode system is not final, it would be futile to attempt a detailed calculation accounting for non-uniform current densities and minor perturbations in the field. To simplify the problem it is assumed that, if any design is to acceptable, the eddy currents must be small. The fringe effects, (i.e., surface currents) will then be small. Thus, the current density profile in the conductor

will be approximately that which would be found under DC operating conditions. If this is not the case the system would be unacceptable due to the eddy current power losses.

Thus, in order to provide some estimate of the importance of various design parameters on the size of eddy currents, the system illustrated in Figure 2 was analyzed in some detail.

Figure 2

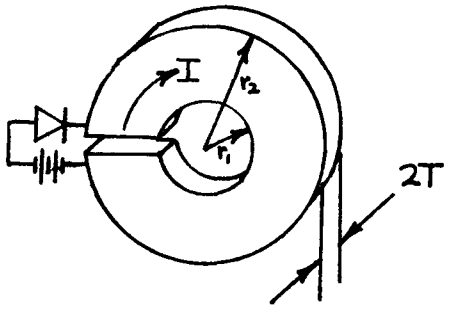

The detail is to assure that for the representative system above, the answers will be essentially correct. The reader may then extrapolate the results to more complex systems for order of magnitude estimates.

The assumptions made for this analysis were:

1. The current due to the diode is uniform within the conductor.
2. The field within the hole is uniform.
3. The field outside the conductor is zero.
4. The field within the conductor is linear.
5. The gap in the cylinder is negligible

Assumption No. 1 has already been discussed. The assumption that the field within the hole is approximately uniform is best demonstrated by comparing the assumption with exact numerical calculations. Comparisons are shown below in Figure 3 for a long thick cylinder. In assumption No. 3 it is implicitly assumed that there are many units of the form shown in Figure 2 lined in series. Figure 3 also demonstrates the accuracy of assumptions 3 and 4. Assumption 5 is minor but cannot be justified.

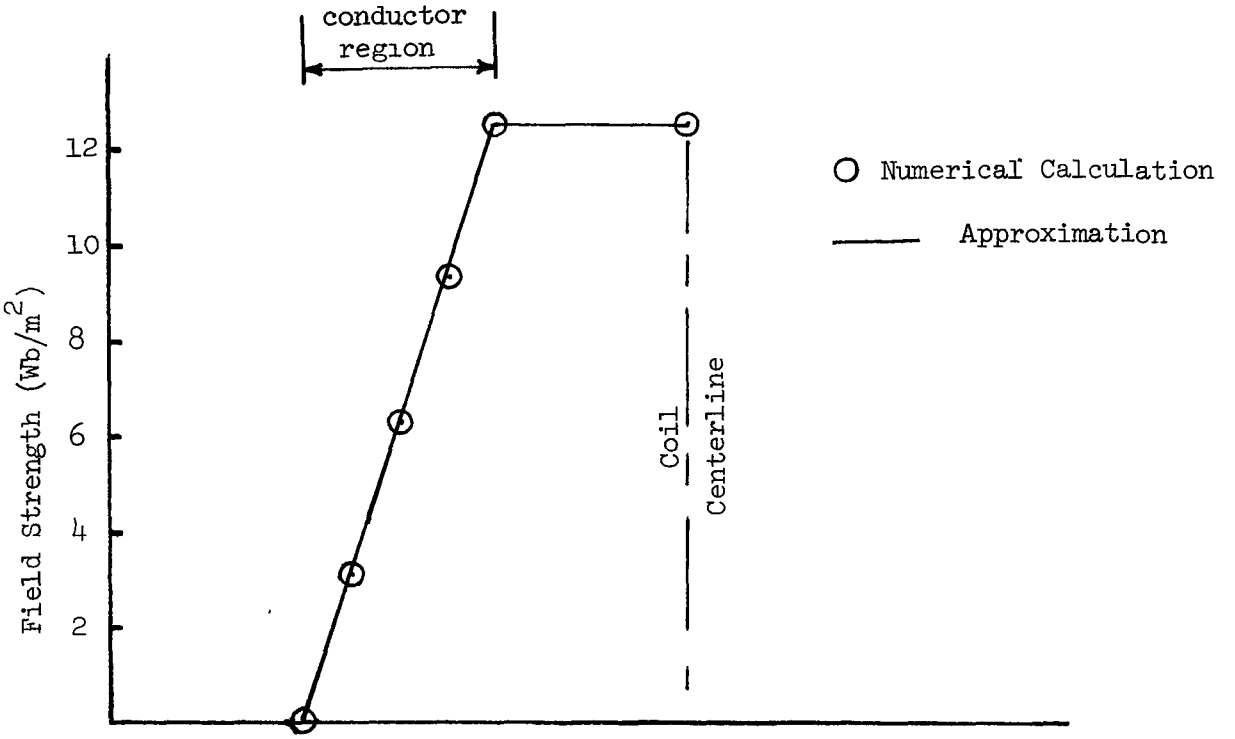

Figure 3 Calculated and Approximated Loop Field Strengths

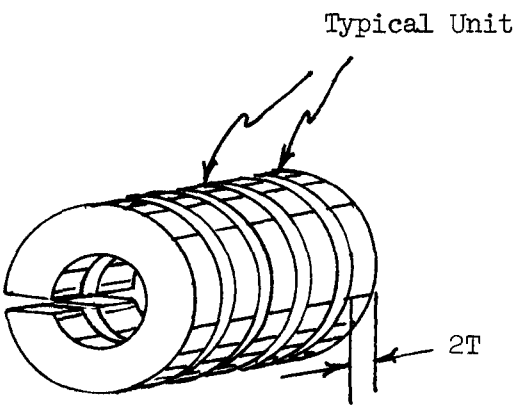

Figure 4 Current Loops in Series

Magnetic Field

With the assumptions above the approximate magnetic field can be expressed analytically.

$$B_{\text{¢}} = \int_{-T}^{+T} \int_{r_1}^{r_2} \frac{\mu_o}{2} \frac{J\, r^2\, drdz}{(Z^2 + r^2)^{3/2}}$$

This expression is a differential form of the centerline field due to a single turn of an infinitely thin conductor, where r is the radial coordinate and z is the axial coordinate. J is the current density (assumed to be uniform). The permittivity of air μ_o is $4\pi \times 10^{-7}$ newtons/amp^2.

Intergrating we obtain

$$B_{\text{¢}} = \mu_o\, J\, T \ln \left[\frac{r_2 + \sqrt{r_2^2 + T^2}}{r_1 + \sqrt{r_1^2 + T^2}} \right]$$

For this calculation we shall assume $T = \infty$. That is, we have a long set of closely spaced units, each with a length of L.

Then

$$B_{\text{¢}} = \mu_o\, J(r_2 - r_1) \quad \text{limit } T \to \infty$$

Imposing assumptions 2, 3, and 4, we have the general expression for the field as a function of the radius

$$B(r) = B_{\text{¢}} \qquad 0 \leq r \leq r_1$$

$$B(r) = B_{\text{¢}} \frac{(r_2 - r)}{(r_2 - r_1)} \qquad r_1 \geq r \leq r_2$$

Eddy Current Flow

The current generated by the alternating magnetic field will be in a direction opposite to that generated by the diode. Because of the diode's presence, the only complete current path is as shown in Figure 5.

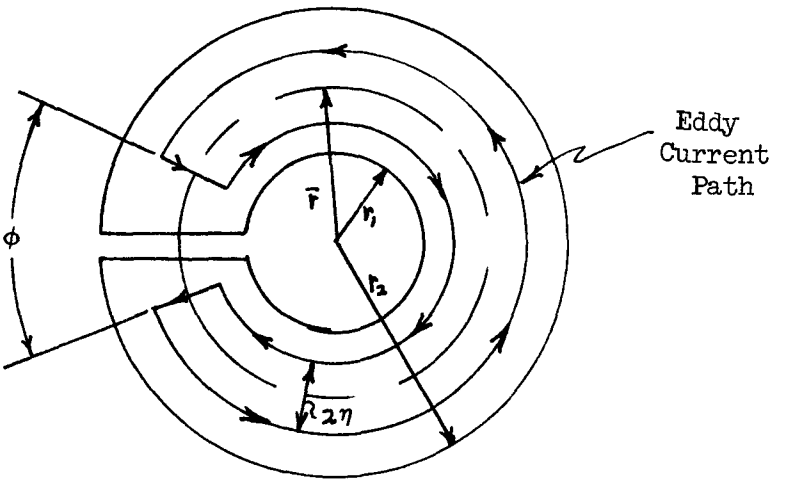

Figure 5

By symmetry

$$\phi = A + B\eta$$

The boundary conditions are

$$\phi = 0, \quad \eta = \frac{r_2 - r_1}{2} \quad \text{and} \quad \phi = 2\pi, \quad \eta = 0$$

Thus

$$\phi = 2\pi\left[1 - \frac{2\eta}{(r_2 - r_1)}\right]$$

The path length can then be shown to be

$$L(\eta) = 4\eta + \left(\frac{r_2 + r_1}{r_2 - r_1}\right) 4\pi\eta$$

The geometry used in the calculations of the area enclosed by a circuit path is shown in Figure 6.

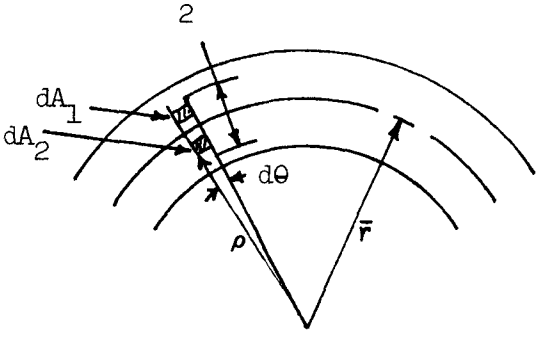

Figure 6

The EMF around the eddy current path is

$$\delta\mathcal{E} = \oint_{\text{path length}} \vec{E} \cdot \vec{dl} = \left[\frac{\partial}{\partial T} \int_{\text{area}} B \, dA \right] \sqrt{2}\pi f$$

where f is the frequency in Hz. Expressing this equation in polar coordinator, as shown in Figure 6 and integrating over ρ and Θ yield

$$\delta\mathcal{E} = \sqrt{2}\,\pi f \int_{\bar{r}-\eta}^{\bar{r}} \pi B t \, \frac{(r_2 - \rho)\, 4\eta\rho\, d\rho}{(r_2 - r_1)^2} + \sqrt{2}\,\pi f \int_{\bar{r}-\eta}^{\bar{r}} \pi B t \, \frac{(\rho - r_1)(2\bar{r} - \rho)\, 4\eta\, d\rho}{(r_2 - r_1)^2}$$

Expanding terms in ρ and integrating

$$\delta\mathcal{E} = \frac{2^{5/2}\,\pi^2\, f\, B t}{2} \, \eta^2 \left[\bar{r}t - \frac{2}{3}\eta^2 \right]$$

where $t = r_2 - r_1$

The eddy current resulting from this driving force is

$$\delta I_E = \frac{\delta\mathcal{E}}{R(\eta)}$$

where $R(\eta)$ is the resistivity of a differential segment along the path $L(\eta)$ shown in Figure 7.

$$R(\eta) = \frac{t^2\eta + 8\pi^2\bar{r}^2\eta}{\bar{r}L\,\sigma\pi\, d\eta}$$

where σ is the conductivity of the loop material

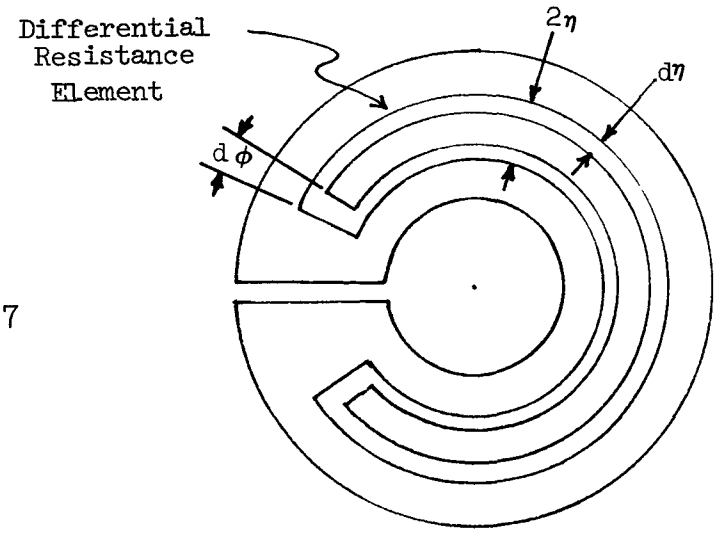

Figure 7

The differential eddy current is then given by

$$\delta I_E = \frac{2^{5/2}\,\pi^3\,L\bar{r}\sigma f\,B_\xi}{t(t^2 + 8\,\pi^2\bar{r}^2)}\,\eta\left(\bar{r}t - \frac{2}{3}\eta^2\right)d\eta$$

Power Losses

The power consumed in the elemental path is just $\delta I_E\,\delta\mathcal{E}$. The total power lost to eddy currents in the conductor is thus given by

$$\int_0^{t/2}\delta I_E\,\delta\mathcal{E} = \int_0^{t/2}\frac{2^5\,\pi^5\,L\bar{r}\,\sigma\,f^2\,B_\xi^2}{t^3(t^2 + 8\,\pi^2\bar{r}^2)}\,\eta^3\left[\bar{r}t - 2/3\,\eta^2\right]^2\,d\eta$$

Performing the integration and substituting for B_ξ^2 leads to the following result for the power lost, P_{eddy}

$$P_{eddy} = \frac{2^5\,\pi^5\,\sigma\,f^2\,\mu_o^2\,J^2\bar{r}t^5}{t^2 + 8\,\pi^2\bar{r}^2}\left[\frac{\bar{r}^2}{64} - \frac{\bar{r}t}{288} - \frac{t^2}{4608}\right]$$

Since $t \leq 2r$; the factor of $8\,\pi^2$ in the denominator makes the 1st term in the denominator negilible compared to the second. Additional simplication results by substituting I = JLt, to give:

$$P_{eddy} = 4\pi^3\sigma\,f^2\,\mu_o^2\,I^2(\bar{r}/L)\,t^3\left[\frac{1}{64} - \frac{(t/\bar{r})}{288} + \frac{(t/\bar{r})^2}{4608}\right]$$

Retaining only the 1st term in t gives a conservative approximation which is within a factor of 2 for most design calculations

$$P_{eddy} \approx (\pi^3/16)\ f^2\ \mu_o^2\ \sigma\ (\bar{r}/L)\ t^3 I^2$$

It is informative to examine the sum of the resistive and eddy current losses, P_T in the loop. The resistive losses for this geometry can be shown to be

$$P_R = \frac{2\ I^2}{L\sigma \ln\left(\frac{2\bar{r} + t}{2\bar{r} - t}\right)}$$

and the total is

$$P_T = \frac{I^2 \Theta}{L}$$

where Θ is a parameter which has the units of resistivity and contains the geometrical dependence for the power loss

$$\Theta = \frac{\pi^3\ f^2\ \mu_o^2\ \sigma\ \bar{r}\ t^3}{16} + \frac{2\pi}{\sigma \ln\left(\frac{2r + t}{2r - t}\right)}$$

Θ has been plotted in Figure 8 for two values of $\bar{r}$. It can be seen that Θ is fairly linear in $\bar{r}$. The optimum thickness is relatively independent of $\bar{r}$, however, and for sodium is ~7 cm.

Summary and Conclusions

An analysis of the power losses due to eddy currents in a cylindrical loop conducter has been made. The losses increase linearly with the average radius of the loop and decrease linearly with the length. The strongest dependence is on thickness, where the losses increase as the cube of this dimension. The losses also increase as the square of the frequency used.

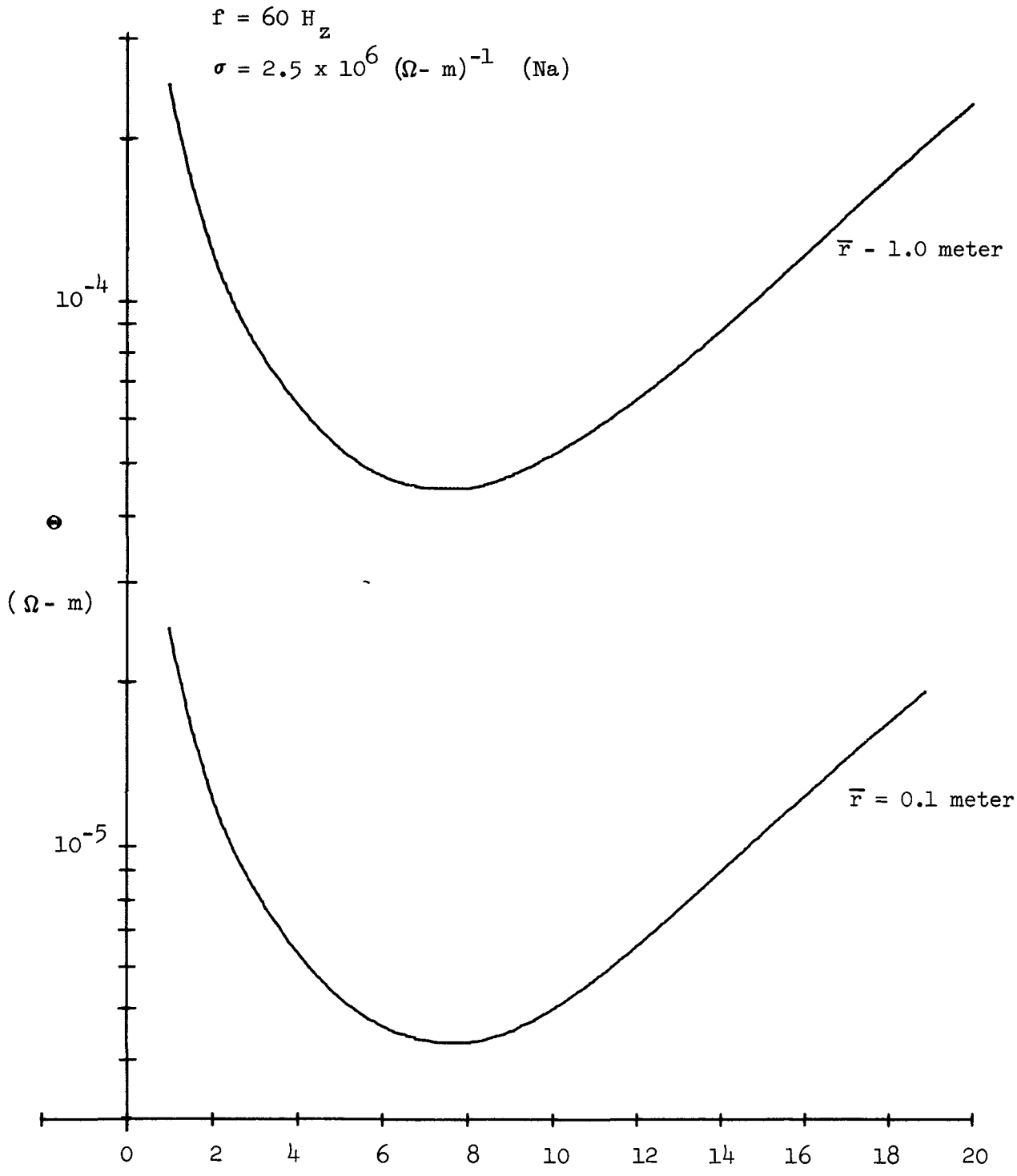

Figure 8 Loop "Resistivity" Θ

APPENDIX I-3

THX - Sodium Heat Transfer in a Fossil Fuel Furnace

Introduction

A simplified scoping analysis was performed to study the heat transfer from a coal fired furnace to a thermionic heat exchanger in a topping cycle application. The analysis was intended to provide a preliminary estimate of the heat transfer characteristics of the liquid metal loop which would be required, and to provide preliminary information and recommendations on suitable materials.

Two possible cases were examined. In the first, liquid sodium is circulated through the furnace, and delivers heat to a THX. The THX is external to the furnace. Figure 1 illustrates this case schematically. In the second case furnace flue gases are circulated directly through the THX module. The gases heat liquid sodium within the THX, which then delivers the heat to the thermionic emitters. Figure 2 illustrated this case schematically.

Both cases were studied with THX emitter temperatures of 2000^{o}F and emitter heat fluxes of 30w/cm^{2} (95000 Btu/hr-ft^{2}). The THX reference design data used in this analysis, is shown in Table 1 and the topping system flow diagram is shown in Figure 3.

Heat Transport

The heat transport process was characterized by the transfer of heat from hot flue gases to a heat exchange surface, to liquid sodium, and finally to the thermionic emitter wall.

The heat flux at the heat exchange surface may be estimated by

$$Q/A_x = U\,\overline{\Delta T}$$

where the log mean temperature drop, $\overline{\Delta T}$, along the surfaces is given by

$$\overline{\Delta T} = (\Delta T_{fg} - \Delta T_{Na})/\ln(\Delta T_{fg}/\Delta T_{Na})$$

TABLE I

REFERENCE THX CHARACTERISTICS

Reference Values - Double Ended Axial Configuration

D = 200 cm

N = 100 tubes

J = 10 amp/cm^2

Density of structural metal = 8 g/cm^3 - i.e. Inconel

Thickness of structural metal = 2 mm

Density of liquid metal = 0.7 g/cm^3 - i.e. Na

Cost of liquid metal = \$.20/lb - i.e. Na

T_E(^oF)	T_C(^oF)	ϕ'_C(ev)	Calandria Height(cm)	V_{opt}(v)	Efficiency (%)	Maximum Total Output Power (Kwe)
2400	1200	1.9	51	.22	6	460
		1.5	73	.45	12	1600
2000	1200	1.5	52	.28	11	500
		1.0	61	.33	14	1000
	600	1.0	94	.58	23	2400
1800	1200	1.5	45	.17	7	390
		1.0	61	.25	11	670
	600	1.0	84	.47	20	1700
1600	600	1.0	76	.37	18	1200

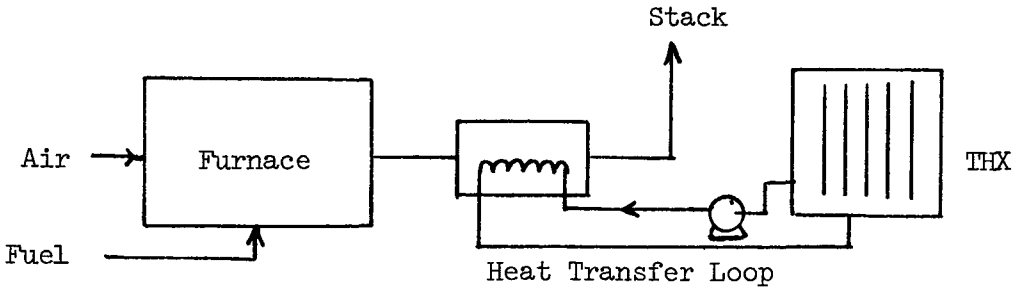

Figure 1 THX Configuration A

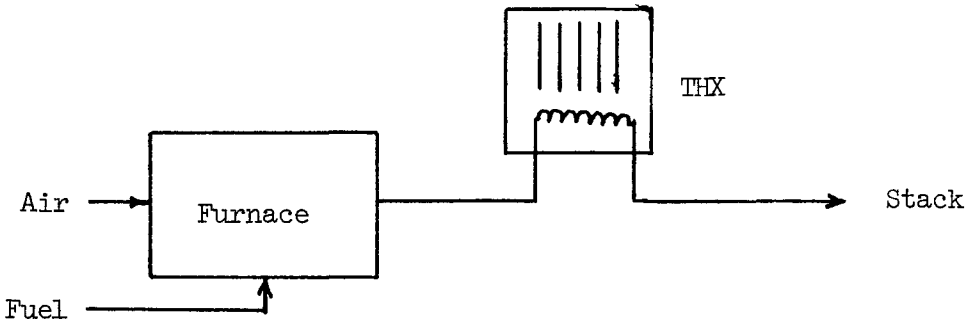

Figure 2 THX Configuration B

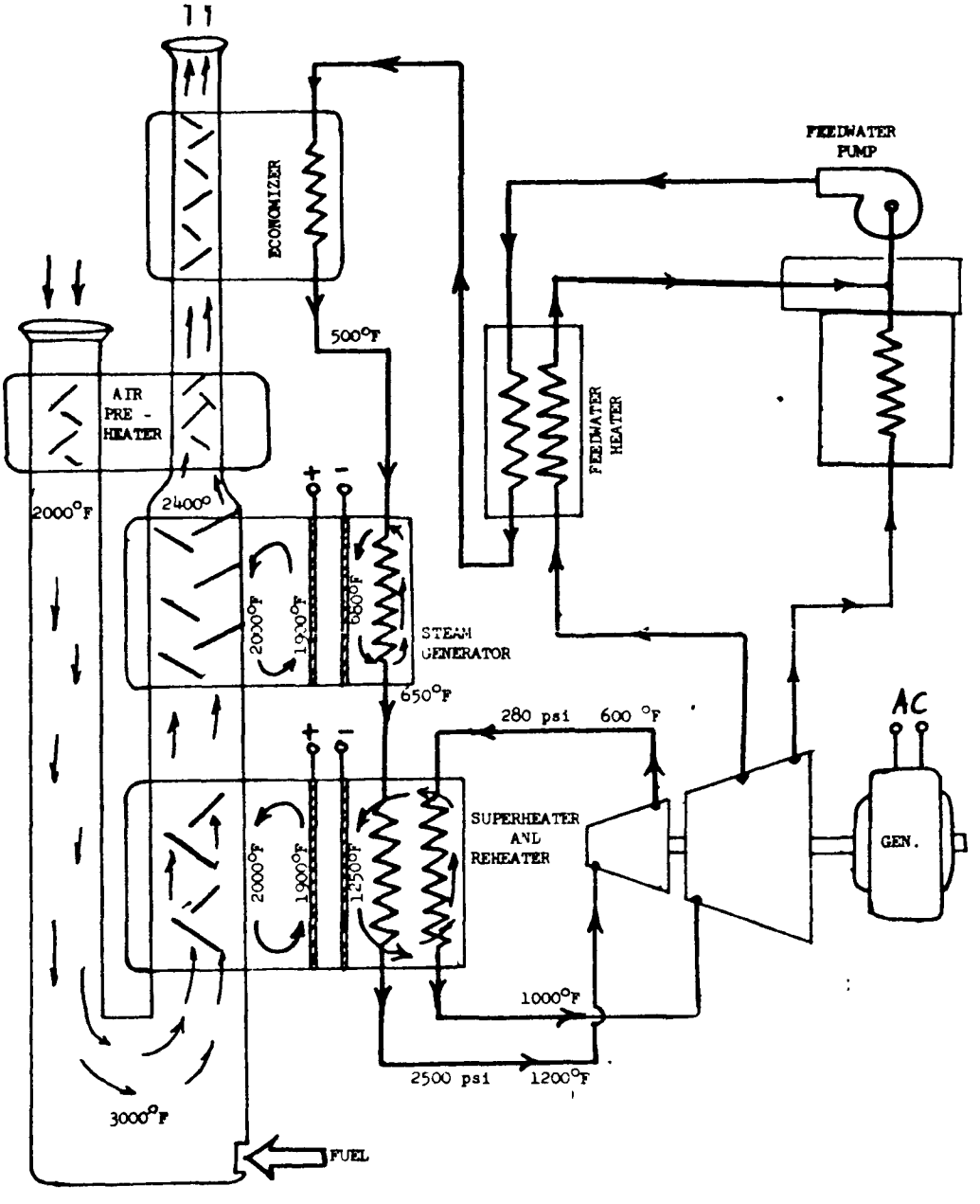

Figure 3 Flow Diagram of Thermionic Topping System

where ΔT_{fg} is the flue gas temperature drop and ΔT_{Na} is the liquid sodium temperature rise.

and the resistance function, U, is given by

$$U = 1/(1/h_h + 1/h_{bd} + x_w/k_w + 1/h_c)$$

The values used for the heat transfer parameters were

h_h	= hot side film coefficient	10 Btu/hr-ft^2/^{o}F
h_{hd}	= hot side cooling film coefficient	2,000 Btu/hr-ft^2/^{o}F
x_w	= wall thickness	1/16 inch
k_w	= thermal conductivity of tube wall	10 Btu/hr-ft^{o}F
h_c	= cold side film coefficient	1000-5000 Btu/hr-ft^2/^{o}F (Na)

The values for k_w are typically between 10 and 30 for steel, near 15 for super-alloy such as Inconel, Hastelloy, Haynes 188, a Mar-M-200, near 10 for Al_2O_3, and BeO and about 0.5 for ZrO_2.

Because of its small value h_h effectively controls the heat transfer through the system

To first order, the temperature drop across each heat transfer region may be estimated by dividing the heat flux in each region by its conductance. Thermal entrance effects and variations in conductivity or other physical properties with temperature may then be ignored. With the specified emitter heat flux of 30w/cm^2 (95,000 Btu/m-ft^2) the temperature drop across the emitter wall (ΔTk_1) is 32^{o}F for a 40 mill wall, and 48^{o}F for a 60 mill wall. Pi correlations for the liquid sodium film coefficient in the THX emitter geometries were not found in the literature but for liquid metals in turbulent flow and small L/D ratios (as in the THX) one might anticipate h$\approx$1000 to 2000 Btu/hr-ft^2/ft. For L/D ratios of 60 and flows of 5 ft/sec. film coefficients as high as 9000 Btu/hr-ft^2 have been obtained. Using a value of 2000 Btu/hr-ft^2 ^{o}F results in a 47^{o}F temperature drop across the film adjacent to the THX emitter walls (ΔT_{h2}). Similarly the drop across the film between liquid sodium and the material separating it from the flue gases would be 47^{o}F (ΔT_{h1}) and the drop across the

material itself would be 30-50°F (ΔT_{k2}). The drop across the boundary layer on the flue gas side (ΔT_{hs}) would be 50°F. The flue gas temperature drop through each THX is constrained by the system design to 300 °F. Figure 4 summarizes the temperature drops through the system.

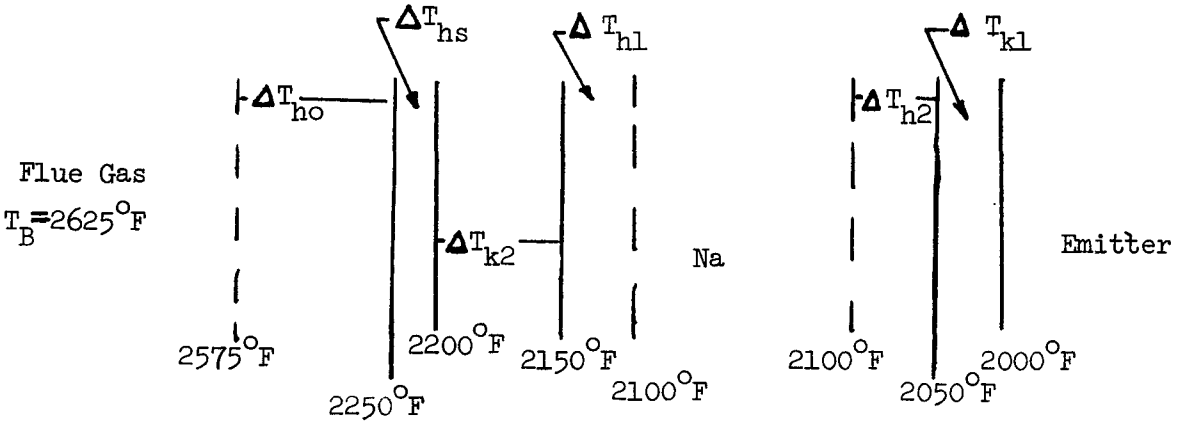

In the second case, the total heat flow to the THX must be provided by convective heat transfer from the flue gases to the sodium containment. This amounts to 1.4×10^7 Btu/hr for the THX operating at an emitter heat flux of 30 w/cm^2 (95,000 Btu/hr-ft^2)with an emitter area of 150 ft^2.

Since $$Q = H_o A_{air} \Delta T_{air}$$

where $H_o \approx 10$ Btu/ft^2-ft^2/°F and ΔT_{air} is constrained to 300°F, the required heat transfer area, A_{air} is

$$A_{air} = 4750 \text{ ft}^2$$

For the first case, where sodium coolant loops are introduced into the furnace, the heat may be provided by radiative as well as conductive heat transfer. In typical combustion furnaces transferring heat to a tube bank the nominal gain is 30%, i.e., 3,225 ft^2 would be sufficient area to transfer the heat load.

Flow Rate

The equation controlling the liquid sodium flow rate required to:

$$Q = W\ C\Delta T$$

where Q is the heat gained by the sodium in one pass, W is the mass flow rate, C is the heat capacity of sodium, and ΔT is the sodium temperature rise. Operation of the THX module allows a ΔT in the sodium of $100^{\circ}F$. For liquid sodium at the temperatures of interest C is approximately 0.3. Then, for a heat requirement of 1.4×10^6 Btu/hr a mass flow rate of 4.8×10^5 lbs/hr may be calculated. Since sodium has a mass of 40 lbs/ft^3, the flow rate, required is 1.2×10^4 ft^3/hr. For a THX of collandria design with 100 - 6" diameter emitter tubes the resulting sodium flow rate is approximately ten feet per minute.

Similarly for the furnace flue gases a heat transfer to the sodium of 1.4×10^7 Btu/hr is required. The crossectional area required, at a furnace gas velocity of $\sim$2000 ft/minute (near the typical maximum) is 30 square feet.

Materials

The classes of materials considered were those used in the chemical process industry and in the aircraft turbine engine industry, typically useful above $1500^{\circ}F$. These types were:

1. Stainless steel related (high Cr types) - 446, 310, SR18, 22-16 CuMo.
2. Nickel base superalloys - Inconels, Hastealloys, Waspalloy, Thora dispersed nickel, Mar-M-200,and Rene alloys.
3. Cobalt Base Superalloys - Haynes 188, Haynes 25 and Mar-M-322
4. Refractory Metals - Tungsten, Tantalum, Columbium, etc., and their alloys
5. Any of above with coatings; coating could be oxide coatings typical of turbine engines, or NiAl, FeCrMo, superalloy coatings (vapor deposited) such as waspalloy, and cladding coatings such as inconels + niobium.

Examples of the characteristics of some of these materials are summarized in Table 2.

Table 2

Alloy	Oxidation Resistance to	Rupture Stress -100 Hrs. @ 1800°F Psi	Creep Stress 1% @ 10000 Hrs. Psi (temp)
ST.ST.310	2000°F	1,600	1,000 (1500°F)
ST.ST.446	1900°F	400	300 (1400°F)
Hastealloy	2200°F	3,000	Unknown
Inconel 601	2300°F	3,000	3,000 (1500°F)
Inconel 702	2400°F	3,000	3,000 (1500°F)
HN (cast)	2400°F	Unknown	200 (2100°F)
Haynes 25	2200°F	5,000	4,000 (1600°F)
Waspalloy	2400°F	8,000	6,000 (1600°F)
Mar-M-200	2200°F	10,000+	9,000 (1600°F)

Extrapolation of any of these to 2200-2400°F shows 100 HR rupture strengths or 10,000 HR creep stress below the 100 Psi sodium vapor pressure in the THX and heat exchanger indicating the need to remain below 2200°F with presently available materials. Above 200°F incompatibility with sodium becomes a problem for the ferrous based alloys. All of the above are available in mill runs - typically 2-10,000 lbs. They are all available in sheet and tube with the exception of MAR-M-200 and HN, both of which are cast alloys, HN is typically used in the radiant section of boiler furnaces. MAR-M-200 is typically used as turbine blades or buckets in jet engines. Weldability of the latter two are poor at best. All of the other alloys have acceptable forming and welding characteristics. The materials listed are generally in the $2-5.00/lb range except for MAR-M-200 and HN, which require more expensive casting procedures.

The strength of the refractory metals is sufficient to the higher temperatures contemplated, but their oxidation resistence is very poor. Their cost is high, in the range of $33/lb. Other exotics (i.e., Silicon Nitride) have interesting properties (SiN-O creep at 2700°F is 50000 psi; 65000 psi rupture

at 2900°F) but information on availability, workability,and costs was not available at the time of this report. The most primising approach seems to be niobium tubing with inconel or related sleeves for oxidation resistance. Further data is being accumulated for NiAl coatings as well as Al_2O_3, ZrO_2, and MgZr coatings, and vapor deposited Waspalloy.

Summary and Conclusions

With the present state of the art a heat transfer area of 3000-4000 ft^2 will be necessary to provide 1.4×10^7 Btu/hr to a THX module. While this is a reasonable amount if sodium coolant pipes are used in a furnace, the direct heating of the THX module with furnace flue gases appears doubtful because of the restricted volume available.

For emitter temperatures above 2000°F refractory materials will probably be necessary to meet creep and rupture strength requirements. A superalloy sheath or other coating will be needed to provide oxidation resistence. Between 1500°F and 2000°F super alloys may be suitable alone, but development will be required. Below 1500°F there is considerable experience with super-alloys in both liquid sodium and flue gas environments.